

UNIVERSIDADE FEDERAL DO PARÁ
INSTITUTO DE TECNOLOGIA
PROGRAMA DE PÓS-GRADUAÇÃO EM ENGENHARIA ELÉTRICA

METODOLOGIAS DE DISCRETIZAÇÃO ESPACIAL SEM MALHA BASEADAS
NOS POTENCIAIS DE COULOMB E LENNARD-JONES PARA O MÉTODO
RADIAL DE INTERPOLAÇÃO POR PONTOS (RPIM) APLICADAS PARA
SOLUÇÃO NUMÉRICA DAS EQUAÇÕES DE MAXWELL

WASHINGTON CÉSAR BRAGA DE SOUSA

TD 13 / 2017

UFPA / ITEC / PPGEE
Campus Universitário do Guamá
Belém-Pará-Brasil
2017

UNIVERSIDADE FEDERAL DO PARÁ
INSTITUTO DE TECNOLOGIA
PROGRAMA DE PÓS-GRADUAÇÃO EM ENGENHARIA ELÉTRICA

WASHINGTON CÉSAR BRAGA DE SOUSA

METODOLOGIAS DE DISCRETIZAÇÃO ESPACIAL SEM MALHA BASEADAS
NOS POTENCIAIS DE COULOMB E LENNARD-JONES PARA O MÉTODO
RADIAL DE INTERPOLAÇÃO POR PONTOS (RPIM) APLICADAS PARA
SOLUÇÃO NUMÉRICA DAS EQUAÇÕES DE MAXWELL

TD 13 / 2017

UFPA / ITEC / PPGEE
Campus Universitário do Guamá
Belém-Pará-Brasil
2017

UNIVERSIDADE FEDERAL DO PARÁ
INSTITUTO DE TECNOLOGIA
PROGRAMA DE PÓS-GRADUAÇÃO EM ENGENHARIA ELÉTRICA

WASHINGTON CÉSAR BRAGA DE SOUSA

METODOLOGIAS DE DISCRETIZAÇÃO ESPACIAL SEM MALHA BASEADAS
NOS POTENCIAIS DE COULOMB E LENNARD-JONES PARA O MÉTODO
RADIAL DE INTERPOLAÇÃO POR PONTOS (RPIM) APLICADAS PARA
SOLUÇÃO NUMÉRICA DAS EQUAÇÕES DE MAXWELL

Tese submetida à
Banca Examinadora do
Programa de Pós-Graduação
em Engenharia Elétrica da
UFPA para a obtenção do
Grau de Doutor em
Engenharia Elétrica na área
de Telecomunicações.

UFPA / ITEC / PPGEE
Campus Universitário do Guamá
Belém-Pará-Brasil
2017

Sousa, Wahington César Braga de, 1980-

Metodologias de discretização espacial sem malha baseadas nos potenciais de Coulomb e Lennard-Jones para o método radial de interpolação por pontos (RPIM) aplicadas para solução numérica das equações de Maxwell / Washington César Braga de Sousa.-2017.

Orientador : Rodrigo Melo e Silva de Oliveira Tese (Doutorado) - Universidade Federal do Pará, Instituto de Tecnologia, Programa de Pós-Graduação em Engenharia Elétrica, Belém, 2017.

1. Campos eletromagnéticos – modelos matemáticos. 2. Maxwell, equações de. 3. Métodos de simulação. I. Título.

CDD 23. ed. 530.141

UNIVERSIDADE FEDERAL DO PARÁ
INSTITUTO DE TECNOLOGIA
PROGRAMA DE PÓS-GRADUAÇÃO EM ENGENHARIA ELÉTRICA

METODOLOGIAS DE DISCRETIZAÇÃO ESPACIAL SEM MALHA BASEADAS NOS
POTENCIAIS DE COULOMB E LENNARD-JONES PARA O MÉTODO RADIAL DE
INTERPOLAÇÃO POR PONTOS (RPIM) APLICADAS PARA SOLUÇÃO NUMÉRICA DAS
EQUAÇÕES DE MAXWELL

AUTOR: WASHINGTON CÉSAR BRAGA DE SOUSA

TESE DE DOUTORADO SUBMETIDA À AVALIAÇÃO DA BANCA EXAMINADORA APROVADA
PELO COLEGIADO DO PROGRAMA DE PÓS-GRADUAÇÃO EM ENGENHARIA ELÉTRICA DA
UNIVERSIDADE FEDERAL DO PARÁ E JULGADA ADEQUADA PARA OBTENÇÃO DO GRAU
DE DOUTOR EM ENGENHARIA ELÉTRICA NA ÁREA DE TELECOMUNICAÇÕES.

APROVADA EM 04/ 12/ 2017

BANCA EXAMINADORA:

Prof. Dr. Rodrigo Melo e Silva de Oliveira
(ORIENTADOR - PPGEE/UFPA)

Prof. Dr. Wilson Ricardo Matos Rabelo
(COORDENADOR - UFPA)

Prof. Dr. Dmitriev Victor
(MEMBRO - PPGEE/UFPA)

Prof. Dr. Rubem Gonçalves Farias
(MEMBRO - UFPA)

Prof. Dr. Fabrício José Brito Barros
(MEMBRO - PPGEE/UFPA)

Prof. Dr. Licinius Dimitri Sá de Alcantara
(MEMBRO - UFRA)

Prof. Dr. Jose Ricardo Descardecí
(MEMBRO - UFT)

VISTO:

Prof. Dr. Evaldo Gonçalves Pelaes
(COORDENADOR DO PPGEE/ITEC/UFPA)

“ A distinção entre passado, presente e futuro é apenas uma ilusão teimosamente persistente.”

Albert Einstein

(1879 - 1955)

A Deus por toda existência.

A meus pais, sementes de tudo em minha vida.

A minha irmã e sobrinhos, por tudo que representam para mim.

Agradecimentos

Primeiramente, agradeço ao meu orientador Rodrigo Oliveira pelo excelente, competente e exemplar trabalho de orientação. Muito obrigado! Ao professor Wilson, pelo suporte relativo à teoria de dinâmica molecular.

Agradeço a todos os companheiros do Lemag pelo ótimo relacionamento no laboratório. Principalmente ao Marcelo Brazão pela parceria nesta caminhada.

Ao Felipe por anos de amizade, e por ter me iniciado no caminho da pesquisa.

Aos meus pais Pedro Sousa e Valquíria Braga, por todo amor, carinho e afeto que compartilhamos, por toda a base familiar, apoio e ensinamentos que são o pilar da minha formação pessoal e intelectual.

A minha irmã Priscila, minha sobrinha Jéssika e meu sobrinho Pedro por todo amor e carinho que sentimos.

A Hellen Pompeu por ter sido uma grande esposa e companheira, que esteve ao meu lado, apoiando e incentivando durante a maior parte deste trabalho.

A Isabelle Silva por todo carinho, incentivo, apoio e amor que compartilhamos durante o último ano deste trabalho.

A todas as pessoas que contribuíram de maneira direta ou indireta para a realização deste trabalho.

Lista de Siglas

ABC	<i>Absorbing Boundary Conditions</i>
CLDM	<i>Coulomb's Law Discretization Method</i>
CPML	<i>Convolutional Perfectly Matched Layer</i>
DR	<i>Desvio Relativo</i>
ECGGM	<i>Electric Charge Gaussian Gradation Method</i>
FDM	<i>Finite Difference Method</i>
FDTD	<i>Finite-Difference Time-Domain</i>
FEFD	<i>Finite Element Frequency Domain</i>
FEM	<i>Finite Element Method</i>
IE	<i>Integral Equations</i>
LJDM	<i>Lennard-Jones Discretization Method</i>
LSFCM	<i>Local Shape Factor Calibration Method</i>
MDR	<i>Máximo Desvio Relativo</i>
MER	<i>Máximo Erro Relativo</i>
MoM	<i>Methods of Moments</i>
PEC	<i>Perfect Electrical Conductor</i>
PO	<i>physical optics</i>
RCS	<i>Radar Cross Section</i>
RDMQ	<i>Raiz do Desvio Médio Quadrático</i>
REMQ	<i>Raiz do Erro Médio Quadrático</i>
RNA	<i>Arranjo Nodal de Referência</i>
RPIM	<i>Radial Point Interpolation Method</i>
TMz	<i>Transversal Magnético z</i>
UPML	<i>Uniaxial Perfectly Matched Layer</i>

Lista de Símbolos

Ω e Ω_a	Domínio de Análise
Ω_S	Domínio de Suporte
Ω_{SR}	Domínio de Suporte para o Método RPIM
Ω_{SC}	Domínio de Suporte para o Método CLDM
Ω_{SL}	Domínio de Suporte para o Método LJDM
\bar{x} e \bar{x}_i	Elemento do Conjunto V
$f(\bar{x})$	Função Exata
$f^a(\bar{x})$	Função Aproximada de $f(\bar{x})$
Φ	Função de Forma
$B_i(\bar{x})$	Função de Base
$R_i(\bar{x})$	Função de Base Radial
$P_i(\bar{x})$	Função de Polinomial
c	Fator de Forma
Err^a	Erro de Aproximação
$Err^{a\%}$	Erro Percentual de Aproximação
$Err_{\partial x}^a$ e $Err_{\partial y}^a$	Erro de Aproximação para as Derivadas Parciais
$u(r_{ij})$	Potencial de Lennard-Jones
\vec{F} ou \vec{F}^L	Vetor Força de Lennard-Jones
\vec{F}^C	Vetor Força de Coulomb
\vec{F}^A	Vetor Força Intramolecular
\vec{F}^E	Vetor Força Intermolecular
r_0	Distância entre átomos onde $\vec{F}^L = 0$
a	Átomos (Partículas Atômicas)

Rb	Região de Borda
Υ	Fator Multiplicado para Força de Coulomb
\vec{E}	Vetor Intensidade de Campo Elétrico
\vec{H}	Vetor Intensidade de Campo Magnético
\vec{D}	Densidade de Fluxo Elétrico
\vec{B}	Densidade de Fluxo Magnético
ϵ_o	Permissividade Elétrica do Vácuo
μ_o	Permeabilidade Magnética do Vácuo
ϵ	Permissividade Elétrica
μ	Permeabilidade Magnética
σ	Condutividade Elétrica
σ_α	Condutividades para UPML
t	Tempo
x, y e z	Coordenadas do Sistema Cartesiano
E_x, E_y e E_z	Componente do Campo Elétrico
H_x, H_y e H_z	Componentes do Campo Magnético
$\frac{df}{d\alpha}$	Derivada de f em relação a α
$\frac{\partial f}{\partial \alpha}$	Derivada Parcial de f em relação a α
(i, j)	Endereçamento no Espaço Discretizado
N_t	Índice Temporal
C_0	Velocidade da Luz no Vácuo: $2,99792 \times 10^8$ m/s
$\Delta_{\bar{x}min}, \Delta_x$ e Δ_y	Incrementos Espaciais
Δ_{dp}	Incrementos Espaciais para Deslocamento Progressivo
δ_{dp}	Fator do Deslocamento Progressivo
Δ_t	Incremento Temporal

A_{α}^n	Componente α de \vec{A} discretizada no instante n
$\vec{\nabla} \times \vec{A}$	Rotacional de \vec{A}
$p(t)$	Sinal de Excitação
A_p	Amplitude do Sinal de Excitação
τ	Parâmetro Relativo à Largura Temporal do Pulso Monociclo Gaussiano
t_0	Instante do Centro do Pulso Monociclo Gaussiano
f_r	Frequência Referencial para o Cálculo do RCS _{2-D}
bw	Largura de banda definida para o pulso Monociclo Gaussiano
ξ_R	Erro Relativo
ξ_{MER}	Máximo Erro Relativo
ξ_{REMQ}	Raiz do Erro Médio Quadrático
ξ_{DR}	Desvio Relativo
ξ_{MDR}	Máximo Desvio Relativo
ξ_{RDMQ}	Raiz do Desvio Médio Quadrático

Sumário

1	Introdução	1
1.1	Objetivo	8
1.2	Estrutura do Trabalho	9
2	Metodologia	10
2.1	Qualidade da Discretização Espacial para Métodos <i>Meshless</i>	12
2.2	Metodologia Proposta	15
3	Artigo 1 - <i>Coulomb's Law Discretization Method: a New Methodology of Spatial Discretization for the Radial Point Interpolation Method</i>	18
4	Artigo 2 - <i>Electric Charge Gaussian Gradation Method (ECGGM): a technique for improving material interface representations for the radial point interpolation method</i>	36
5	Artigo 3 - <i>A Meshless Discretization Methodology Based on Lennard-Jones Forces</i>	50
6	Aplicação do método LJDM na geração de domínios tridimensionais	55
6.1	RPIM aplicado nas equações de Maxwell 3D	55
6.2	Caso 1 - ressonador condutor perfeito na forma de um quarto de anel 3D .	57
7	Considerações Finais e Propostas para Trabalhos Futuros	65

Lista de Figuras

2.1	Discretização espacial para um dado domínio da análise, que possui duas regiões distintas, sendo que uma das regiões está contida na outra. a) Espaço de análise a ser discretizado, b) discretização com malha estruturada, c) discretização com malha não-estruturada, d) discretização sem malha (<i>meshless</i>).	11
2.2	Qualidade da variação direcional da distância entre nós. a) Variação direcional uniforme, b) Variação direcional não uniforme.	13
2.3	Qualidade da representação dos contornos das interfaces entre regiões. a) Interface entre regiões com contorno circular, b) Representação da interface usando malha estruturada retangular, d) Representação da interface através de discretização <i>meshless</i> (usando o esquema de representação por partículas fixas).	13
2.4	Qualidade da conformidade. Notar a transição suave entre geometrias (circulares e retangulares).	14
2.5	Qualidade da uniformidade do domínio de suporte $\Omega_S(\bar{x}_i)$ relativo ao nó \bar{x}_i . a) Domínio de suporte uniforme, b) Domínio de suporte não uniforme.	14
2.6	Conjunto de nós e células: (a) Domínio Preliminar Ω_P distribuído com base no arranjo nodal de referencia (RNA) usados para o LJDM e (b) Malha baseada na célula de Yee.	14
6.1	Representação do ressonador condutor perfeito na forma de um quarto de anel 3D. a) seção transversal no plano-xy e b) Projecção tridimensional (3D).	57

6.2	Sinal de excitação com largura de banda igual a $bw \approx 4\text{GHz}$ e a frequência máxima de $f_{\text{max}} = 5\text{GHz}$. a) Sinal gaussiano modulado no domínio do tempo, b) Espectro de frequência do sinal gaussiano modulado.	58
6.3	Discretização espacial na região próxima ao ressonador obtida após 65 iterações do método LJDM para $\delta_{\text{dp}} = 0.25$. a) Seção transversal no plano-xy, b) Visão 3D (tridimensional).	60
6.4	Distribuição da componente E_z total, seção transversal no plano-xy em $z = 0.005$. a) $t = 0.58\text{ns}$, b) $t = 0.96\text{ns}$, c) $t = 1.34\text{ns}$, d) $t = 1.93\text{ns}$, f) $t = 3.27\text{ns}$, g) $t = 4.91\text{ns}$	62
6.5	Comparação dos resultados no domínio da frequência para os métodos RPIM (com LJDM), RPIM (distribuição retangular), FDTD e solução de referência.	63

Lista de Tabelas

6.1	Parâmetros de simulação	61
-----	-----------------------------------	----

Resumo

Neste trabalho, três novos métodos de interação entre partículas baseados na lei de Coulomb e potencial de Lennard-Jones foram desenvolvidos e computacionalmente implementados visando gerar discretização espacial totalmente *meshless* que possa ser aplicada ao *Radial Point Interpolation Method* (RPIM) na solução de equações diferenciais parciais. Estes novos métodos, chamados de *Coulomb Law Discretization Method* (CLDM), *Electric Charge Gaussian Gradation Method* (ECGGM) e *Lennard-Jones Discretization Method* (LJDM), empregam versões adaptadas de equações das forças vetoriais de Coulomb e Lennard-Jones para obter uma distribuição equilibrada de nós no espaço (estado de equilíbrio), com o intuito de alcançar alta qualidade na discretização espacial de estruturas complexas. Para este objetivo, uma nova métrica de qualidade é introduzida. O trabalho está apresentado na forma de agregação de três artigos científicos, os quais apresentam respectivamente os métodos: CLDM, ECGGM e LJDM. Os métodos RPIM e UPML (*Uniaxial Perfectly Matched Layers*) são usados para resolver as equações de Maxwell no domínio do tempo para problemas 2D (modo TMz) e 3D. Os métodos CLDM, ECGGM e LJDM (cada um em conjunto com o método RPIM), são aplicados em problemas de espalhamento eletromagnético, com base em cilindros metálicos circulares, elípticos e triangulares (caso 2D). Para o caso 3D é aplicado o método LJDM/RPIM. Os resultados obtidos estão de acordo com soluções analíticas.

Palavras-chave: Discretização Sem Malha (*Meshless discretization*), RPIM, Lei de Coulomb, Gradação Gaussiana, Potencial de Lennard-Jones, Dinâmica Molecular, equações de Maxwell.

Abstract

In this thesis, three new particle interaction methods based on the Coulomb's and Lennard-Jones' potentials have been developed (and computationally implemented), aiming to generate meshless spatial discretization which can be used to the Radial Point Interpolation Method (RPIM) for solving partial differential equations. These new methods, called Coulomb Law Discretization Method (CLDM), Electric Charge Gaussian Gradation Method (ECGGM) e Lennard-Jones Discretization Method (LJDM), employ adapted versions of Coulomb's and Lennard-Jones' vector forces equations for obtaining a balanced distribution of nodes in space (equilibrium state), in order to achieve high discretization quality of space and complex structures. For this aim, a new quality metrics is introduced. This doctoral thesis is presented as an aggregation of three scientific papers, which present respectively the methods: CLDM, ECGGM and LJDM. The RPIM and the uniaxial perfectly matched layers (UPML) are used for solving Maxwell's equations in time domain for 2D (TMz mode) and 3D problems. The CLDM, ECGGM and LJDM methods (each in conjunction with the RPIM method) are applied to electromagnetic scattering problems, based on circular, elliptic and triangular metal cylinders (2D case). The LJDM / RPIM method is applied to the 3D case. The obtained results are in accordance with analytical solutions.

Key words: Meshless Discretization, RPIM, Coulomb's Law, Gaussian Gradation, Lennard-Jones Potential, Molecular Dynamics, Maxwell's equations.

Capítulo 1

Introdução

O ser humano, durante toda sua evolução, tem desenvolvido diversas formas de entender o espaço-tempo e os fenômenos ao seu redor. Atualmente, as tecnologias computacionais vêm evoluindo exponencialmente, possibilitando ao ser humano representar e simular o universo à sua volta, utilizando métodos computacionais cada dia mais precisos.

Basicamente, os métodos computacionais são um conjunto de ferramentas, técnicas, algoritmos e formulações, utilizados para obter solução computacional de fenômenos físicos onde uma abordagem analítica é extremamente complexa ou impossível [1]. Na área de engenharia voltada para estudos de fenômenos eletromagnéticos regidos pelas equações de Maxwell [2], os métodos computacionais mais utilizados para resolver estas equações são os baseados no *Finite-Difference Method* (FDM) [3, 4] e no *Finite Element Method* (FEM) [5, 6, 7], ambos considerados métodos tradicionais e utilizam discretização espacial que representa um domínio (e objetos nele inseridos) através de malhas computacionais.

Apesar de serem métodos robustos e bastante estudados, os métodos tradicionais possuem problemas relacionados à representação de formas geométricas complexas (não Cartesianas) [8]. Por este motivo, uma nova abordagem conhecida como métodos *meshless*, vem sendo utilizada de forma expressiva, uma vez que permitem representação numérica precisa de geometrias não-retangulares, sem necessidade de malhas para resolver equações diferenciais parciais [9].

Os métodos *meshless* surgem em 1977 com o *Smooth Particle Hydrodynamics* (SPH) [10], primeiro método sem malha formulado para resolver problemas astrofísicos, e em

seguida, diversos outros métodos foram propostos como resultado de várias melhorias do método SPH. Em 1998, é publicado o *Meshless Local Petrov-Galerkin* (MLPG) [11], considerado o primeiro método verdadeiramente sem malha, pois sua formulação evita a utilização de *grid*.

Posteriormente, baseados no método MLPG, Liu e Gu desenvolvem o *Point Interpolation Method* (PIM) [12] e, em 2000, Wang e Liu propõem o *Radial PIM* (RPIM) [13], um método baseado no PIM e em funções de base radial. Em 2009, RPIM foi aplicado para resolver as equações de Maxwell em três dimensões [14].

Em 2011, Machado e Oliveira et al. publicaram um novo método, chamado *Local Shape Factor Calibration Method* (LSFCM) [15], para melhorar a precisão numérica de interpolações do método RPIM, calculando fatores de forma otimizados para cada domínio de suporte. Os métodos sem malha são assim chamados porque o espaço de análise é discretizado por intermédio de um grupo de nós (domínio Ω) [16], onde não existe um esquema predefinido, elemento (como em FEM) ou formações celulares (como no *Finite-Difference Time-Domain Method* - FDTD) [4].

A influência que os nós em Ω exercem entre si é dada usando subconjuntos de nós vizinhos (os domínios de suporte, indicados por $\Omega_{SR}(\bar{x})$) [13] para cada nó $\bar{x} \in \Omega$. Desta forma, os problemas complicados relacionados à malha, deixam de existir. No entanto, a distribuição dos pontos precisa ser tal que garanta a representatividade de todo o domínio, o que exige métodos criteriosos de discretização espacial.

A abordagem mais utilizada para método *meshless* é a discretização por métodos tradicionais baseados na triangulação de Delaunay [17] ou no diagrama de Voronoi [18]. Neste tipo de discretização, é gerada uma malha não estruturada de boa qualidade que serve apenas como guia para a distribuição dos nós no domínio. A popularidade desta abordagem dá-se pela grande utilização do método FEM e a variedade de ferramentas existentes, que geralmente são comerciais.

Durante o período das atividades relacionadas a este projeto de doutorado em engenharia elétrica, foram desenvolvidos três novos métodos de discretização espacial totalmente *meshless* baseados nos conceitos físicos de interação entre partículas para gerar domínios que possam ser utilizados por métodos *meshless* (mais especificamente o método RPIM)

na solução de equações diferenciais parciais.

Para garantir resultados satisfatórios do método RPIM aplicado a problemas eletromagnéticos, é importante que os três métodos desenvolvido neste trabalho consigam gerar discretização espacial totalmente *meshless*, que:

- seja conformal, ou melhor, represente de forma precisa objetos não retangulares e favoreça a geração de um conjunto de nós (domínio) com transições suaves nos espaços que circunda objetos geometricamente diferentes.
- represente adequadamente toda a região de análise, mantendo elevada qualidade da discretização espacial *meshless*;
- consiga reduzir os problemas relacionados às variações espaciais significativas do campo eletromagnético próximo dos cantos e bordas (interfaces entre materiais) dos espalhadores imersos na região de análise, sem necessitar aumentar a resolução da discretização espacial (densidade de nós do domínio) em todo espaço de análise.
- consiga preservar o arranjo nodal de referência (RNA) em todo o domínio Ω ; Para realizar os cálculos relacionados à propagação do campo eletromagnético é necessário que em determinados pontos do domínio Ω seja calculado o campo elétrico (subconjunto de nós elétricos) e em outros seja calculado o campo magnético (subconjunto de nós magnéticos). O arranjo nodal de referência (RNA) é a configuração geométrica local que define as posições relativas entre os nós onde esses campos (elétrico e magnético) são calculados. Este arranjo nodal é concebido de forma a se calcular adequadamente o rotacional dos campos.

As pesquisas realizadas motivaram a publicação de três artigos científicos em periódicos da área. Estes artigos são listados a seguir, em ordem cronológica dos métodos desenvolvidos:

1. Artigo 1 - SOUSA, Washington C. B. ; DE OLIVEIRA, Rodrigo M. S. Coulomb's Law Discretization Method: a New Methodology of Spatial Discretization for the Radial Point Interpolation Method. IEEE Antennas & Propagation Magazine, v. 57, pp. 277-293, 2015. Classificação A2 no sistema QUALIS/CAPES;

2. Artigo 2 - DE OLIVEIRA, Rodrigo M. S. ; BRANDAO, M. B. S. ; SOUSA, W. C. B. Electric Charge Gaussian Gradation Method (ECGGM): a technique for improving material interface representations for the radial point interpolation method. International Journal of Numerical Modelling: Electronic Networks, Devices and Fields, DOI: 10.1002/jnm.2303, 2017. Classificação B1 no sistema QUALIS/CAPES;
3. Artigo 3 - DE OLIVEIRA, Rodrigo M. S. ; SOUSA, Washington C. B. ; RABELO, Wilson. A Meshless Discretization Methodology Based on Lennard-Jones Forces. IEEE Antennas and Wireless Propagation Letters, v. 16, pp. 1492-1495, 2017. Classificação A1 no sistema QUALIS/CAPES.

O artigo 1 introduz um simples e eficaz método autoadaptativo de discretização espacial *meshless* chamado *Coulomb's Law Discretization Method* (CLDM), o qual se baseia na dinâmica analítica da lei de Coulomb para gerar a distribuição dos nós nos domínios que possam ser usados pelo método RPIM na solução de equações diferenciais parciais.

Esse método não está associado a qualquer técnica tradicional que use malha (conhecida pelos autores) e, sendo assim, pode ser considerado um método discretização espacial completamente *meshless*. Além disso, neste artigo é introduzida uma métrica para avaliação da qualidade da discretização espacial *meshless*, que usa diretamente o RPIM.

A ideia principal do CLDM é utilizar a repulsão entre partículas carregadas (cargas com sinais iguais) para obter domínios (distribuição de nós) que sejam capazes de representar (adequadamente) regiões de análise formadas por estruturas complexas, mantendo o estado de equilíbrio do sistema e garantindo assim a elevada qualidade na discretização espacial dos domínios gerados.

Por ser baseado em forças repulsivas, o CLDM acaba produzindo um conjunto de nós Ω que se comporta como uma nuvem de elétrons. Este sistema físico favorece a discretização espacial conformal *meshless*, ou seja, favorece a geração de um conjunto de nós com transições suaves nos espaços que envolvem objetos geometricamente diferentes. Porém, não favorece automaticamente a manutenção de um nível aceitável de preservação do arranjo nodal de referência (RNA), o qual é a configuração geométrica local que define as posições relativas entre os nós onde campos elétrico e magnético são calculados. Esta

possibilidade de modificação drástica do RNA gera dificuldade na convergência do método CLDM resultando em problemas na definição de um critério de parada.

A implementação deste método teve início no projeto de mestrado desenvolvido pelo autor desta tese e finalizou no primeiro ano deste projeto de doutorado resultando no artigo 1. Sua versão final contém correções em relação à descrita na dissertação [19], as quais diferenciam substancialmente o método apresentado na dissertação para o descrito no artigo 1. As correções mais significativas podem ser vistas nas equações (15) a (23), na seção 3 (*The Coulomb's Law Discretization Method* - CLDM) do artigo 1.

O artigo 2 introduz o *Electric Charge Gaussian Gradation Method* (ECGGM), um novo método de discretização espacial que utiliza funções Gaussianas para aprimorar o CLDM, possibilitando o aumento (de forma natural e controlável) da densidade de nós do domínio, nas regiões próximas às bordas e cantos das formas geométricas (espalhadores metálicos) imersos na região de análise.

A discretização do espaço de análise realizada pelo método CLDM é baseada na ideia da repulsão entre cargas levando em consideração que é atribuído um valor único (e global) de carga elétrica para todos os nós pertencentes ao domínio Ω (usado na discretização espacial *meshless*).

Inicialmente, no CLDM, os nós do conjunto usado na discretização espacial são posicionados usando um arranjo nodal de referência (RNA) baseado em uma malha FDTD. Posteriormente, os nós mais próximos das interfaces entre regiões vizinhas são movidos para as interfaces entre materiais. Por fim, os nós que não foram colocados nas interfaces entre regiões são reposicionados no espaço sucessivamente ao longo do tempo, aplicando um processo iterativo que usa a segunda lei do movimento de Newton excitada pelas resultantes das forças eletrostáticas de Coulomb. Com este processo, o CLDM é capaz de produzir domínios com discretização espacial conformal, que podem ser usados para realizar análises completas de propagação eletromagnética usando as equações discretizadas de Maxwell com RPIM.

Conforme detalhado no capítulo 11 de Taflove e Hagness [4], observam-se variações espaciais substanciais de campos eletromagnéticos próximos dos cantos e bordas de objetos na região de análise. Para resolver esse problema usando CLDM e RPIM, seria necessário

aumentar a resolução da discretização espaciais em todo espaço de análise numérico.

Neste trabalho, desenvolveu-se pela primeira vez uma técnica de discretização espacial *meshless* que possibilita transições graduais dos níveis de discretização para uma dada região de análise. Essas transições dos níveis de discretização são realizadas externamente aos espalhadores metálicos imersos na região de interesse, de tal forma que a densidade do domínio é gradualmente reduzida a partir dos limites desses espalhadores (onde há uma distribuição mais refinada dos nós) para os seus espaços circundantes (onde a distribuição menos densa dos nós é formada). É possível implementar este efeito no CLDM usando uma transição gradual da magnitude da carga elétrica dos nós próximos das interfaces entre material. A transição suave de cargas proposta é baseada em uma distribuição gaussiana espacial centrada nas interfaces entre materiais para sua vizinhança externa imediata.

O método ECGGM (em conjunto com RPIM) produz melhora substancial nos resultados obtidos pelos CLDM/RPIM, porque a densidade de nós pode ser aumentada somente para regiões onde o campo eletromagnético apresenta grandes variações no espaço. Sendo assim, esse método apresenta duas vantagens principais sobre o CLDM: 1º - precisão de cálculo aprimorada para RPIM (Máximo Erro Relativo - MRE de cerca de 5% em relação às soluções analíticas) e 2º - aumento do nível de discretização (número de nós) apenas perto das interfaces, evitando alta densidade de nós em toda a região de análise, reduzindo o tempo de cálculo e os requisitos de memória para RPIM e CLDM para um determinado nível de precisão.

E finalmente, no artigo 3, um terceiro método baseado na física de interação entre partículas (dinâmica molecular) regida pelo potencial de Lennard-Jones, foi desenvolvido e implementado computacionalmente para a geração de discretização espacial *meshless*.

A nova metodologia, denominada *Lennard-Jones Discretization Method* (LJDM), emprega uma versão adaptada da equação de força vetorial de Lennard-Jones (LJ) para a obtenção de discretização espacial conformal de alta qualidade e elevada manutenção do arranjo nodal de referência (RNA), gerando domínios (mais próximos do estado de equilíbrio) com alta representatividade das regiões de análise.

Como visto anteriormente no método CLDM, pode-se usar a repulsão entre cargas

para gerar uma distribuição equilibrada de nós no espaço (estado de equilíbrio), pois quando submetido apenas a forças repulsivas, o conjunto de nós Ω se comporta como uma nuvem de elétrons, o que favorece a discretização espacial conformal *meshless*. Porém, o método não garante a manutenção do RNA, gerando problemas para calcular o operador rotacional.

Ajustes manuais dos parâmetros durante o processo de discretização usando CLDM podem ajudar a manter o RNA. Porém, este processo é realizado de forma não determinista (e depende subjetivamente da experiência de usuário). Mesmo assim, sem o ajuste periódico desses parâmetros, podem ocorrer instabilidades locais de RNA após certa quantidade de iterações do método CLDM, tornando difícil a definição precisa de um critério de parada.

O LJDM surge com o objetivo de ser um método de discretização espacial *meshless* melhorado, baseado no potencial de Lennard-Jones (LJ), o qual pode representar sistema de partícula no estado sólido, líquido ou gasoso. A força atrativa do potencial LJ atua na ligação entre partículas (pode ser usada para colocar o sistema nos estados sólido ou líquido) e a parcela repulsiva impede o colapso, preservando assim o RNA.

Neste trabalho, a parte repulsiva da força de LJ impede que as partículas (nós em Ω) fiquem muito próximas, enquanto a contribuição atrativa impede automaticamente a quebrar o RNA. Estas duas partes trabalham juntas para garantir uma conexão estável entre as partículas (nós) em Ω e para produzir discretização espacial *meshless* conformal. Sendo assim, o método LJDM pode ser visto como uma melhoria do CLDM.

Em todos os artigos, os métodos RPIM e UPML (*Uniaxial Perfectly Matched Layers*) são usados para resolver equações de Maxwell no domínio do tempo para problemas 2D (modo TMz). Os métodos CLDM, ECGGM e LJDM (cada um em conjunto com o método RPIM), são aplicados em problemas de espalhamento eletromagnético, com base em estruturas geométricas 2D (bidimensionais). Os resultados obtidos estão em conformidade com soluções analíticas.

Esta tese de doutorado foi baseada na agregação dos três artigos científicos em questão e no caso de validação do método LJDM aplicado a problemas de propagação eletromagnética no espaço tridimensional (3D).

1.1 Objetivo

O objetivo principal deste trabalho foi propor e implementar três novos métodos de discretização espacial totalmente *meshless*. Estes métodos utilizam conceitos físicos de interação entre partículas para gerar a domínios (distribuição dos nós) que represente adequadamente toda uma região de análise. Os domínios gerados podem ser usados pelo método RPIM associado às equações de Maxwell, para solucionar problemas de propagação eletromagnética.

De forma mais específica, estes três métodos aplicam os efeitos associados às forças vetoriais que atuam em sistemas de partículas específicos, para gerar discretização espacial que não possua associação com métodos tradicionais, ou seja, totalmente *meshless*.

Os objetivos específicos deste trabalho são:

- Gerar discretização espacial *meshless* conformal que consiga representar adequadamente toda uma região de interesse, representando-se de forma adequada objetos com geometria não compatível com o sistema Cartesiano de coordenadas.
- Garantir elevados níveis da qualidade da discretização e uma métrica associada ao método RPIM para avaliação desta qualidade.
- Resolver problemas relacionados às variações espaciais substanciais do campo eletromagnético próximo dos cantos e bordas dos espalhadores metálicos imersos na região de análise, sem necessidade de aumentar a resolução da discretização espacial em todo espaço de análise.
- Gerar discretização espacial *meshless* que consiga preservar o arranjo nodal de referência (RNA) para o domínio Ω final.
- Definir um critério de parada para os métodos propostos neste trabalho.
- Aplicar o método LJDM a problemas de propagação eletromagnética no espaço tridimensional 3D.

1.2 Estrutura do Trabalho

Esta tese de doutorado foi baseada na agregação dos três artigos científicos apresentados anteriormente e sua estrutura foi dividida em 7 capítulos, de modo a facilitar o entendimento das pesquisas realizadas.

- Capítulo 1 (Introdução): este capítulo possui a introdução geral do trabalho, a apresentação e descrição dos artigos científicos agregados, o objetivo geral e os objetivos específicos que nortearam as pesquisas desenvolvidas e a estrutura do trabalho;
- Capítulo 2 (Metodologia): neste capítulo, são descritas de forma resumida as bases teóricas gerais e específicas que nortearam o desenvolvimento de cada método presente neste trabalho. Maiores detalhes podem ser conferidos nos artigos científicos anexados.
- Nos Capítulos 3, 4 e 5 estão apresentados na íntegra e respectivamente os artigos: "Artigo 1 - *Coulomb's Law Discretization Method: a New Methodology of Spatial Discretization for the Radial Point Interpolation Method*", "Artigo 2 - *Electric Charge Gaussian Gradation Method (ECGGM): a technique for improving material interface representations for the radial point interpolation method*" e "Artigo 3 - *A Meshless Discretization Methodology Based on Lennard-Jones Forces*".
- Capítulo 6 (Aplicação do método LJDM na geração de domínios tridimensionais) - este capítulo trata do caso de validação 3D (tridimensional) baseado no problema de propagação eletromagnética dentro de uma cavidade metálica no formato de um quarto ($1/4$) de anel. Este caso de validação serve para avaliar a aplicação do método LJDM na geração de domínios tridimensionais. Os resultados obtidos são comparados com solução disponível na literatura e com resultado gerado via FDTD, com o intuito de identificar vantagens do método LJDM.
- Capítulo 7 (Considerações finais): o capítulo final expõe as considerações finais e propostas para trabalhos futuros.

Capítulo 2

Metodologia

Os métodos de discretização do espaço geram pontos (nós) que representam um região de análise (Fig.2.1(a)) a partir de um conjunto finito de elementos com dimensionamento controlado, de tal forma que não haja superposição nem espaçamento entre os elementos [20]. Estes métodos podem ser classificados segundo a existência ou não de malha [21].

A malha é uma estrutura que segue um padrão pré-estabelecido e serve para definir uma relação de dependência ou conectividade entre os nós. Ela é a base para a formulação dos métodos numéricos convencionais. Existem dois tipos básicos de malhas: as estruturadas e as não-estruturadas.

A malha do tipo estruturada, Fig.2.1(b), é também conhecida como grade ou *grid*, pois os nós são ordenados pela grade de forma sistemática. A determinação dos nós vizinhos para cada nó da malha é bem simples, dada sua ordenação. Entretanto, esta malha não se adapta bem a problemas com geometrias curvas ou até mesmo retas e planos inclinados. Este tipo de malha é usado pelo método de diferenças finitas (FDM).

Já a malha não-estruturada, Fig.2.1(c), é um tipo de malha composta por elementos que podem assumir formas geométricas diversas, sendo capaz de se ajustar bem a geometrias complexas com inclinações e discretizar curvas em um conjunto de segmentos ou planos. Normalmente, são utilizadas formas triangulares para definir os elementos em problemas bidimensionais (Fig.2.1(c)) e formas tetraédricas para os tridimensionais. Sendo assim, este tipo de malha é muito usada pelo método de elementos finito (FEM). Ressalta-se que a malha não-estruturada não pode ser representada por uma matriz sim-

ples (tal como a estruturada) e que o método das diferenças finitas pode ser adaptado para malhas não estruturadas [4]. A discretização por malha não-estruturada é um método robusto e amplamente usado na solução de problemas eletromagnéticos, mas possui limitações na geração de um grupo de nós que represente bem o problema e para que seja numericamente de boa qualidade e não é adequada para tratar problemas no domínio do tempo [4].

Existem outros métodos além dos convencionas, chamados de sem malha (*meshless*). Esses métodos são considerados independentes de malhas, pois a discretização do espaço é feita através de um conjunto de nós espalhados sobre o domínio do problema [22], Fig.2.1(d), e não necessitam diretamente de informações sobre conectividade para interpolações de variáveis de campo. A ausência de conectividade torna fácil a resolução de alguns problemas relacionadas aos métodos com malhas. No entanto, a falta de malha introduz outras dificuldades. Para os métodos sem malha, as relações entre os nós são determinadas a partir da análise da vizinhança de cada um dos nós. Para um nó \bar{x}_i qualquer, a vizinhança é normalmente uma região circular centrada no nó \bar{x}_i e o conjunto de nós que pertence a esta vizinhança é comumente chamado de domínio de suporte $\Omega_{SC}(\bar{x}_i)$ (ou, $\Omega_{SL}(\bar{x}_i)$).

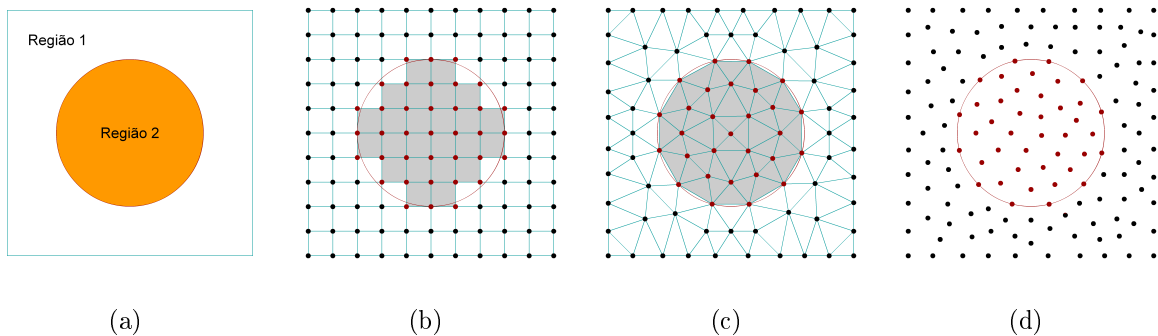


Figura 2.1: Discretização espacial para um dado domínio da análise, que possui duas regiões distintas, sendo que uma das regiões está contida na outra. a) Espaço de análise a ser discretizado, b) discretização com malha estruturada, c) discretização com malha não-estruturada, d) discretização sem malha (*meshless*).

2.1 Qualidade da Discretização Espacial para Métodos

Meshless

A qualidade da discretização espacial afeta a precisão dos resultados numéricos. A principal dificuldade, na geração de uma discretização espacial de alta qualidade, está associada a um conjunto de parâmetros que definem a qualidade numérica da discretização. Para os métodos sem malha *meshless*, os parâmetros que definem a qualidade da discretização espacial são [21, 22, 15]:

- Variação direcional controlada da distância entre os nós (espaçamento uniforme): as distâncias entre os nós devem ser aproximadamente iguais para todas as direções (Fig.2.2). Neste trabalho, esta condição é conseguida através da minimização da energia potencial entre partículas (átomos ou moléculas).
- Representação precisa dos contornos: para os problemas que envolvem regiões as quais possuem diferentes materiais, as geometrias das interfaces entre as regiões devem ser respeitadas. Um conjunto de nós fixos (partículas fixas) é usado para representar os contornos das interfaces (Fig.2.3).
- Conformidade: a distribuição de nós deve favorecer transições suaves entre as diferentes geometrias (Fig.2.4), as quais normalmente fazem parte do espaço livre discretizado. Nota-se que este requisito também é compatível com o princípio da energia potencial mínima.
- Uniformidade da distribuição de nós em $\Omega_{SC}(\bar{x}_i)$ (Fig.2.5): para (cada) domínio de suporte $\Omega_{SC}(\bar{x}_i)$ pertencente a Ω , a densidade de nós deve ser conservada em seu domínio espacial (em torno de \bar{x}_i). Isto é muito importante, para calcular corretamente a interpolação de funções em Ω_C [15].
- Preservação do arranjo nodal de referência (RNA): Um domínio Ω usado na solução de problemas eletromagnéticos, pode ser definido como um conjunto de dois subdomínios, um no qual será calculado o campo elétrico e no outro o campo magnético. Os nós pertencentes a cada um desses subdomínios são chamados de elétricos e

magnéticos, respectivamente. Esses dois subdomínios estão conectados entre si, com base no arranjo nodal de referencia (RNA), que é a configuração geométrica local que define as posições relativas entre os nós elétricos e magnéticos, Fig.2.6. O RNA é importante, pois garante a característica rotacional do campo eletromagnético no espaço.

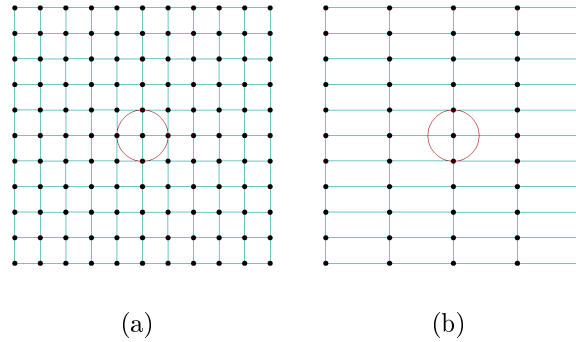


Figura 2.2: Qualidade da variação direcional da distância entre nós. a) Variação direcional uniforme, b) Variação direcional não uniforme.

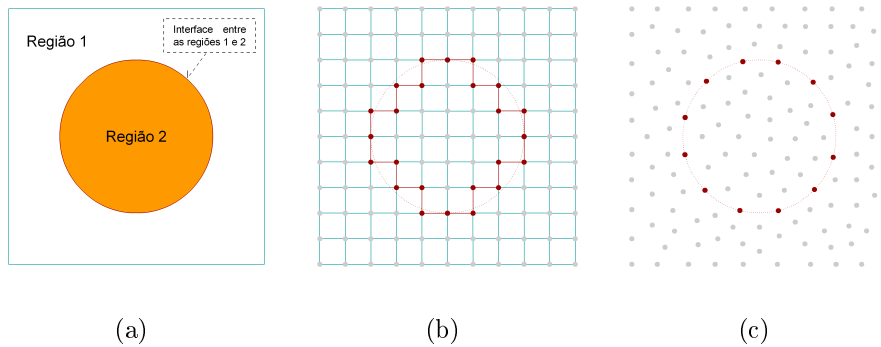


Figura 2.3: Qualidade da representação dos contornos das interfaces entre regiões. a) Interface entre regiões com contorno circular, b) Representação da interface usando malha estruturada retangular, d) Representação da interface através de discretização *meshless* (usando o esquema de representação por partículas fixas).

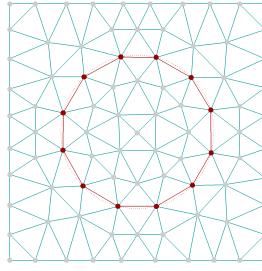


Figura 2.4: Qualidade da conformidade. Notar a transição suave entre geometrias (circulares e retangulares).

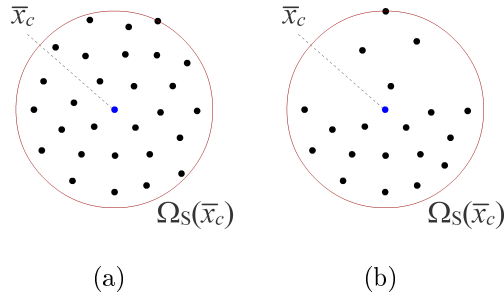


Figura 2.5: Qualidade da uniformidade do domínio de suporte $\Omega_S(\bar{x}_i)$ relativo ao nó \bar{x}_i .
a) Domínio de suporte uniforme, b) Domínio de suporte não uniforme.

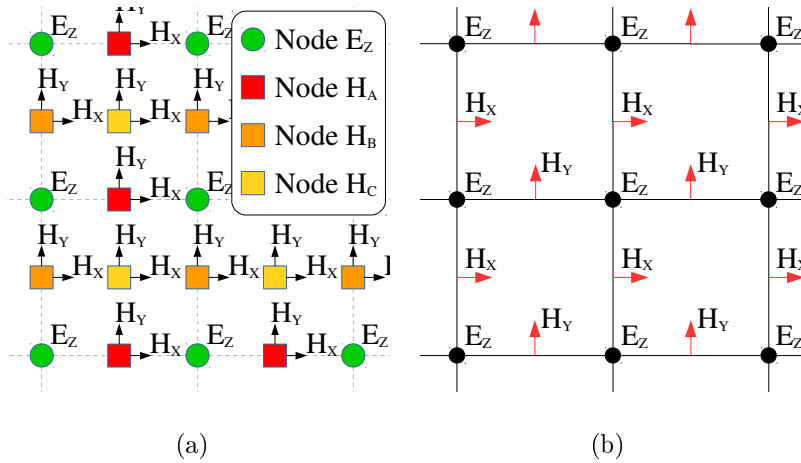


Figura 2.6: Conjunto de nós e células: (a) Domínio Preliminar Ω_P distribuído com base no arranjo nodal de referencia (RNA) usados para o LJDM e (b) Malha baseada na célula de Yee.

2.2 Metodologia Proposta

De acordo com a literatura, a maioria das técnicas usadas para discretização espacial *meshless* são baseadas em procedimentos desenvolvidos inicialmente para os métodos tradicionais baseados em malhas [23, 24, 25].

Neste trabalho, são propostas três novas técnicas de discretização espacial puramente *meshless* baseada na física de interação entre partículas para gerar a distribuição do conjunto de nós de um dado domínio de análise, de forma a satisfazer todas as características de uma boa discretização espacial. A ideia principal é considerar cada nó do domínio de análise como uma partícula (carga ou átomo que compõe moléculas, dependendo do método a ser utilizado) e fazer com que eles interajam entre si de acordo com os conceitos da força vetorial que atua na dinâmica entre partículas (adotada por cada método especificamente), proporcionando os deslocamentos necessários para gerar a representação discreta ideal do espaço de análise.

Os conceitos newtonianos e numéricos abordados nas equações de (15) a (23) do artigo 1, podem ser aplicados para diversos tipos de forças e por este motivo são utilizados em todos os três métodos desta tese. O que diferencia cada método é principalmente a equação da força utilizada: os métodos CLDM e ECGGM utilizam a lei de Coulomb, enquanto que o método LJDM utiliza a força de Lennard-Jones. Sendo assim, considerando um conjunto de nós (partículas) móveis, no qual o princípio da mínima energia potencial total não é satisfeito para um instante de tempo T , cada partícula móvel (pertencente a Ω) interage com as outras, simultaneamente, com a finalidade de minimizar as forças resultantes que atuam sobre cada partícula.

A reprodução numérica desses princípios físicos pode ser utilizada com o intuito de obter representações espaciais discretas de elevada qualidade (com objetos complexos imersos no espaço de análise), de forma que as quais podem ser utilizadas na solução de equações diferenciais parciais com métodos *meshless*. De forma geral, para alcançar este objetivo, os três métodos propostos nesta tese possuem quatro etapas subsequentes:

1. Geração do domínio preliminar - nesta primeira etapa é criado um conjunto de nós que descreve a região de análise, distribuído com base em uma malha estruturada simples. Destaca-se que esta malha é usada apenas como uma referência inicial.

O domínio preliminar deve ser capaz de: garantir o equilíbrio molecular inicial, facilitar a identificação dos domínios de suporte, satisfazer alguns dos parâmetros da discretização espacial *meshless* (tais como a uniformidade dos domínios de suporte), garantir a eficiência dos métodos de truncagem espacial aplicados para as forças vetoriais utilizadas por cada método e para as equações de Maxwell com RPIM (tal como a UPML);

2. Definição dos domínios de suporte (especificamente para o processo de discretização)
 - A aplicação das forças vetoriais utilizadas pelos métodos desenvolvidos nesta tese em um domínio de análise (Ω_P) implica que cada nó \bar{x}_i em Ω_P comporta-se como uma partícula livre no espaço e recebe a influência de todos os outros nós pertencentes ao domínio total (Ω). A implementação deste processo se torna inviável para um domínio total (Ω) com uma grande quantidade de nós. Uma solução viável de otimização é aplicar a ideia de domínios de suporte (ou subdomínios) para cada nó em (Ω_P), o que só é possível devido ao fato de que as forças (de Coulomb e Lennard-Jones) utilizadas nos três métodos desenvolvidos neste trabalho são inversamente proporcionais a potências da distância.
3. Definição das interfaces entre os diferentes materiais - Os limites (interfaces) entre duas ou mais formas geométricas (compostas por materiais com características eletromagnéticas diferentes) pertencentes a região de análise, são representados no domínio por meio de um conjunto de nós fixos. Esta representação é feita deslocando os nós mais próximos de uma interface e fixando-os sobre a mesma. O deslocamento pode ser classificado como instantâneo ou progressivo. O deslocamento é instantâneo quando os nós são deslocados e fixados diretamente na interface logo na primeira iteração, de forma que este tipo de deslocamento foi usado pelo CLDM nos artigos 1 e 2. Já o deslocamento progressivo é um processo no qual a cada iteração do método os nós (mais próximos) sofrem um pequeno deslocado em direção à interface. Este deslocamento é feito de forma progressiva até que os nós alcancem a interface.
4. Reposicionamento iterativo de nós e avaliação da qualidade da discretização - A cada iteração, após o processo de deslocamentos, alguns nós livres próximos dos

nós movidos pelo deslocamento progressivo passam a estar fora de suas posições de equilíbrio entre forças, interferindo com a qualidade da discretização espacial. Nova configuração de equilíbrio entre forças pode ser obtido através da utilização de procedimento iterativo baseado na força vetorial de Coulomb (CLDM e ECGGM) ou Lennard-Jones (LJDM). Esta etapa realiza aplicações sucessivas da equação de movimento (21) do Artigo 1 sobre os nós (partículas) móveis do domínio Ω , com o intuito de fazer com que o sistema aproxime-se do estado mínimo de energia potencial, obtendo assim, uma distribuição espacial de nós com características compatíveis aos parâmetros que define a qualidade da discretização espacial *meshless*, apresentados na seção 2.1. Desta forma, os métodos de discretização espacial *meshless* propostos visam satisfazer o conjunto de critérios que definem a qualidade da discretização espacial. A cada iteração desta etapa é realizada a avaliação da qualidade da discretização e a métrica de avaliação desenvolvida está diretamente associada ao método RPIM. Verifica-se que distribuições de nós com elevada qualidade produzem estabilidade numérica e sistemas numéricos bem condicionados, como detalhado nos três artigos.

Os conceitos abordados aqui independem de paradigmas computacionais [26], de tal forma que o desenvolvimento computacional pode ser realizado utilizando qualquer linguagem computacional como *C++*, *Java*, *Fortran*, etc [27]. Para os resultados obtidos neste trabalho optou-se pela programação em linguagem *C++* [28], por ser uma linguagem robusta que possibilita a implementação de software com elevado nível de desempenho computacional, bastante difundida nos meios acadêmico e comercial. É neste contexto que a proposta deste trabalho surge.

A seguir serão apresentados, na íntegra, os três artigos científicos que foram publicados em periódicos de boa classificação CAPES ao longo dos anos do curso de doutorado em engenharia elétrica. Neles podem ser encontrados maiores detalhes a respeito de cada método desenvolvido em questão.

Capítulo 3

Artigo 1 - *Coulomb's Law Discretization*

Method: a New Methodology of Spatial

Discretization for the Radial Point

Interpolation Method

IEEE Antennas and Propagation Magazine, Vol. 57, No. 2, April 2015

QUALIS (CAPES): A2

Coulomb's Law Discretization Method: A New Methodology of Spatial Discretization for the Radial Point Interpolation Method

Washington César Braga de Sousa and Rodrigo Melo e Silva de Oliveira

Federal University of Pará (UFPA), Institute of Technology (ITEC),
Post-Graduation Course in Electrical Engineering (PPGEE), 66075-110 Belém-PA, Brazil
E-mails: csaksousa@gmail.com; rmso@ufpa.br

Abstract

In this paper, a new particle interaction method based on Coulomb's force law has been developed and computationally implemented for performing meshless spatial discretization. The new methodology, which is named Coulomb's Law Discretization Method (CLDM), employs an adapted version of the Coulomb's vector force equation for obtaining a balanced distribution of nodes in space (equilibrium state), in such a way to achieve high discretization quality of space and complex structures. For this aim, a new quality metrics is introduced. The radial point interpolation method (RPIM) and the uniaxial perfectly matched layers (UPML) are used for solving Maxwell's equations in time domain for 2D problems. The CLDM/RPIM methods are applied to electromagnetic scattering problems and for designing hybrid photonic band-gap filters, based on circular and triangular metallic cylinders. The obtained results are in accordance with analytical solutions.

Keywords: Coulomb's Law Discretization Method (CLDM); meshless discretization; coulomb's law; radial point interpolation method (RPIM); 2-D Maxwell's equations

1. Introduction

The importance of meshless (or mesh-free) methods has been expressively rising since they enable accurate numerical representation of nonrectangular geometries with no need of meshes for solving partial differential equations. These methods emerged in 1977 with the smooth particle hydrodynamics (SPH) [1], the first meshless method formulated to solve astrophysics problems. Thereafter, the following methods were proposed, i.e., reproduced kernel particle method [2] and corrected SPH [3], which presented several improvements over the SPH method. Subsequently, based on the meshless local Petrov–Galerkin (MLPG), Liu and Gu developed the point interpolation method (PIM) [4]. In 2000, Wang and Liu introduced the radial PIM (RPIM) [5], a method based on PIM and on radial basis functions. In 2009, RPIM was applied for solving Maxwell's equations in three dimensions [6]. In 2011, Machado *et al.* published a new method, which is called local shape factor calibration method (LSFCM) [7], for improving numerical precision of interpolations by calculating optimized shape factors for each support domain.

The meshless methods are so called because the analysis space is discretized by means of a node group (domain Ω) [8], where there is no predefined element schema (as in finite element method) [9–11] or cell formations [as in finite-difference time-domain (FDTD) method] [12]. The influence that nodes in Ω exert on each other is accounted by using subsets of neighboring nodes (the support domains, which are denoted by $\Omega_{SR}(\bar{x})$) [13] for each node $\bar{x} \in \Omega$. This way, the complicated problems related to meshing processes [9–11] cease to exist. A natural thought is that, for meshless methods, analysis domain can be represented by a set of randomly distributed nodes. This is true provided that discretization quality parameters are satisfied and the contours (relative to the problem) are represented accurately [14], requiring specialized methods of spatial discretization.

Nowadays, it seems that the most used discretization technique is unstructured meshing [6], in which the set of nodes is extracted from unstructured meshes. Other approaches have been developed [13, 15, 16], but the most notorious methods are based on Voronoi diagram [17] and Delaunay triangulation [14].

In this context, the main objective of this paper is to present a simple yet effective and autoadaptive meshless spatial discretization method based on analytical dynamics of Coulomb's force law to generate the node distribution for analysis domain

$\Omega_a \subseteq \Omega$. The proposed method is named Coulomb's Law Discretization Method (CLDM) in this paper, and it is not associated to any traditional meshing technique (known to authors). For this reason, it can be considered a completely meshless discretization approach. In addition, it is introduced a meshless discretization quality metrics, which is measured by using RPIM itself. In addition to being a meshless discretization method, CLDM is relatively simple to be computationally implemented.

This paper is organized as follows. Section 2 presents a review of RPIM's basic concepts and essential physical aspects related to Coulomb's law for the development of the proposed discretization technique, which is presented and discussed in Section 3; In Section 4, the new quality metrics for meshless discretization is introduced and a technique for improving the discretization quality is presented. Section 5 shows results obtained by using CLDM/RPIM, which are validated using analytical solutions and compared with numerical results produced with FDTD and CLDM/Delaunay; The numerical techniques proposed in this work are applied for designing PBG filters in Section 6; final remarks are provided in Section 7.

2. Theoretical Background

2.1 RPIM

The basic principle of meshless methods is to obtain an approximation $f^a(\bar{x})$ for a function of interest $f(\bar{x})$ for each node $\bar{x} \in \Omega$ [19] by using radial basis functions and samples $f_j(\bar{x})$ of $f(\bar{x})$ on neighbor nodes j around \bar{x} . In order to solve differential equations, approximations for derivatives of $f(\bar{x})$ are also of interest.

In general, the radial basis functions cannot shape every kind of function; thus, a polynomial basis is included [20]. This way, the approximation $f^a(\bar{x})$ may be defined as

$$f^a(\bar{x}) = \sum_{l=1}^n R_l(\bar{x})a_l + \sum_{j=1}^m P_j(\bar{x})b_j, \quad (1)$$

which can be written in matrix form as

$$f^a(\bar{x}) = R^T(\bar{x})a + P^T(\bar{x})b, \quad (2)$$

where $R^T(\bar{x}) = [R_1(\bar{x}), R_2(\bar{x}), \dots, R_n(\bar{x})]$ is the matrix of radial basis functions, $a = [a_1, a_2, \dots, a_n]^T$ are the coefficients of each radial basis function, $P^T(\bar{x}) = [P_1(\bar{x}), P_2(\bar{x}), \dots, P_m(\bar{x})]$ is the vector of polynomial basis, $b = [b_1, b_2, \dots, b_m]^T$ are the coefficients of each polynomial term, n is the number of nodes in $\Omega_{SR}(\bar{x})$, and m is the number of polynomial terms. If two-dimensional (2-D) problems are considered, $\bar{x} = (x, y)$, $P^T(\bar{x}) = [1, x, y, x^2, xy, y^2, \dots]_m$, and

$$R_j(\bar{x}) = e^{-\frac{c}{r_{\max}}(\sqrt{(x-x_j)^2+(y-y_j)^2})^2}, \quad (3)$$

where r_{\max} is the radius of $\Omega_{SR}(\bar{x})$, $\bar{x}_j = (x_j, y_j)$ is the j th node in $\Omega_{SR}(\bar{x})$, and c is known as the shape factor [7]. The vector

of polynomial basis $P^T(\bar{x})$ is usually considered to be [21]

$$P^T(\bar{x}) = [1, x, y]. \quad (4)$$

2.2 RPIM Applied to Maxwell's Equations

Maxwell's equations [22] are a set of partial differential equations that describe the physics associated to electromagnetic wave propagation. In this paper, the transverse-magnetic mode with respect to z (TM_z) is used in rectangular coordinates [22], where the Maxwell's equations in two dimensions can be written as

$$\frac{\partial E_z}{\partial t} = \frac{1}{\epsilon} \left(\frac{\partial H_y}{\partial x} - \frac{\partial H_x}{\partial y} \right), \quad (5)$$

$$\frac{\partial H_x}{\partial t} = -\frac{1}{\mu} \left(\frac{\partial E_z}{\partial y} \right) \quad (6)$$

and

$$\frac{\partial H_y}{\partial t} = \frac{1}{\mu} \left(\frac{\partial E_z}{\partial x} \right). \quad (7)$$

The expressions (1)–(4) can be used to construct the so-called shape functions $\phi(\bar{x}) = [\phi_1(\bar{x})\phi_2(\bar{x}) \dots \phi_n(\bar{x})]$ (specific for each support domain), as described in [5], in such a way that

$$f^a(\bar{x}) = \sum_{j=1}^n f_j(\bar{x})\phi_j(\bar{x}). \quad (8)$$

The spatial derivatives of the fields' components can be obtained by computing $\partial\phi_j/\partial x$ and $\partial\phi_j/\partial y$. This way, (5)–(7) can be approximated by

$$E_{z,i}^{N_t+1} = E_{z,i}^{N_t} + \frac{\Delta_t}{\epsilon} \left(\sum_{j=1}^n H_{y,j}^{N_t} \frac{\partial\phi_j}{\partial x} - \sum_{j=1}^n H_{x,j}^{N_t} \frac{\partial\phi_j}{\partial y} \right), \quad (9)$$

$$H_{x,i}^{N_t+1} = H_{x,i}^{N_t} - \frac{\Delta_t}{\mu} \left(\sum_{j=1}^n E_{z,j}^{N_t} \frac{\partial\phi_j}{\partial y} \right) \quad (10)$$

and

$$H_{y,i}^{N_t+1} = H_{y,i}^{N_t} + \frac{\Delta_t}{\mu} \left(\sum_{j=1}^n E_{z,j}^{N_t} \frac{\partial\phi_j}{\partial x} \right). \quad (11)$$

where $t = N_t \times \Delta_t$ is the time (in seconds), Δ_t is the RPIM time step, and i is the index of the node placed at \bar{x} . It must be emphasized that, in this paper, n ranges from 8 to 16, according to the considered support domain. The radii of all support domains are approximately equal (maximum distance from \bar{x} to $\bar{x}_j, \forall \bar{x}_j \in \Omega_{SR}(\bar{x})$).

In this paper, the vector of polynomial basis (4) has been modified to ensure independence of the interpolation coefficients on \bar{x} , such that

$$P^T(\bar{x}_j) = [1, x_j - x, y_j - y]. \quad (12)$$

In order to truncate the analysis space, the uniaxial perfect matched layers (UPML) [23] formulation has been employed for absorbing the fields at the limits of Ω (standard procedure for treating open problems [12]). It is also noteworthy that the Gauss's laws are automatically satisfied by Faraday's and Ampere's equations when written in rectangular coordinates [12].

2.3 Coulomb's Law and Analytical Dynamics

Coulomb's inverse-square law is seen today as a classic law of electrostatics developed in 1785 by Charles Coulomb. This law describes the electrostatic force interaction between electrically charged particles, and it was essential to the development of electromagnetic theory as it builds the foundation of the electric field concept.

Coulomb's law states that the magnitude of the electrostatic force \vec{F} resultant of the interaction between two point charges (q_1 and q_2) is directly proportional to the scalar multiplication of the magnitudes of charges and inversely proportional to the square of the distance r between them [24]. The electrostatic force \vec{F} promotes attraction if the two charges have different signs (see Figure 1a), or repulsion otherwise (Figure 1b and c).

After detailed experiments, Coulomb found out that the force produced by charge q_1 acting on charge q_2 in free space is completely described as a vector by

$$\vec{F}_{1,2} = \frac{1}{4\pi\epsilon_0} \frac{q_1 q_2}{|\vec{r}_{1,2}|^3} \vec{r}_{1,2} \quad (13)$$

in which $\vec{r}_{1,2} = \vec{x}_2 - \vec{x}_1$, \vec{x}_i is the point vector defining the position of q_i in space, and ϵ_0 is the electric permittivity of vacuum.

Coulomb's law (13) is usually described for a system of two charges. However, it is widely known that the total force \vec{F}_{Ri} (resultant force) on a test charge q_i , which is produced by a set of N point charges (q_1, q_2, \dots, q_N), is given simply by the vector sum of forces relative to each of the N charges (principle of superposition) [24]. Mathematically, one has

$$\vec{F}_{Ri} = \sum_{j=1}^N \vec{F}_{j,i}, \quad j \neq i \quad (14)$$

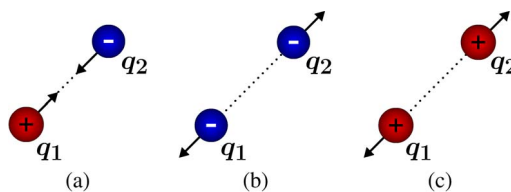


Figure 1. Forces produced by two electrically charged particles. (a) Charges with different signs. (b) and (c) Charges with same sign.

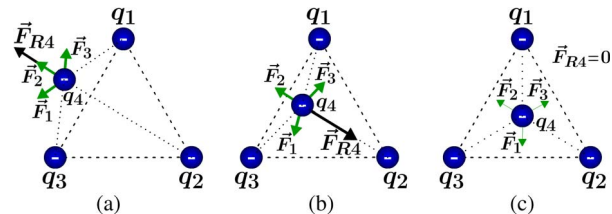


Figure 2. Analytical dynamics applied to a system of four particles with same charge (q_4 is the only particle free to move over space). (a) When q_4 is initially positioned outside the triangle, \vec{F}_{R4} pushes it away. (b) Charge q_4 is dragged by \vec{F}_{R4} to the force equilibrium point if its initial position is inside the triangle. (c) q_4 at the force equilibrium point inside the triangle ($\vec{F}_{R4} = 0$).

By applying Coulomb's law and the principle of superposition to a system of four identical point charges, in which charges $q_1, q_2,$ and q_3 are spatially fixed at the vertices of an equilateral triangle and q_4 is free to move over space, it can be seen that if charge q_4 is positioned outside the triangle, as shown in Figure 2a, the force \vec{F}_{R4} (resultant of the forces acting on q_4) pushes q_4 away from the triangle. However, if q_4 is positioned initially inside the triangle, as shown in Figure 2b, the resultant force \vec{F}_{R4} drags the charge q_4 to the centroid of the triangle, as shown in Figure 2c, which is the position of force equilibrium ($\vec{F}_{R4} = 0$).

Without loss of generality, consider for 2-D space the case in which there is an infinite set of movable particles, all with same electric charge, in force equilibrium state (see Figure 3a). Notice that the charges must be equidistantly positioned. However, if a charge q_i is moved and remains fixed at any position other than its original equilibrium location in the set (see Figure 3b), the system of particles reacts in order to produce a new equilibrium state due to the new location of q_i . As far as q_i is fixed at a new locus, the other particles tend to move, and a new equilibrium state is established (see Figure 3c), in such a way to satisfy the principle of minimum total potential energy (as it is established by analytical dynamics due to the second law of thermodynamics) [25].

This effect is the basis for the discretization method proposed in this paper.

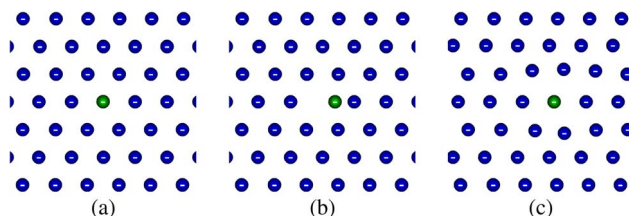


Figure 3. Two-dimensional analytical dynamics applied to an infinite set of charges. (a) Initial equilibrium state. (b) Displacement of a single charge (fixed at a new position). (c) New force equilibrium state is produced.

3. The Coulomb's Law Discretization Method (CLDM)

Consider a set of movable charged particles. If the principle of minimum total potential energy is not satisfied at a given time T , then every movable particle is pushed by each other, simultaneously, in such a way to minimize resultant forces acting on every particle. Now, consider a movable charged particle p_i placed originally at \bar{x}_i (within the set), as illustrated in Figure 3. In this context, according to Newton's second law of motion [26], the resultant force \vec{F}_{Ri} acting on a particle p_i can be written as

$$\vec{F}_{Ri} = m_s \vec{a}_i \quad (15)$$

in which m_s is the mass of p_i , and \vec{a}_i is its acceleration. By writing (15) in terms of the particle's velocity \vec{v}_i , one gets

$$\vec{F}_{Ri} = m_s \vec{a}_i = m_s \frac{\partial \vec{v}_i}{\partial T}. \quad (16)$$

By using finite differences, (16) assumes the form

$$\vec{F}_{Ri}^T = m_s \frac{\vec{v}_i^T - \vec{v}_i^{T-\Delta T}}{\Delta T}, \quad (17)$$

from which \vec{v}_i^T (the velocity of p_i at time T) can be calculated. This way

$$\vec{v}_i^T = \vec{F}_{Ri}^T \frac{\Delta T}{m_s} + \vec{v}_i^{T-\Delta T}, \quad (18)$$

where \vec{F}_{Ri}^T is the resultant force on p_i at time T , $\vec{v}_i^{T-\Delta T}$ is the velocity of p_i at $T - \Delta T$, and ΔT is the CLDM time step.

By using finite differences, the position \bar{x}_i of p_i is associated to the particle's velocity by

$$\frac{\bar{x}_i^{T+\Delta T} - \bar{x}_i^T}{\Delta T} = \vec{v}_i^T, \quad (19)$$

from which

$$\bar{x}_i^{T+\Delta T} = \bar{x}_i^T + \vec{v}_i^T \Delta T. \quad (20)$$

From (18) and (20), it is easy to see that

$$\bar{x}_i^{T+\Delta T} = \bar{x}_i^T + \left(\vec{F}_{Ri}^T \frac{\Delta T}{m_s} + \vec{v}_i^{T-\Delta T} \right) \Delta T. \quad (21)$$

In this paper, it is assumed that $m_s = 1$, for all $p_i \in \Omega$. The vector spatial step $\vec{\Delta}_x^i$ is given by

$$\vec{\Delta}_x^i = \left(\vec{F}_{Ri}^T \frac{\Delta T}{m_s} + \vec{v}_i^{T-\Delta T} \right) \Delta T \quad (22)$$

and

$$\Delta T = \frac{|\vec{\Delta}_x^i|}{\Upsilon}, \quad (23)$$

where $|\vec{\Delta}_x^i|$ is the minimum absolute distance among particles at $T - \Delta T$, $|\vec{v}_{\max}|$ is the maximum absolute particle velocity in Ω at $T - \Delta T$, and Υ is a factor (constant) that assures stability to the method, which is heuristically determined to be $\Upsilon \geq 10$. Notice that ΔT in (17)–(23) is unrelated to RPIM time step Δ_t in (9)–(11).

For a given temporal advance of ΔT , (21) produces a total spatial shift of $\vec{\Delta}_x^i$ on p_i directed by the force vector \vec{F}_{Ri}^T evaluated at T . If $|\vec{\Delta}_x^i|$ is sufficiently small and (21) is successively applied simultaneously for each particle in the set, the physical behavior illustrated in Figure 3 can be reproduced computationally, as long as \vec{F}_{Ri}^T tends to zero as $T \rightarrow \infty$.

The numerical reproduction of the described physical dynamics can be used for obtaining high-quality discrete representations of complex objects immersed in space for solving partial differential equations with meshless methods. In order to define the interfaces between different materials (contours), fixed nodes (seen as unmovable charges) can be used. Movable nodes (charges, as well) can be used for performing optimizable discretization of space. A high-quality node distribution is expected to produce numerical stability and well-conditioned numerical systems, as detailed in [14]. By successively applying (21) to the set of movable nodes, minimum potential energy state can be reached, and the main characteristics of the obtained spatial node distribution tend to be compatible with the parameters defining the quality of spatial discretization, which are as follows [7, 27, 28].

- Controlled directional variation of distance among nodes (uniform spacing): Distances among nodes should be approximately equal for all directions (see Figure 4). In this work, this condition is achieved by minimizing potential energy among charged particles.
- Precise representation of contours: In this paper, for problems involving different materials, a set of

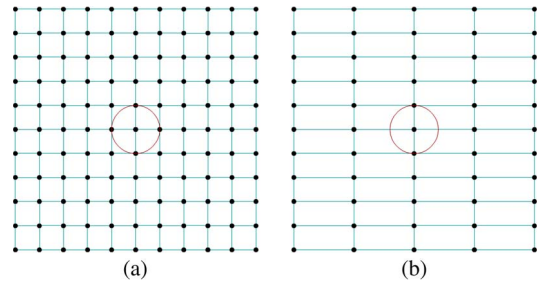


Figure 4. Directional variation quality regarding separation among nodes (uniform node spacing). (a) Uniform directional variation. (b) Nonuniform directional variation.

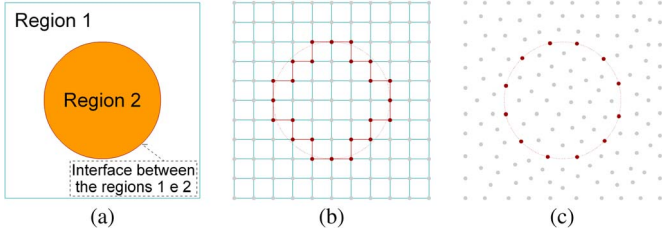


Figure 5. Geometrical quality of interfaces between regions. (a) Circular contour. (b) Representation of interface by using a structured rectangular mesh. (c) Representation of interface by employing a meshless discretization schema (represented by fixed charges).

fixed charged nodes is used to represent the interfacing contours (see Figure 5).

- Smoothing: The node distribution should favor smooth discretization transitions among different geometries (see Figure 6), which typically takes place in free-space discretization. Notice that this requirement is also compatible with minimum potential energy principle.
- Uniformity of node distribution in $\Omega_{SR}(\bar{x})$ (see Figure 7): For (every) support domain $\Omega_{SR}(\bar{x})$ in Ω , density of nodes should be conserved across its spatial domain (around \bar{x}). This is necessary in order to properly compute interpolation of functions and curl operations in $\Omega_{SR}(\bar{x})$ [7]. In this work, this is also fulfilled by minimizing potential energy among nodes.
- An additional quality criterion can be considered, which is introduced in this paper, i.e., assurance of interpolation precision in all support domains, which can be evaluated during the dynamics of the discretization process.

This way, the proposed discretization method (CLDM) aims at the aforementioned set of quality criteria. CLDM is divided into four subsequent steps: 1) preliminary domain

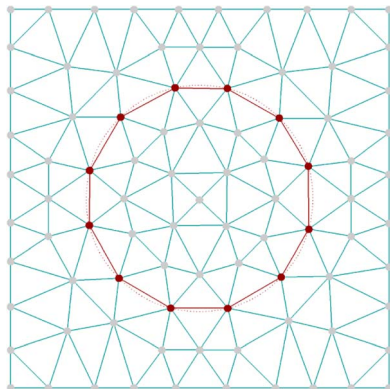


Figure 6. Quality of smoothing (notice the smooth transition between circular and rectangular geometries).

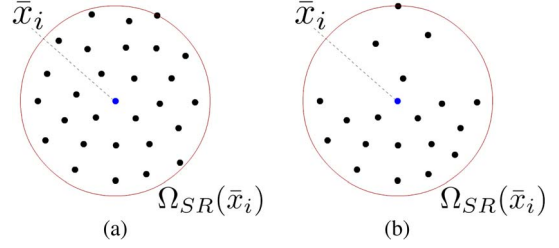


Figure 7. Quality regarding uniformity of node distribution in support domains. (a) Uniform support domain. (b) Nonuniform support domain.

creation; 2) definition of support domains (specifically for the discretization process); 3) definition of interfaces among different materials; and 4) iterative repositioning of nodes by using (14) and (21) with discretization quality evaluation. Each step is detailed as follows.

3.1 Creation of a Preliminary Domain Ω_P

In order to obtain the definitive domain Ω , which is used for performing RPIM simulations, building a preliminary domain Ω_P (from which Ω can be obtained) is required by CLDM. This first step of the proposed method corresponds to setting up a preliminary node distribution in the analysis region (see Figure 8a), which does not necessarily satisfy all quality criteria aimed for meshless discretization. Two possibilities are illustrated in Figure 8b and c.

The preliminary analysis domain $\Omega_{aP} \subseteq \Omega_P$ is a set of nodes \bar{x}_i (where $i = 1, 2, \dots, N$, and N is the number of nodes in Ω_{aP}) that coarsely describes the geometry of the environment to be simulated. In this work, Ω_{aP} consists of a simple structured mesh with evenly distributed nodes, as shown in Figure 8c. This structured mesh is used only as a reference set of nodes for the discretization process, and its importance lies on the fact that it naturally favors the following aspects of interest:

- simple construction of support domains $\Omega_{SC}(\bar{x}_i)$ for CLDM since the node distribution is organized as a structured model;

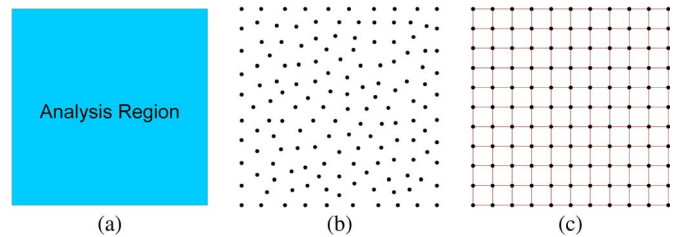


Figure 8. Spatial discretization of the analysis region. (a) Analysis region. (b) Random and disorderly node set. (c) Node set organized as a Cartesian mesh.

- uniformity of node distribution in $\Omega_{SC}(\bar{x}_i)$ (and, in consequence, in Ω_{aP}), favoring force equilibrium;
- truncation of domains for CLDM (as discussed later here) and RPIM (by UPML).

The preliminary spatial discretization Ω_{aP} is also used for defining the minimum distance among nodes $\Delta_{\bar{x}_{\min}}$. Furthermore, two groups of points are created for solving Maxwell's equations, namely, "electric" and "magnetic" nodes, at which the field components of electric and magnetic fields are evaluated each time step. The spatial arrangement of such nodes is based on Yee's cell [29], which is adapted for enabling the application of CLDM. The adaptation is the addition of an electrical node (called pivot node) at the center of Yee's cell, in order to ensure initial electrostatic equilibrium state.

It is assumed in this work that the minimum distance between nodes $\Delta_{\bar{x}_{\min}}$ must be less than or equal to $\lambda_{\min}/10$, for $\lambda_{\min} = C_0/f_{\max}$ (minimum wavelength), where C_0 is the speed of light in vacuum, and f_{\max} is the maximum significant frequency of the applied pulse.

Notice that, to ensure the perfect electrostatic equilibrium, it would be necessary to use an infinite analysis domain with infinite quantity of particles, making CLDM computationally unfeasible. If a restricted region and a finite quantity of movable nodes are considered, mutual repulsion would scatter them out of the analysis region (see Figure 9).

In this paper, a technique for avoiding the behavior presented in Figure 9 is introduced. It consists in the creation of a border region Rb, which is composed of unmovable nodes placed around the analysis domain Ω_{aP} , such as illustrated in Figure 10. The node distribution schema in Rb also follows the adapted Yee's cell (with pivot nodes). The position of an unmovable node is not affected by the other nodes, but fixed charges influence the position of movable nodes in Ω_{aP} which, this way, confines charges in Ω_{aP} .

The border region Rb must be large enough to ensure the stability of the system (typically, larger than the maximum radius of the support domains $\Omega_{SC}(\bar{x}_i)$ for CLDM, as

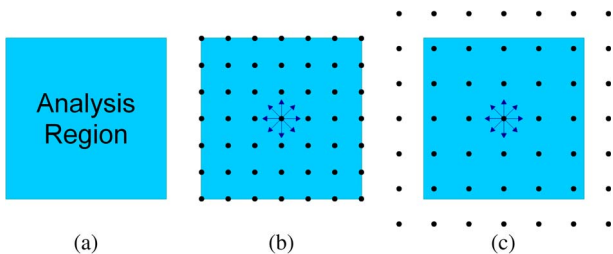


Figure 9. Limitation of analysis domain Ω_{aP} with no use of a truncation technique for CLDM. (a) Analysis region. (b) Ω_{aP} before the application of CLDM. (c) Ω_{aP} after the application of CLDM with no special truncation treatment.

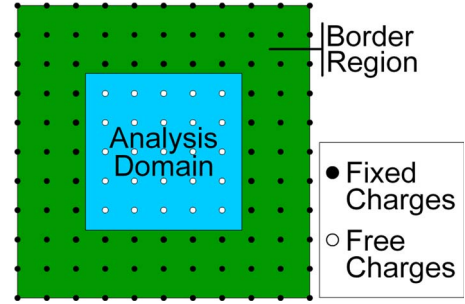


Figure 10. Border region Rb and the analysis domain Ω_{aP} .

described in Section 3.2). This way, the total preliminary domain Ω_P is the union of Ω_{aP} and Rb (see Figure 10).

3.2 Definition of Support Domains $\Omega_{SC}(\bar{x}_i)$ for CLDM

In principle, the application of Coulomb's law in Ω_{aP} implies that each node $\bar{x}_i \in \Omega_{aP}$ behaves as a charge q_i and receives the influence of all other nodes in Ω_P . However, this becomes unfeasible when applied to a domain with a large quantity of nodes as it can require enormous computational effort. In order to optimize this process, the idea of support domains (or subdomains) was applied for each node in Ω_{aP} . Support domains can be used because, as shown by (13), the Coulomb's force \vec{F} is inversely proportional to the square of the distance r between two charges. Thus, for a given set of identical point charges, the resultant force \vec{F}_{Ri} (for a charge q_i) presents stronger dependence on charges closer to q_i (see Figure 11a).

The subset of K nodes ($\bar{x}_j \neq \bar{x}_i$) $\in V$ closer to node $\bar{x}_i \in V$ (where $K < N$, and N is the total number of nodes in the set V) is called *support domain for CLDM* $\Omega_{SC}(\bar{x}_i)$ here (see Figure 12a).

Although $\Omega_{SC}(\bar{x}_i)$ can have different sizes and shapes, in this paper, the research areas are all identical, and they have the form of a circle of radius r (for 2-D problems) centered \bar{x}_i .

Despite that $\Omega_{SC}(\bar{x}_i)$ contains a number of nodes smaller than the total domain's node number, it should be large enough

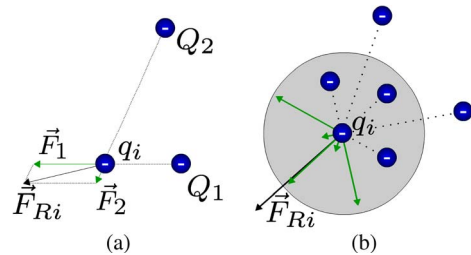


Figure 11. Influence among identical charges. (a) \vec{F}_{Ri} presents stronger dependence on charge Q_1 than on charge Q_2 . (b) \vec{F}_{Ri} is more dependent on charges in the vicinity Ω_{SC} of q_i than on other charges.

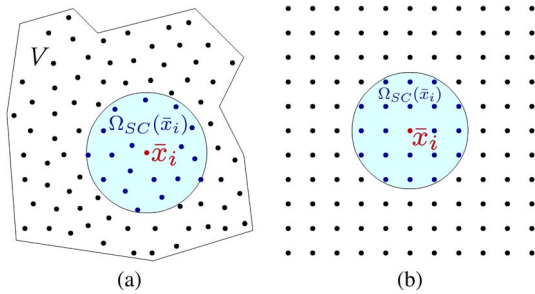


Figure 12. Support domain $\Omega_{SC}(\bar{x}_i) \in V$ centered on \bar{x}_i . (a) Support domain in a random and disordered node distribution. (b) Support domain in an ordered and uniform node distribution.

to properly minimize deviations on computed resultant Coulomb forces. In this work, we have empirically determined that $r = 8\Delta_{\bar{x}_{\min}}$ (see Figure 13) is enough for obtaining the expected behavior. We have observed that neglecting forces \vec{F}_1 with absolute value smaller than 2% of the magnitude of force \vec{F}_2 calculated for two charges separated by the distance $\Delta_{\bar{x}_{\min}}$ does not substantially affect results (final positions of particles are virtually identical for either case). This way, if $r = 8\Delta_{\bar{x}_{\min}}$, then $|F_1| = (1/64)|F_2| \approx 0.016|F_2|$. Notice that this definition implies that each support domain can have a particular number of nodes and this step does not produce disturbances in the preliminary analysis domain Ω_{ap} by itself (it is used exclusively to optimize the computational performance of CLDM). We solved all the six examples presented in this paper, plus five additional problems, using $r = 8\Delta_{\bar{x}_{\min}}$. Each problem was simulated for five discretization levels in the range $\lambda_{\min}/20 - \lambda_{\min}/80$. This way, we have tested the methodology 55 times. The suggested criteria have satisfied every case tested by authors so far, and this way, it seems to be trustworthy for being used in a broad range of electromagnetic problems.

3.3 Representation of Interfaces

In this step, a geometry describing boundaries among two or more media in a given domain Ω_P is defined by

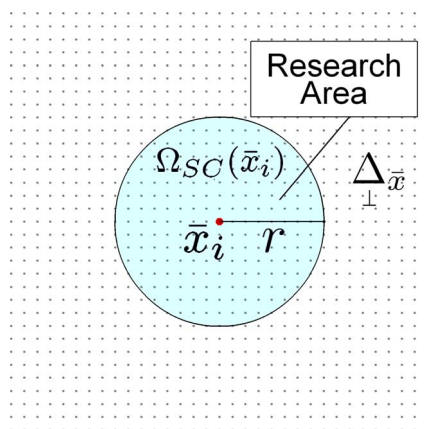


Figure 13. Support domain $\Omega_{SC}(\bar{x}_i)$ in a uniform distribution based on a background mesh, which has a circular search area of radius $r = 8\Delta_{\bar{x}_{\min}}$.

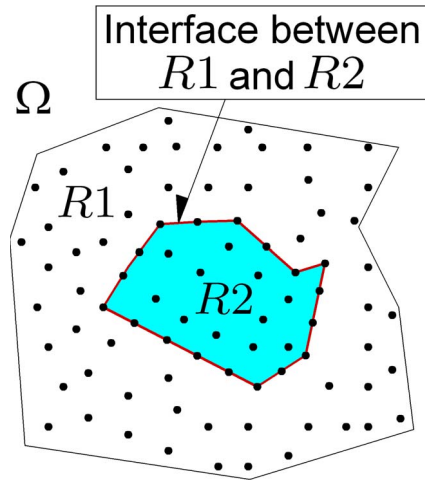


Figure 14. Formatting the interface between $R1$ and $R2$, where $R2 \in R1$, and $R1 \in \Omega_P$.

means of a set of fixed (unmovable) nodes (see Figure 14). The implementation of this step is relatively simple, and it consists in identifying nodes closer to a given interface, to move and fix them to the line defining the interface (see Figure 15).

Despite its simplicity, this step requires some care.

- Two or more nodes may not overlap after the displacement process.
- The distance between neighbor nodes on the interface $\Delta_{\bar{x}_{\min I}}$ should be approximately equal to $\Delta_{\bar{x}_{\min}}$.
- The nodes used to represent the contour of the interface among regions must be converted to fixed nodes (considered as fixed charges).

If any of the aforementioned conditions is not satisfied, discretization quality problems can emerge when CLDM is applied, such as inadequate representation of the interfaces and/or unbalanced distribution of the nodes in the domain can be produced.

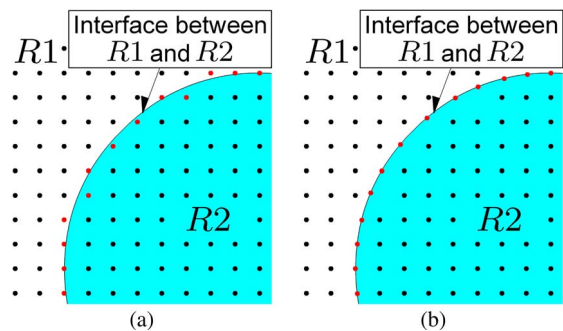


Figure 15. Formatting the interface between $R1$ and $R2$. (a) Identification of nodes near the interface. (b) Displacements and fixing of nodes near the interface.

This step promotes significant modifications on the preliminary analysis domain Ω_{aP} , producing the intermediate analysis domain Ω_{aI} . The reconfigured preliminary total domain Ω_{LP} (with interfaces properly defined and fixed) is referred here as intermediate total domain Ω_I , and $\Omega_I = \Omega_{aI} \cup \text{Rb}$.

3.4 Repositioning of Nodes Using Coulomb's Law

Once the media interfaces are completely defined by using fixed nodes, some nodes become placed off their positions of force equilibrium, interfering with the spatial discretization quality (see Figure 17a). New force equilibrium configuration can be obtained by using an iterative procedure, which is introduced in this paper, which is based on Coulomb's force law. The goal is to minimize potential energy among the charged particles (used later as RPIM nodes) by moving free charges to positions defined by using (14)–(23) for each step. Free charges are those that can move due to the resultant force \vec{F}_R . These charges are distributed over Ω , except the border region Rb and interfaces among different materials (see Figure 16).

The displacement of a charge at \bar{x}_i depends on the resultant force \vec{F}_{Ri} at time T , which is the vector sum of all forces that act on \bar{x}_i due to its interaction with each charge $\bar{x}_j \in \Omega_{SC}(\bar{x}_i)$, where $\bar{x}_j \neq \bar{x}_i$, $j = 1, 2, \dots, K$, and K is the number of nodes on support domain $\Omega_{SC}(\bar{x}_i)$. Obtaining the final positions of all free charges is a process requiring a relatively large number of iterations (see Figure 17) to achieve the expected result. This is due to the fact that ΔT must be sufficiently small in order to guarantee the stability of the iterative method [the stability is controlled by Υ in (23)].

After executing a given iteration of CLDM [application of (21) for each movable particle], the quality of the discretization is evaluated. In principle, this evaluation can be performed in two ways.

- Resultant force evaluation: It is a specific evaluation that verifies the magnitudes of the resultant

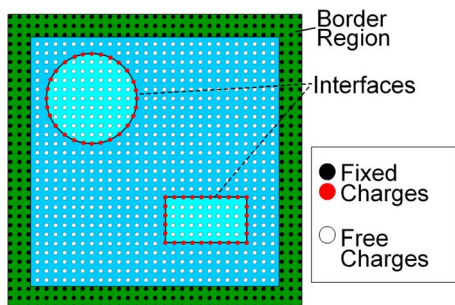


Figure 16. Classification of charges according to their ability to react to the system. Fixed charges in border region Rb (black) and in interface between regions (red). All other charges are free to move (white).

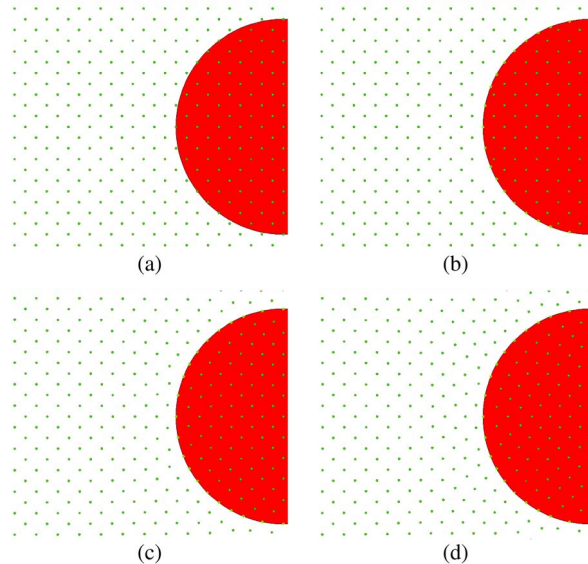


Figure 17. Application of CLDM for 150 iterations. (a) Creation of the preliminary domain Ω_P . (b) Interface representation between regions (Ω_I). (c) Repositioning of nodes after 50 iterations (Ω_C). (d) Repositioning of nodes after 150 iterations (Ω_C).

forces \vec{F}_{Ri} at each node $\bar{x}_i \in \Omega_I$. If all nodes in Ω_I present $|\vec{F}_{Ri}|$ smaller than a reference value (that is, $|\vec{F}_{Ri}| \approx 0$), then the iterative procedure stops.

- RPIM interpolation precision: If the interpolation of a given test function [7] presents acceptable errors for all RPIM support domains (Ω_{SR}), then Ω_I can be used for solving Maxwell's equation via RPIM methodology.

When results of both evaluations are favorable, then Ω_{aI} becomes Ω_{aC} (definitive analysis domain), and Ω_I is referred as Ω_C , that is, $\Omega_C = \Omega_{aC} \cup \text{Rb}$. The process related to evaluation of interpolation quality is detailed in the next section.

The basic algorithm designed to update the position of free nodes is illustrated in Figure 18. Figure 19 shows the flowchart that describes CLDM.

4. Quality of Spatial Discretization

There are several ways to evaluate the discretization quality for a given domain [14]. In this paper, however, it is proposed a quantification based on the percentage RPIM interpolation error Err^a defined in [7] as

$$\text{Err}^a\% = 100 \times \left[\frac{f^a(\bar{x}) - f(\bar{x})}{f(\bar{x})} \right], \quad (24)$$

where $f(\bar{x})$ is the exact value of a reference function f at \bar{x} , and $f^a(\bar{x})$ is the interpolated value of $f(\bar{x})$. The use of a

```

1) CoulombRepositioning2D( $x, y, q, X\Omega_{SC}, Y\Omega_{SC}, V_x, V_y, \Delta\bar{x}, \Delta T, \Upsilon$ )
2)  $N \leftarrow x[i].size$  # gets size of  $\Omega_c$  #
3)  $V_{max} \leftarrow 0$ 
4)  $\Delta\bar{x}_{min} \leftarrow \Delta\bar{x}$ 
5)  $m_s \leftarrow 1$ 
6) for  $i \leftarrow 1$  to  $N$  do
7)    $x[i] \leftarrow x[i] + V_x[i] * \Delta T$  (20)
8)    $y[i] \leftarrow y[i] + V_y[i] * \Delta T$  (20)
9) end for
10) for  $i \leftarrow 1$  to  $N$  do
11)    $F_x[i] \leftarrow 0$ 
12)    $F_y[i] \leftarrow 0$ 
13)    $n\Omega_r \leftarrow X\Omega_{SC}[i].size$  # gets size of  $\Omega_{SC}(\bar{x}_i)$  #
14)   for  $j \leftarrow 1$  to  $n\Omega_r$  do
15)      $x1 \leftarrow X\Omega_{SC}[i][j]$ 
16)      $y1 \leftarrow Y\Omega_{SC}[i][j]$ 
17)      $r \leftarrow \sqrt{(x1 - x[i])^2 + (y1 - y[i])^2}$ 
18)      $F_x[i] \leftarrow F_x[i] + (q[i] * q[j]/r^3) * (x1 - x[i])$ 
19)      $F_y[i] \leftarrow F_y[i] + (q[i] * q[j]/r^3) * (y1 - y[i])$ 
20)     if  $\Delta\bar{x}_{min} > r$  then  $\Delta\bar{x}_{min} = r$  end if
21)   end for
22)    $V_x[i] \leftarrow F_x[i](\Delta T/m_s) - V_x[i]$  (18)
23)    $V_y[i] \leftarrow F_y[i](\Delta T/m_s) - V_y[i]$  (18)
24)    $V \leftarrow \sqrt{V_x[i]^2 + V_y[i]^2}$ 
25)   if  $V_{max} < V$  then  $V_{max} = V$  end if
26) end for
27)  $\Delta T \leftarrow \frac{\Delta\bar{x}_{min}}{\Upsilon}$  (23)
28) end CoulombRepositioning2D

```

Figure 18. Pseudocode for updating the position of free nodes used to discretize the analysis region.

reference function is justified by the fact that the computation of spatial partial derivatives of a given field component is obtained by multiplying the derivatives of shapes functions ($\partial\phi_j/\partial x$ and $\partial\phi_j/\partial y$) by samples of the field component of interest in Ω_{SR} , as shown in (9)–(11). As in [7], the reference function is considered to be

$$f(\bar{x}) = f(x, y) = \sin(kx) + \sin(ky), \quad (25)$$

which contains the minimum wavelength λ_{min} of interest (critical case), and k is the maximum associated wave number ($k = 2\pi/\lambda_{min}$). Notice that if the RPIM interpolation of spatial derivatives can be obtained satisfactorily for the reference function (25), the spatial distribution of points in Ω_{SR} will produce precise interpolations for other functions as long as their maximum wave number is smaller or equal to k , as shown in [7]. The choice of (25) as test function is strongly related to the empirical spatial discretization condition $\Delta_{min} \leq \lambda_{min}/10$ adopted for standard FDTD simulations [12], which aims at precisely representing the smaller propagating wavelength in analysis space.

In this context, the quality of the spatial meshless discretization Q can be defined as

$$Q = \frac{1}{\max(|Err^a\%|)}, \quad (26)$$

in which $\max(|Err^a\%|)$ is the absolute value of the maximum interpolation error found in Ω_{aC} among all its support

domains. The discretization quality Q proposed here is a convenient solution as long as it assesses the interpolation precision (which is dependent on spatial discretization) all over Ω_{aC} directly by using RPIM interpolations. This way, it is possible to determine if numerical divergences will emerge during the RPIM simulations (numerical solution of Maxwell's equations). The maximum tolerated absolute interpolation error, which is obtained heuristically, is $|Err^a_{max}| = 10^{-4}\%$ (that is, $Q_{min} = 10^4$).

During the CLDM optimization process, if support domains in which $|Err^a| > |Err^a_{max}|$ are found between two consecutive steps, LSFCM [7] is applied to adjust the values of c [the shape factor in (3)] for reducing $|Err^a|$. If the condition $|Err^a| > |Err^a_{max}|$ is still verified for any support domain, this procedure (executing a CLDM step followed by LSFCM

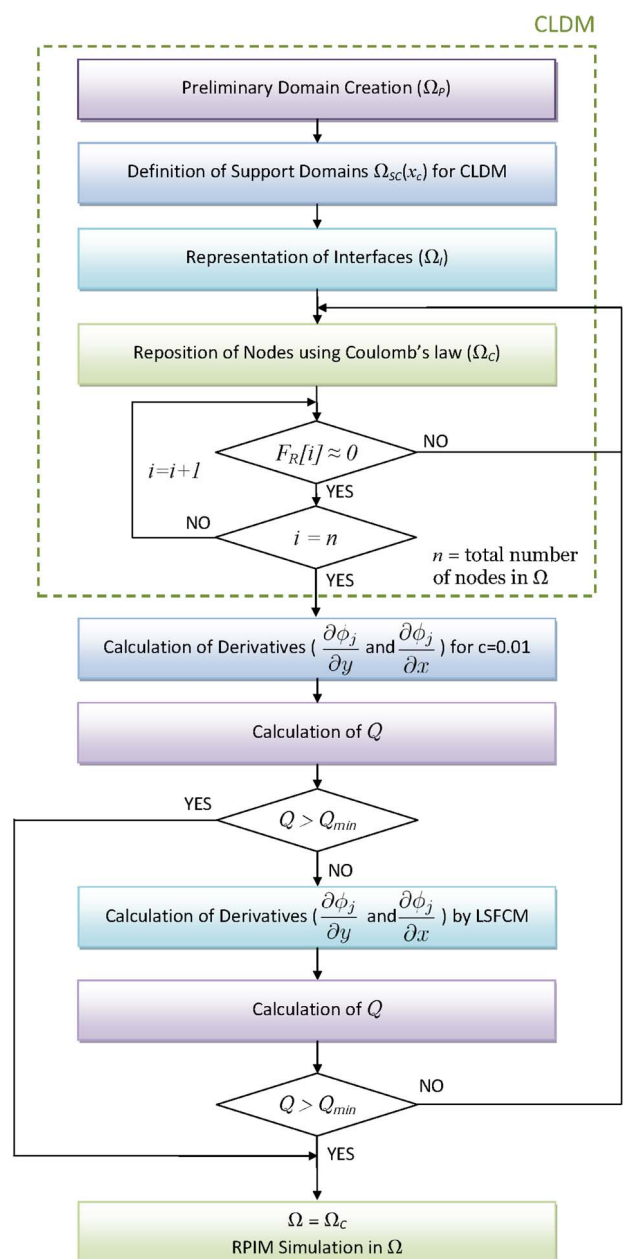


Figure 19. Flowchart of CLDM associated to LSFCM.

optimization for c) is repeated until the quality of the spatial discretization reaches or exceeds Q_{\min} and then Ω_{aC} becomes Ω_a (definitive analysis domain) and Ω_C is turned into Ω , that is, $\Omega = \Omega_a \cup \text{Rb}$. Finally, Figure 19 shows the flowchart that describes the CLDM algorithm associated to Q evaluation ($Q \geq Q_{\min}$ is used as stop criterion).

5. Numerical Validation and Analysis of Results

This section shows three simulations and their results, in order to validate the CLDM with LSFCM and RPIM-2D methods [7] implemented for this work. The first two are electromagnetic scattering analyses for different scattering cylinders. The third is an analysis of electromagnetic waves propagation over a photonic band gap (PBG)-based filter. For every RPIM-Delaunay simulation, which is used for confrontation of results, LSFCM was employed for avoiding temporal progression of numerical instabilities.

5.1 Validation Case 1: RCS of Triangular Cylinder Scatterer

The electromagnetic scattering of a given object can be evaluated by calculating its radar cross section (RCS). The RCS is a far-field parameter that compares the incident electric field with the scattered field for a given frequency [22]. For this validation case, the equation developed by Bavelis in [30] was used to numerically calculate RCS_{2-D} by using near field (obtained here by means of numerical simulations).

The scatterer considered for this example is a metallic triangular cylindrical structure, which is infinite along the z -axis,

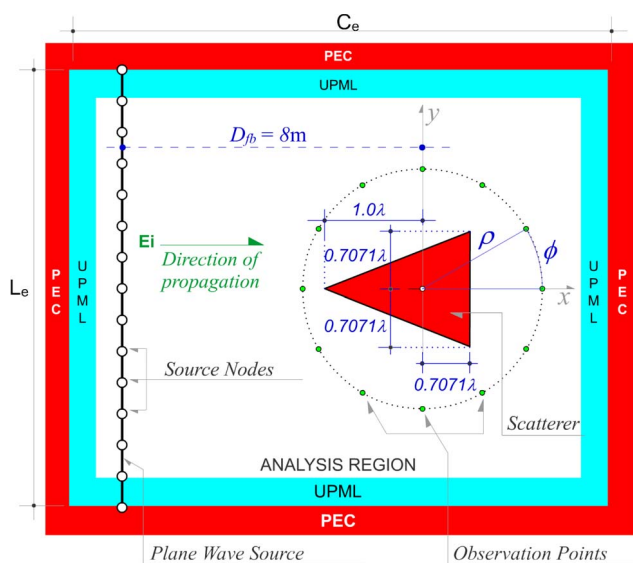


Figure 20. Transverse section of the triangular cylinder (x - y plane) (validation case 1).

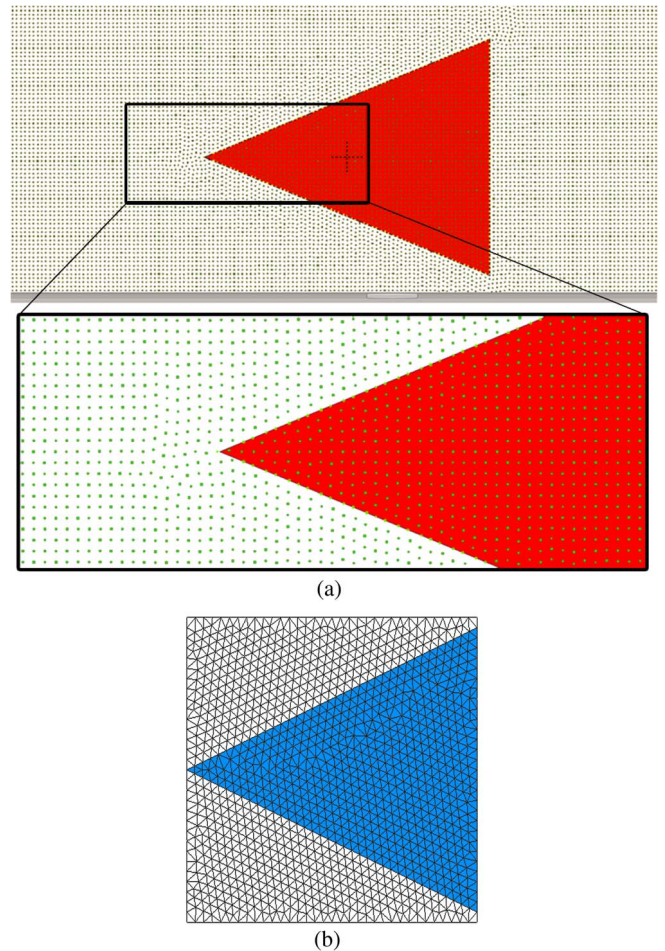


Figure 21. Distribution of spatial discretization nodes for modeling the triangular scatterer (validation case 1). (a) Node set obtained by using CLDM. (b) Delaunay-triangulation-based mesh.

and its cross section is an isosceles triangle with base $\sqrt{2}\lambda$ and height $(1 + \sqrt{2})\lambda$ (see Figure 20). This cylinder is surrounded by free space where an electromagnetic plane wave propagates. Figure 21 shows the spatial discretization obtained by CLDM (see Figure 21a) and by Delaunay triangulation (see Figure 21b) for performing RPIM simulations. Delaunay-based mesh is used for comparison of results only.

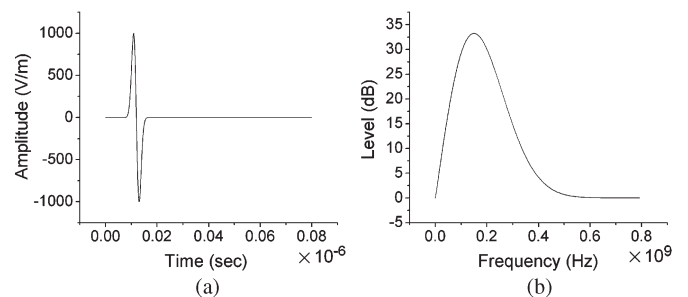


Figure 22. Gaussian monocycle pulse (validation cases 1 and 2). (a) Time domain. (b) Frequency domain.

Table 1. Simulation parameters for validation cases 1 and 2.

PARAMETERS	RPIM_CLDM	RPIM_Delaunay	FDTD
Size of analysis region + UPML= $L_e \times C_e$ (m)	12×15	12×15	12×15
f_c (GHz) (central frequency of the excitation pulse)	0.3	0.3	0.3
dt (s)	2×10^{-11}	2×10^{-11}	2×10^{-11}
$\lambda_{min} = C_0/f_{max}$ (m) (minimum wavelength)	0.5	0.5	0.5
$\Delta_{x_{min}} = \Delta x = \Delta y$ (m) (minimum distance among nodes)	$\lambda_{min}/20$	$\lambda_{min}/20$	$\lambda_{min}/20$
Number of observation points	200	150	200
Number of time steps	4000	4000	4000

A plane wave was modeled for acting as excitation source. The time dependence of the excitation pulse (Gaussian monocycle) is given by

$$p(t) = A_p \sqrt{\frac{2e}{\tau^2}} (t - t_0) e^{-\frac{(t-t_0)^2}{\tau^2}}, \quad (27)$$

where t is the time given in seconds, $A_p = 1$ V/m, $\tau = 200 \times 10^{-11}$ s, $f_c = 0.300$ GHz (frequency of maximum spectral amplitude), $bw = 0.600$ GHz (3-dB upper frequency/bandwidth), and $t_0 = 1200 \times 10^{-11}$ s. Figure 22 shows plots of the excitation pulse. The temporal and spectral shapes of the pulse are shown in Figure 22a and b, respectively.

The observation points are distributed over a virtual circle in the near-field region surrounding the triangle (see Figure 20). The virtual circle's radius is $\rho = 1.5$ m, and its

center coincides with the centroid of the triangle. The simulation parameters are shown in Table 1.

The RCS calculation requires the evaluation of the total and incident fields. For this reason, the simulations were performed with the scatterer (total field) and with no scatterer (incident field). Figure 23 shows the temporal progression of the propagation of $|E_z|$ for both situations.

After performing the simulations, RCS is calculated by using the near fields obtained from RPIM and FDTD simulations, and the numerical results were compared with the analytical solution provided by [30]. As shown in Figure 24, the RCS solution obtained by using RPIM with CLDM produces smaller maximum deviation from analytical solution than solutions calculated by employing FDTD or RPIM with Delaunay mesh. The accurate numerical

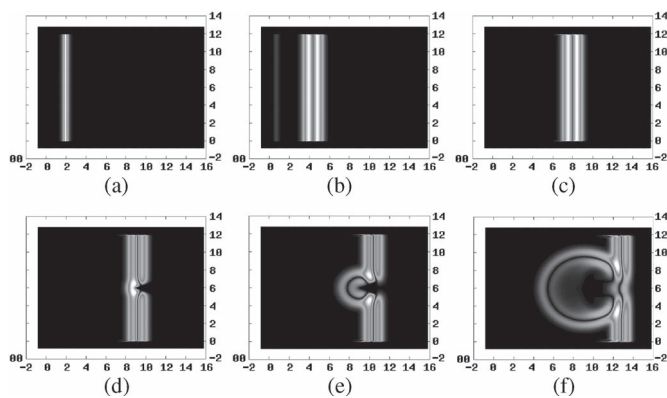


Figure 23. Spatial distribution of $|E_z|$: incident field for validation cases 1 and 2 [(a) $t = 8.0$ ns, (b) $t = 20.0$ ns, and (c) $t = 32.0$ ns] and total field for validation case 1 [(d) $t = 36.0$ ns, (e) $t = 40.0$ ns, and (f) $t = 48.0$ ns].

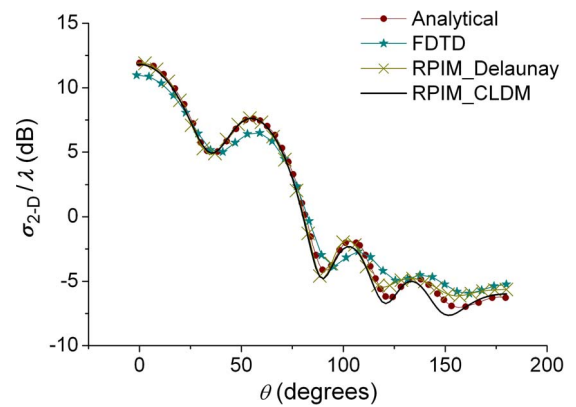


Figure 24. RCS of triangular scatterer (validation case 1): comparison among analytical curve ($\theta = \phi - \pi$) and solutions from FDTD and RPIM (with CLDM node set and the Delaunay triangular mesh).

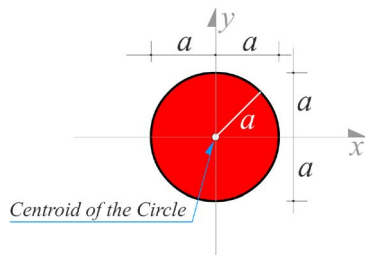


Figure 25. Circular cylinder scatterer and its dimensions (validation case 2).

solution for this problem properly validates the CLDM technique and our computer implementation. Notice that, in order to obtain stable solutions with the RPIM-Delaunay methodology, LSFCM had to be employed in order to minimize interpolation errors.

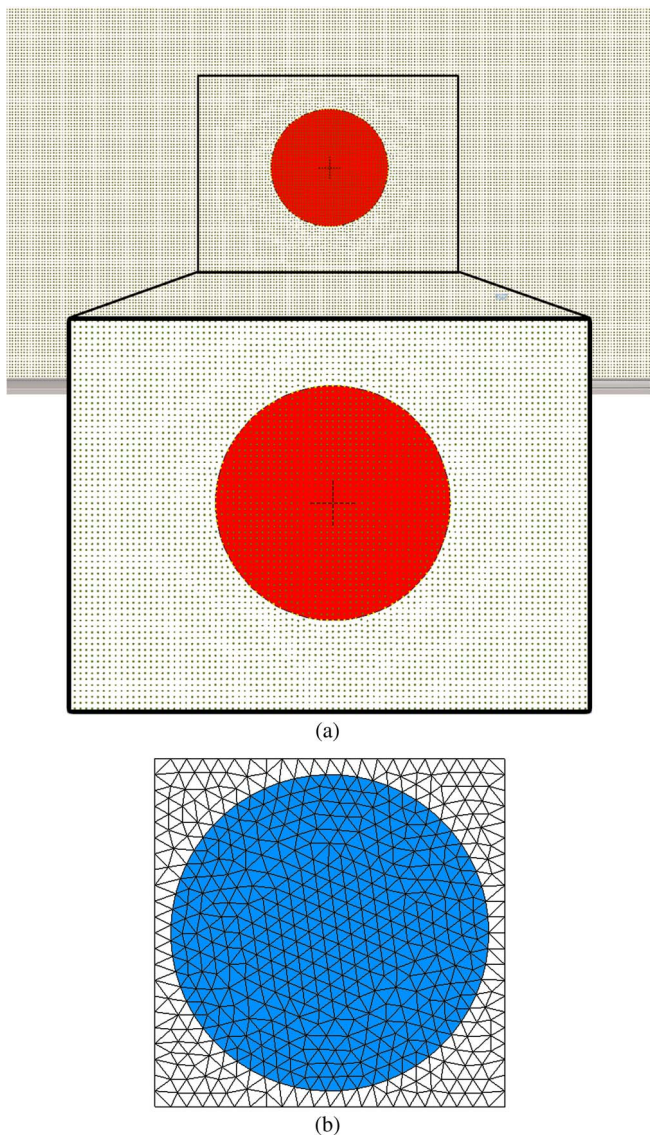


Figure 26. Spatial discretization for circular scatterer (validation case 2) obtained by using (a) CLDM and (b) Delaunay triangulation.

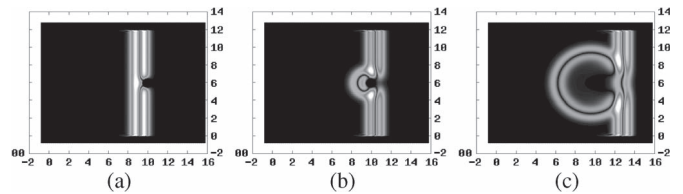


Figure 27. Spatial distribution of $|E_z|$ (total field) for validation case 2. (a) $t = 36.0$ ns. (b) $t = 40.0$ ns. (c) $t = 48.0$ ns.

5.2 Validation Case 2: RCS of Circular Cylinder Scatterer

In this case, the problem setting is similar to that of validation case 1. However, the scatterer considered is a metallic circular cylinder with cross section of radius $a = \lambda/2$ (see Figure 25). Figure 26 shows discretization node sets obtained by CLDM (see Figure 26a) and by Delaunay triangulation (see Figure 26b).

Such as in validation case 1, a plane wave was modeled to excite the present problem. The excitation pulse is described by (27). The remaining simulation parameters are shown in Table 1. In order to obtain field data for calculating RCS, several observation points were distributed over a virtual circle of radius $\rho = 1.5$ m, which is concentric with the metallic scatterer. Figure 27 shows the temporal evolution of electric field distribution (RPIM/CLDM simulation) for the problem at hand.

After performing the transient simulations, RCS was calculated, and the numerical results were compared with the analytical solution provided by [30]. As shown in Figure 28, once more, the RCS values obtained via RPIM are closer to the analytical solution than to the FDTD solution. Figure 29 shows the percentage error as a function of the angle θ for each simulation result. Notice that FDTD produces a maximum deviation from analytical solution of

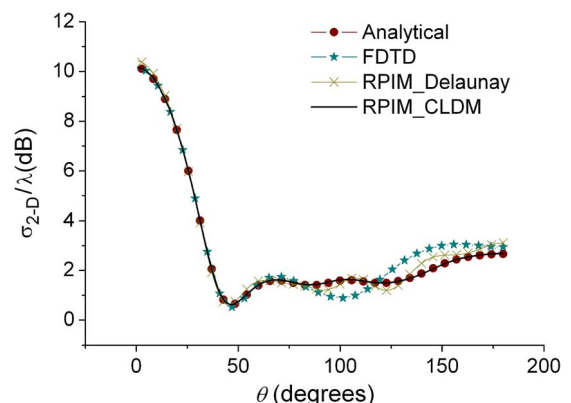


Figure 28. RCS for circular scatterer (validation case 2): comparison among analytical curve ($\theta = \phi - \pi$) and numerical solutions from RPIM (CLDM node set and Delaunay-based mesh) and FDTD.

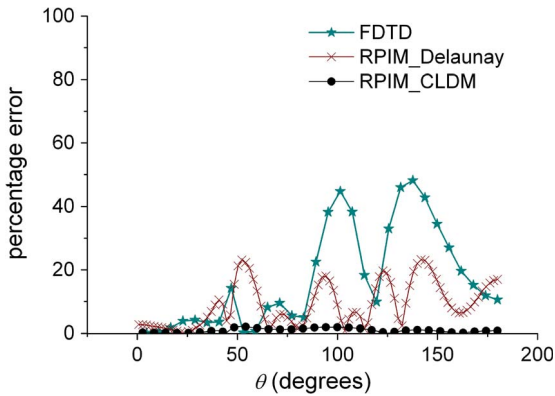


Figure 29. Percentage error for RCS of a circular scatterer (validation case 2): comparison among RPIM (CLDM), RPIM (Delaunay triangulation), and FDTD.

approximately 50%, RPIM with an unstructured mesh shaped with Delaunay discretization produces a deviation of 24% and RPIM with CLDM node set generates a maximum deviation of 3% for this problem. Notice that the improved calculation precision associated to CLDM is related to the discretization quality Q . As illustrated in Table 3, CLDM produced a node set with discretization quality approximately eight times greater than that of the Delaunay-based mesh. This way, the obtained results reinforce the validation of the CLDM discretization methodology. Observe that interpolation errors were minimized with LSFCM for the RPIM-Delaunay simulation.

5.3 Validation Case 3: Metallic PBG Structures

The third validation case consists on electromagnetic plane wave scattering over a metallic PBG [12] structure described by Tarot *et al.* in [31] (see Figure 30a). The structure presents three layers of scatterers for the x -direction and an infinite number of layers for the y -direction. The z -dimension of the scatterers is also considered to be infinite, and for this reason, the TM_z mode is considered for executing 2-D simulations. The basic element of the metallic PBG structure is a perfect electrical conductor (PEC) cylinder with radius $a_1 = 0.5$ mm. The longitudinal period P_l is equal to the transverse period P_t ($P_l = P_t = 12$ mm). The area of analysis region with UPML is 24×160 mm, the time step is set to $\Delta_t = 2.5 \times 10^{-13}$ s, the minimum wavelength considered is $\lambda_{\min} = C_0/f_{\max} = 10$ mm, and the minimum distance among nodes $|\Delta_{\bar{x}\min}| = \lambda_{\min}/40 = 0.25$ mm.

A plane wave source was used as excitation, and the used pulse (Gaussian monocycle) is described by $p(t)$ given by (27), where $A_p = 1$ V/m, $\tau = 230 \times 10^{-13}$ s, $f_c = 10.085$ GHz (frequency of maximum spectral amplitude), $bw = 28$ GHz (3-dB upper frequency/bandwidth), $t_0 = 2250 \times 10^{-13}$ s, and t is the time. Figure 31 shows plots of the excitation pulse. Additional simulation parameters are shown in Table 2.

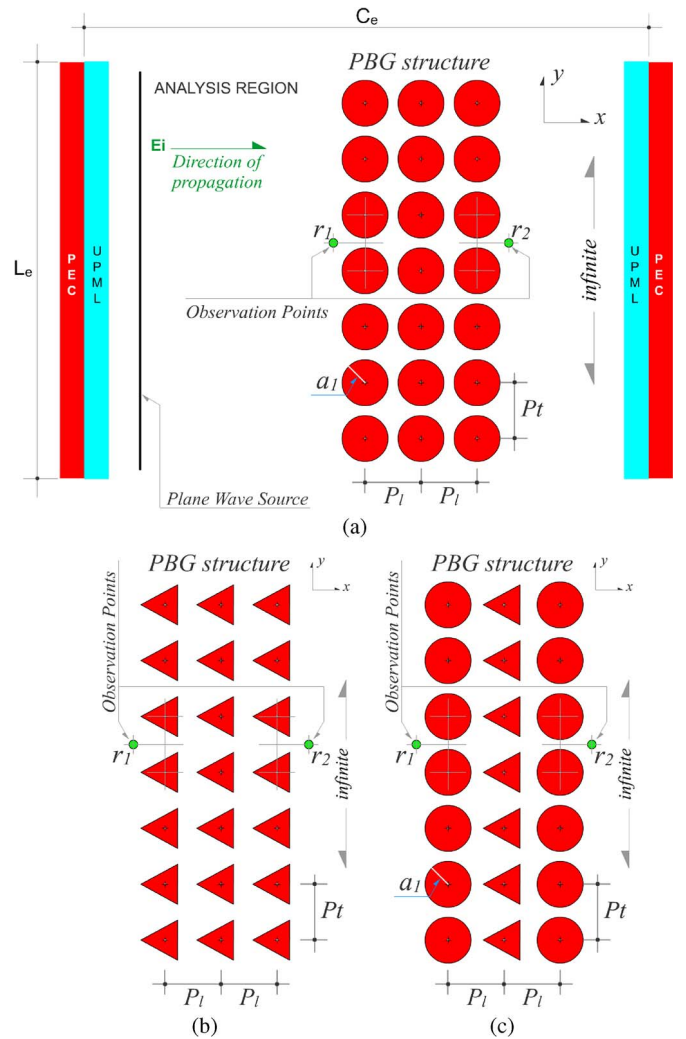


Figure 30. Cross sections. (a) Two-dimensional representation of the validation PBG structure (x - y plane) (validation case 3). (b) PBG filter with triangular cylinder as base-element (simulation 2). (c) Geometrically hybrid PBG filter (simulation 3).

Figure 32a shows comparisons of reflection coefficients, and Figure 32b compares transmission coefficients (both parameters were calculated by using FDTD, RPIM, and the analytic solution obtained by Tarot *et al.* in [31]). As shown in Figure 32, all over the analyzed band (from 2.0 to 20.0 GHz), the results obtained by using the RPIM with CLDM are closer to the

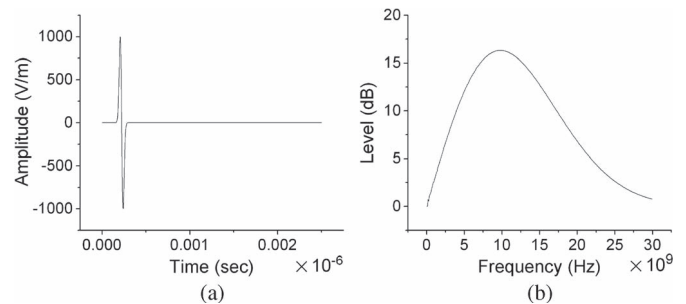


Figure 31. Gaussian monocycle pulse (validation case 3 and simulations 1, 2, and 3). (a) Time domain. (b) Frequency domain.

Table 2. Simulation parameters for validation case 3 and simulations 1, 2, and 3.

PARAMETERS	RPIM_CLDM	RPIM_Delaunay	FDTD
Size of analysis region + UPML = $L_e \times C_e$ (mm)	24×160	24×160	24×160
f_c (GHz) (central frequency of the excitation pulse)	11.085	11.085	11.085
dt (s)	2.5×10^{-13}	2.5×10^{-13}	2.5×10^{-13}
$\lambda_{min} = C_0/f_{max}$ (mm) (minimum wavelength)	10	10	10
$\Delta \bar{x}_{min} = \Delta x = \Delta y$ (mm) (minimum distance among nodes)	$\lambda_{min}/40$	$\lambda_{min}/40$	$\lambda_{min}/40$
Number of time steps	10000	10000	10000

analytical solution than the results calculated via the FDTD and RPIM with Delaunay mesh with the same discretization level due to improved discretization quality Q . Table 3 shows the total number of field components updated each time step, the total time required for concluding simulations, and the Q -parameter for validation cases 1–3, for each method employed. Although Delaunay-based meshes presented Q -factors greater than the reference value of 10^4 , results previously shown indicate that it is possible to improve Q if CLDM is used, as also shown in Table 3. Additionally, one should notice that it is not a straightforward process to obtain an unstructured mesh with $Q \geq 10^4$ because traditional meshing algorithms work with different quality parameters for distinct goals [9–11]. In this work, authors needed at least an entire day for producing such a mesh in a trial-and-error basis. With CLDM, about 10 min is required to produce the node set, with the automated procedure presented in this paper.

6. Hybrid PBG Filters

This section presents a study regarding RPIM with CLDM/LSFCM to design hybrid PBG filters. The filters to be synthesized and studied are made up of circular and triangular cylinders. In order to provide better understanding of the new hybrid structure, two additional cases are previously analyzed: a PBG structure with electrically large circular cylinders and a filter made up of triangular elements.

The simulations here have the same parameters of validation case 3 in Section 5.3. In simulation 1, the basic element's radius of the PBG structure was set to $a_2 = 2$ mm ($P_l = P_t = 12$ mm) (see Figure 30a). In simulation 2, a PEC triangular cylinder is used as base element of this PBG structure (see Figure 30b), and its cross section is an equilateral triangle of edge $l = 5.3871$ mm and area S_{triangle} equal to the circular cross section area S_{circle} of simulation 1. Finally, in simulation 3 (see Figure 30c), the two basic elements of the previous simulations (1 and 2) are used to create a hybrid PBG structure, which presents a geometrical longitudinal hybridization of elements. The signal propagation obtained by using RPIM methodology, for simulation 3 and validation case 3, is shown in Figure 34.

Figure 33 shows the spatial discretization obtained by using CLDM for discretizing the analysis region for simulation 3. It can be noted that CLDM's adaptiveness naturally allows modeling several different types of structures (with different geometrical configurations) in the same region, satisfying the discretization quality criteria previously stated. The spatial distribution of $|E_z|$ (total field) for validation case 3 is shown in Figure 34.

The results obtained via the CLDM/LSFCM/RPIM methods for validation case 3 are compared with those of simulations 1, 2, and 3. Figure 35a and b shows the reflection and transmission coefficients, respectively.

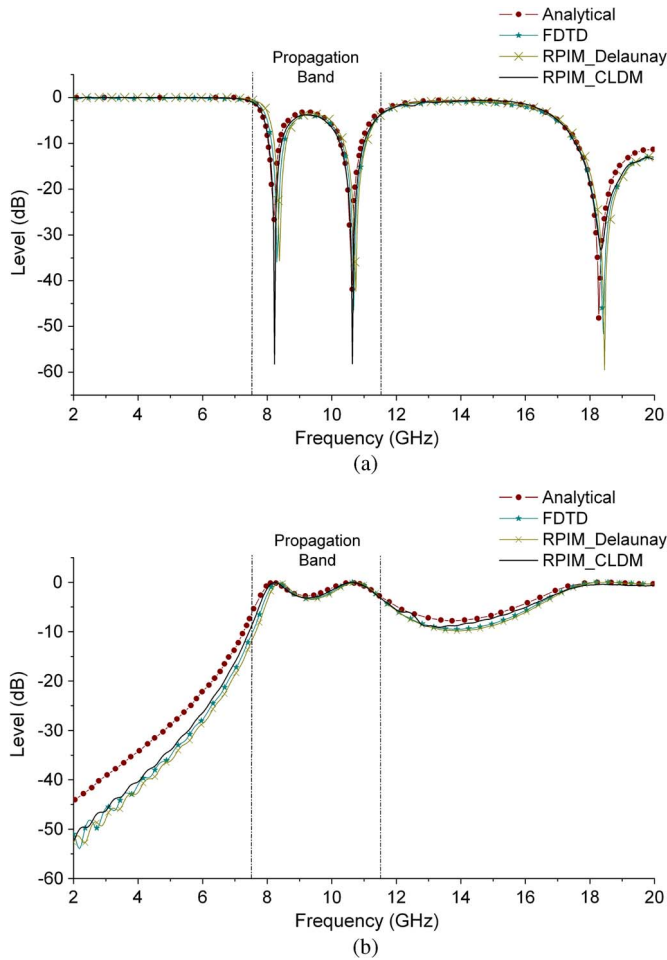


Figure 32. Scattering parameters for validation case 3. (a) Reflection coefficients (observation point: r_1). (b) Transmission coefficients (observation point: r_2).

Based on Figure 35a and b, we can make the following comments.

- 1) For simulation 1, the cylinder diameter was increased four times (if compared with validation case 3 scatterer), which caused the transmission band to shift from the range 7.5–11.5 to 11.5–14.0

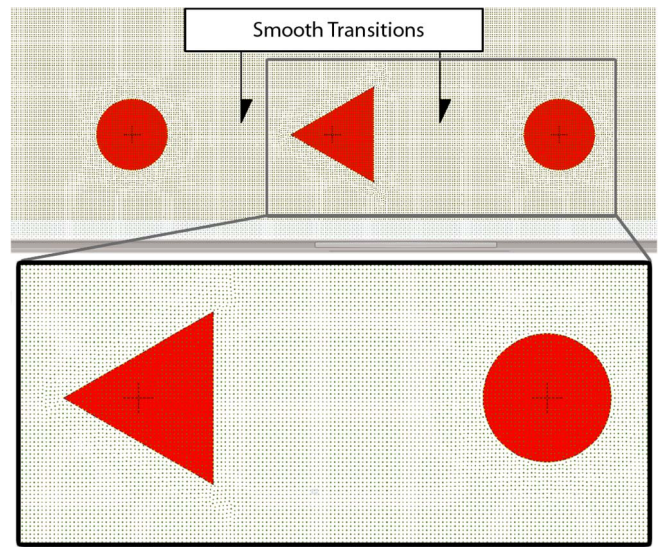


Figure 33. Spatial discretization of the region close to scatterers (simulation 3). Distribution of the nodes placed around the scatterers obtained by CLDM.

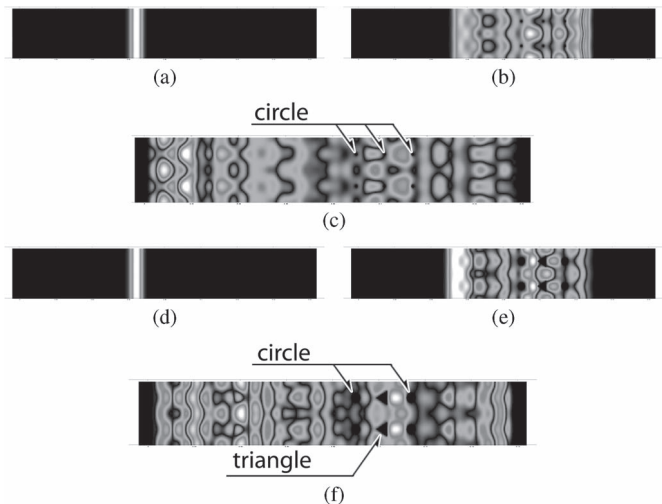


Figure 34. Spatial distribution of $|E_z|$ (total field) for validation case 3 [(a) $t = 0.4$ ns, (b) $t = 0.6$ ns, and (c) $t = 0.9$ ns] and for simulation 3 [(d) $t = 0.4$ ns, (e) $t = 0.6$ ns, and (f) $t = 0.7$ ns].

Table 3. Processing time and simulation conditions.

Simulation	Method	Proc. Time (s)	Field Componets	$Q/10^6$
Validation Case 1	FDTD	28.78	136383	—
	RPIM_CLDM	151.89	318227	6.214
	RPIM_Delaunay	152.79	319053	0.537
Validation Case 2	FDTD	28.76	136383	—
	RPIM_CLDM	151.88	318227	7.802
	RPIM_Delaunay	152.42	318458	0.993
Validation Case 3	FDTD	55.54	119886	—
	RPIM_CLDM	293.80	279734	5.745
	RPIM_Delaunay	294.62	280109	0.828

7. Conclusion

In this paper, a meshless discretization method, which is called Coulomb's Law Discretization Method (CLDM), has been introduced. The method is based on Coulomb's law, and virtual charges are used for performing spatial discretization. Basically, two groups of particles are set up: movable and unmovable charges. Unmovable particles are used to describe interfaces among different media to be simulated and to create a border region for avoiding particles to disperse from analysis domain. Movable particles are employed to create smooth transitions on discretization among the various objects immersed in space. The particle accommodation process (which produces force balance among particles) is obtained naturally by using Coulomb's law analytical dynamics. In order to assure numerical stability for RPIM, interpolation quality (as defined in this paper) is surveilled and improved by using LSFCM where necessary (local optimization of shape factor c) during the discretization process.

CLDM was applied successfully to problems involving electromagnetic scattering and PBG filters with complex geometries. High accuracy is observed for CLDM/LSFCM/RPIM when analytical solutions are used as reference because meshless geometric representation (by CLDM) is conformal, differently from FDTD grids, which suffers with the staircase approximation for nonrectangular structures. In addition, the precision of interpolations is improved by employing local optimization of c . Notice that, as shown in this paper, CLDM discretization node sets tend to be produced with higher discretization quality Q than Delaunay-based meshless. CLDM can be adapted for increasing the discretization level for specific regions of the numerical space. However, stability problems are presented by RPIM under these conditions, and further research is suggested for future improvements.

Circular and triangular contours have been used because of the availability of analytical solutions for 2-D scattering problems. However, CLDM is not restricted to basic shapes in geometry. As a proposal for future investigations, complex shapes (such as spirals and fractals) can be considered.

It is worth mentioning that the developed method is considerably simpler to implement than traditional unstructured meshing algorithms. Although about 10 min was necessary to produce the larger meshless domain in this work, on a single core of the 2.33-GHz Q8200 processor, it is important to notice that CLDM is highly parallelizable, a benefit that can tremendously reduce processing time if multicore processors or graphics processing units are used.

8. References

- [1] R. Gingold and J. Monaghan, "Smoothed particle hydrodynamics—Theory and application to non-spherical stars," *Monthly Notices Roy. Astron. Soc.*, vol. 181, pp. 375–389, Nov. 1977.

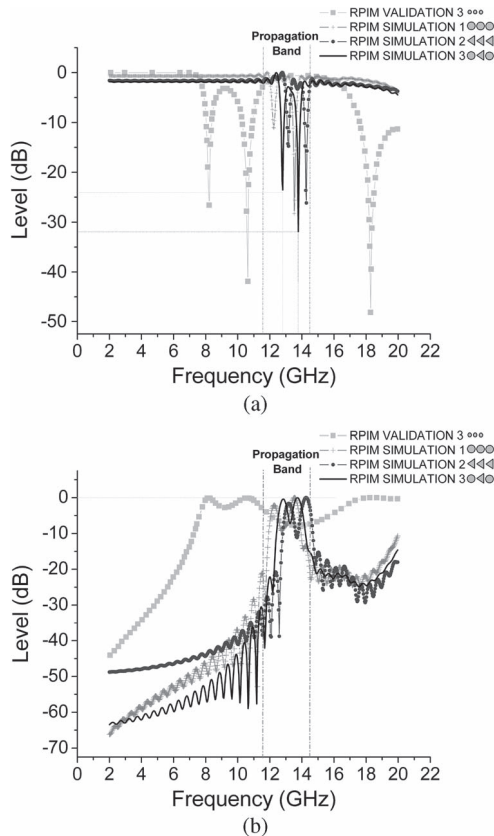


Figure 35. Comparison of results for validation case 3 and simulations 1, 2, and 3. (a) Reflection coefficients (observation point in r_1). (b) Transmission coefficients (observation point in r_2).

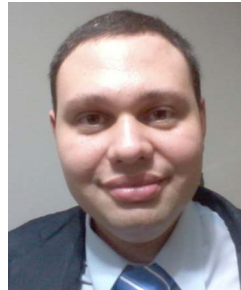
GHz. In practice, this occurred because the spacing among PEC cylinders was reduced. Furthermore, it was noted that the minimum reflection levels (shifted from 8.1 and 10.6 GHz to 12.3 and 13.5 GHz) increased from -26 and -42 dB to -11 and -27 dB, respectively.

- 2) For simulation 2, the substitution of circular cylinder by triangular cylinder (which preserves the cylinder area of simulation 1) caused the transmission band shift from 11.5–14.0 to 12.9–14.5 GHz. Furthermore, it is also noted that the minimum reflection levels (shifted from 12.3 and 13.5 GHz to 13.1 and 14.2 GHz) changed from -11 and -27 dB to -15 and -25 dB, respectively.
- 3) Finally, for simulation 3 (wherein triangles are alternated with circles), it was noted that the minimum reflection levels occur at frequencies 12.8 and 13.8 GHz, between the frequencies of minimal reflection levels obtained for simulations 1 and 2, which is expected physically. Furthermore, the reflection levels on these frequencies decreased to -24 and -50 dB, respectively. We emphasize that the reflection level for 13.8 GHz (simulation 3) is smaller than the one obtained by Tarot *et al.* in [31] for 10.6 GHz (validation case 3).


- [2] M. Xu, P. Thompson, and A. Toga, "Adaptive reproducing kernel particle method for extraction of the cortical surface," *IEEE Trans. Med. Imag.*, vol. 25, no. 6, pp. 755–767, Jun. 2006.
- [3] J. Bonet and S. Kulasegaram, "Remarks on tension instability of Eulerian and Lagrangian Corrected Smooth Particle Hydrodynamics (CSPH) methods," *Int. J. Numer. Methods Eng.*, vol. 52, no. 11, Dec. 2001.
- [4] G.-R. Liu and Y. Gu, "A point interpolation method," in *Proc. 4th Asian-Pac. Conf. Comput. Mech.*, Singapore, Dec. 1999, pp. 1009–1014.
- [5] J. G. Wang and G. R. Liu, "Radial point interpolation method for elastoplastic problem," in *Proc. 1st Int. Conf. Struct. Stability Dyn.*, Taipei, Taiwan, Dec. 2000, pp. 703–708.
- [6] Y. Yu and Z. Chen, "A 3-D radial point interpolation method for meshless time-domain modeling," *IEEE Trans. Microw. Theory Techn.*, vol. 57, no. 8, pp. 2015–2020, Aug. 2009.
- [7] P. L. Machado et al., "An automatic methodology for obtaining optimum shape factors for the radial point interpolation method," *J. Microw. Optoelectron. Electromagn. Appl.*, vol. 10, no. 2, pp. 389–401, 2011.
- [8] S. Lipschutz and M. Lipson, *Schaum's Outline of Discrete Mathematics*. New York, NY, USA: McGraw-Hill, 2007.
- [9] T. Hughes, *The Finite Element Method: Linear Static and Dynamic Finite Element Analysis*, 1st ed. New York, NY, USA: Dover, 2000.
- [10] P. P. Silvester and R. L. Ferrari, *Finite Elements for Electrical Engineers.*, 3rd ed. ed. New York, NY, USA: Cambridge, Univ. Press, 1996.
- [11] K.-J. Bathe, *Finite Element Procedures*, 1st ed. Englewood Cliffs, NJ, USA: Prentice-Hall, 1996.
- [12] A. Taflove and S. Hagness, *Computational Electrodynamics: The Finite-Difference Time-Domain Method*, 3rd ed. Artech House Antennas and Propagation Library, Norwood, MA, USA: Artech House, 2005.
- [13] Q. Du, M. Gunzburger, and L. Ju, "Meshfree, probabilistic determination of point sets and support regions for meshless computing," *Comput. Methods Appl. Mech. Eng.*, vol. 191, no. 13, pp. 1349–1366, 2002.
- [14] C. Nunes, R. Mesquita, and D. Lowther, "Remeshing driven by smooth-surface approximation of mesh nodes," *IEEE Trans. Magn.*, vol. 43, no. 4, pp. 1541–1544, Apr. 2007.
- [15] K. Shanazari and M. Hosami, "A two-dimensional adaptive nodes technique in irregular regions applied to meshless-type methods," *Eng. Anal. Boundary Elements*, vol. 36, no. 2, pp. 161–168, 2012.
- [16] L. P. Amorim, R. C. Mesquita, D. Burgarelli, and N. Z. Lima, "Point cloud generation for meshless methods," in *Iberian Latin American Congress On Computational Methods In Engineering*, 2011.
- [17] A. Okabe, B. Boots, K. Sugihara, and S. N. Chiu, *Spatial Tessellations - Concepts and Applications of Voronoi Diagrams*, 2nd ed. Hoboken, NJ, USA: Wiley, 2000.
- [18] J. Shewchuk, *Delaunay Refinement Mesh Generation*, 2nd ed. Hoboken, NJ, USA: Wiley, 2000.
- [19] G. Liu, *Meshfree Methods: Moving Beyond the Finite Element Method*, 2nd ed. Boca Raton, FL, USA: CRC Press, 2010.
- [20] J. G. Wang and G. R. Liu, "A point interpolation meshless method based on radial basis functions," *Int. J. Numer. Methods Eng.*, vol. 54, no. 11, pp. 1623–1648, Aug. 2002.
- [21] T. Kaufmann, C. Engstrom, C. Fumeaux, and R. Vahldieck, "Eigenvalue analysis and longtime stability of resonant structures for the meshless radial point interpolation method in time domain," *IEEE Trans. Microw. Theory Techn.*, vol. 58, no. 12, pp. 3399–3408, Dec. 2010.
- [22] C. Balanis, *Advanced Engineering Electromagnetics*. Hoboken, NJ, USA: Wiley, 1989.
- [23] S. Gedney, "An anisotropic perfectly matched layer-absorbing medium for the truncation of FDTD lattices," *IEEE Trans. Antennas Propag.*, vol. 44, no. 12, pp. 1630–1639, Dec. 1996.
- [24] M. N. Sadiku, *Elements of Electromagnetics*, 5th ed. London, U.K.: Oxford Univ. Press, 2009.
- [25] J. Har and K. Tamma, *Advances in Computational Dynamics of Particles, Materials and Structures*, 1st ed. London, U.K.: Wiley, 2012.
- [26] M. Beatty, *Principles of Engineering Mechanics: Dynamics - The Analysis of Motion*, Mathematical Concepts and Methods in Science and Engineering. New York, NY, USA: Springer-Verlag, 2006, vol. 2.
- [27] S. Li and W. K. Liu, *Meshfree Particle Methods.*, 1st ed. New York, NY, USA: Springer-Verlag, 2007.
- [28] S. A. Viana, "Meshless methods applied to computational electromagnetics." Ph.D. dissertation, Univ. Bath, Somerset, U.K., 2006.
- [29] K. Yee, "Numerical solution of initial boundary value problems involving Maxwell's equations in isotropic media," *IEEE Trans. Antennas Propag.*, vol. 14, no. 3, pp. 302–307, May 1966.
- [30] K. Bavelis, "Finite-element time-domain modelling of cylindrical structures with a modal non-reflecting boundary condition," Ph.D. dissertation, Philos. Eng., School Eng., Univ. Warwick, Coventry, U.K., 2010.
- [31] A.-C. Tarot, S. Collardey, and K. Mahdjoubi, "Numerical studies of metallic PBG structures," *Progr. Electromagn. Res.*, vol. 41, pp. 133–157, 2003.



Washington César Braga de Sousa received the Bachelor's degree in computer science, the Bachelor's degree in electrical engineering, and the Master's degree in electrical engineering from Federal University of Pará (UFPA), Belém, Brazil, in 2003, 2008, and 2013, respectively. He is currently working toward the Doctoral degree at UFPA.



Rodrigo Melo e Silva de Oliveira was born in Brasília, Brazil, in 1980. He received the Bachelor's degree in electrical engineering and the Master's and Doctoral degrees from Federal University of Pará (UFPA), Belém, Brazil, in 2002, 2004, and 2008, respectively.

Since February 2008, he has been with the Institute of Technology (ITEC), UFPA, where he is currently a Professor and a Researcher. He has authored and coauthored about 80 technical publications regarding the application of computational electro-dynamics to model complex structures, optimization techniques, and numerical methods. 

Capítulo 4

Artigo 2 - *Electric Charge Gaussian*

Gradation Method (ECGGM): a technique for improving material interface representations for the radial point interpolation method


International Journal of Numerical Modelling, 2017;

e2303.

<https://doi.org/10.1002/jnm.2303>

QUALIS (CAPES): B1

Electric Charge Gaussian Gradation Method (ECGGM): A technique for improving material interface representations for the radial point interpolation method

Rodrigo M. S. de Oliveira  | Marcelo B. S. Brandão | Washington C. B. Sousa

Institute of Technology (ITEC), Federal University of Pará (UFPA), PO Box 8619, Belém, Pará 66073-900, Brazil

Correspondence

Rodrigo M. S. de Oliveira, Institute of Technology (ITEC), Federal University of Pará (UFPA), Belém, PO Box 8619, Pará 66073-900, Brazil.
Email: rmso@ufpa.br

Abstract

An improved meshless discretization methodology, based on the Coulomb's law discretization method, is introduced. With the presented improvement, it is possible to naturally and controllably increase the density of nodes around edges and corners of scatterers immersed in analysis space. This is achieved by gradually modifying node's charges across space according to Gaussian functions. It is observed that higher concentration of nodes in the neighborhood of media interfaces substantially improves the precision of numerical solutions of Maxwell's equations obtained with the radial point interpolation method. This improvement is justified by refined calculation of intense spatial field variations near the boundaries. Several other relevant benefits resulting from the new technique are observed and highlighted.

KEYWORDS

Gaussian gradation of discretization levels and radial point interpolation method (RPIM), meshless discretization

1 | INTRODUCTION

Computer simulations of problems in electrodynamics are performed by using numerical methods, which are based on discrete versions of Maxwell's equations. Among these methods, we can emphasize techniques based on finite-difference time-domain (FDTD),^{1,2} finite element (FEM),^{3,4} and, more recently, on meshless methods. The meshless techniques, such as the radial point interpolation method (RPIM),⁵ have been increasingly used in applications related to electromagnetic problems^{6,7} not only because of the absence of predefined meshes and their intrinsic relatively simple mathematical formulations but also because of the high degree of geometrical compliance offered by such methods for representing nonrectangular objects. Besides, meshless methodologies tend to be computationally more efficient and precise than most FEMs for time-domain analysis.⁸

In 2011, a method for improving interpolation accuracy and robustness of RPIM was introduced by Machado and Oliveira et al. The referred technique is called local shape factor calibration method (LSFCM),⁹ with which one is able to optimize shape factors for each support domain in RPIM, allowing for the execution of electromagnetic simulations of cases requiring points to be positioned closer among each other in support domains than it was previously possible. In short, LSFCM is used to improve interpolation precision and the condition number of RPIM interpolation matrices, providing improved stability to RPIM simulations. In 2015, a meshless discretization approach was introduced by Sousa and de Oliveira,¹⁰ called Coulomb's law discretization method (CLDM). Space and objects immersed in it can be meshlessly discretized with CLDM, which is based on the idea of attributing for all the meshless discretization nodes a single (global) electric charge value. In CLDM, initially the discretization points are positioned using an FDTD mesh-based nodal

arrangement. Then, nodes neighboring media interfaces are instantaneously moved to the media boundaries. Finally, nodes not placed on the media borders are repositioned in space successively over time using an iterative process that uses the Newton's second law of motion excited by resultant Coulomb's electrostatic forces. This way, one can produce conformal discretization node sets with CLDM and perform full-wave analysis using Maxwell's equations discretized with RPIM.

As detailed on chapter 11 of Taflove and Hagness,² substantial spatial variations of electromagnetic fields are observed near corners and edges of objects in analysis region. For solving this problem with CLDM and RPIM, increasing spatial resolution on entire numerical space would be required. Thus, in this work, we develop for the first time a meshless discretization technique for defining gradual transitions of discretization levels. The discretization transitions are performed outwardly the objects, in such a way that node set density is gradually reduced from the scatterers boundaries to their surrounding space (where coarser distribution of nodes is formed). This technique produces substantial overall improvement of results because node density can be increased only for regions where electromagnetic field presents major spatial variations. This is accomplished by implementing, in CLDM, transitions of discretization nodes electric charges magnitudes from the material interfaces to their immediate neighborhood. The proposed gentle charge transition is based on a spatial Gaussian distribution centered at media interfaces. The method developed in this work, named Electric Charge Gaussian Gradation Method (ECGGM), has 2 key advantages over the original CLDM: (1) improved calculation accuracy for RPIM (MRE of about 5% over analytical solutions was observed) and (2) increased discretization level (number of nodes) only near the interfaces, avoiding high density of points over the entire analysis region, thus distinguishably reducing calculation time and memory requirements for RPIM and CLDM for a given precision level.

2 | THEORETICAL BACKGROUND: THE CLDM

In 2015, Sousa and de Oliveira developed in their study¹⁰ a methodology of meshless spatial discretization for RPIM, which is based on 3 classical laws in physics: the Coulomb's law, Newton's second law of motion, and the minimum potential energy principle. In CLDM, the vector form of Coulomb's law, given by

$$\vec{F}_{1,2} = \frac{1}{4\pi\epsilon_0} \frac{q_1 q_2}{|r_{1,2}|^3} \vec{r}_{1,2}, \quad (1)$$

is used in such a way that all nodes in the analysis domain are considered to have a global parameter: electric charge. The nodes are classified as movable and unmovable. The unmovable nodes are those positioned precisely at the interface among different media and, thus, define the geometric features of interest.

In this paper, the two-dimensional transverse-magnetic mode with respect to z (TM $_z$) is considered. To begin the CLDM algorithm, nodes are uniformly distributed in the problem domain according to the reference nodal arrangement of Figure 1A, which is based on the FDTD grid illustrated by Figure 1B. For defining discretization of boundaries among

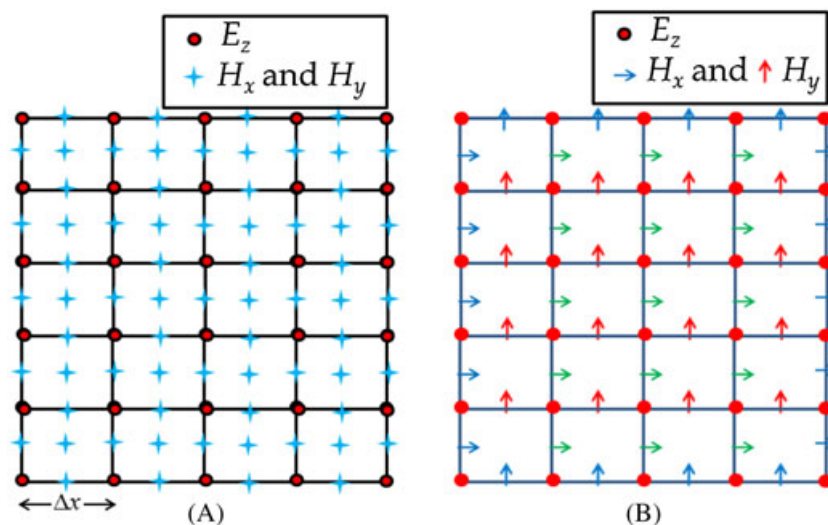


FIGURE 1 Representation of TM $_z$ mode: A, TM $_z$ reference nodal arrangement for radial point interpolation method and B, finite-difference time-domain grid

different media, the charges that are close to the media interfaces are, in a single step, instantaneously moved to scatterers boundary lines and converted into unmovable nodes. This procedure disrupts the force balance originally caused by the structured rectangular node placement. However, it is widely known from the superposition principle that the resultant force \vec{F}_{Ri} on a particle i is given by

$$\vec{F}_{Ri} = \sum_{j=1}^n \vec{F}_{i,j}, j \neq i. \quad (2)$$

The application of \vec{F}_{Ri} given by (2) as force source for Newton's motion equation for each movable charge i gradually tends to restore the force balance among the discretization nodes after successive temporal iterations of Newton's law. As a consequence, a conformal minimum potential energy¹⁰ particle distribution tends to be produced, as predicted by Newton's classical model.

From Newton's second law of motion, the resultant force \vec{F}_{Ri} acting on a particle i with mass m_s can be written as

$$\vec{F}_{Ri} = m_s \vec{a}_i = m_s \frac{\partial \vec{v}_i}{\partial T}. \quad (3)$$

Equation 3 can be approximated using the finite-difference method by

$$\vec{v}_i^T = \vec{F}_{Ri}^T \frac{\Delta T}{m_s} + \vec{v}_i^{T-\Delta T}, \quad (4)$$

where \vec{v}_i^T is the velocity of particle i at time T and ΔT is the time step of CLDM. The new particle position $\vec{x}_i^{T+\Delta T}$ can also be evaluated using the finite-difference technique and the definition of velocity. Mathematically, we have the approximation

$$\vec{x}_i^{T+\Delta T} = \vec{x}_i^T + \vec{v}_i^T \Delta T. \quad (5)$$

By using (4) and (5), we finally obtain the expression used to update the position of each particle i . It is given by

$$\vec{x}_i^{T+\Delta T} = \vec{x}_i^T + \left(\vec{F}_{Ri}^T \frac{\Delta T}{m_s} + \vec{v}_i^{T-\Delta T} \right) \Delta T. \quad (6)$$

For simplicity, it is assumed that $m_s = 1$ for all particles. In addition,

$$\Delta T = \frac{|\vec{\Delta}_{\vec{x}_{min}}^{T-\Delta T}| / |\vec{v}_{\vec{x}_{max}}^{T-\Delta T}|}{\Upsilon}, \quad (7)$$

where $|\vec{\Delta}_{\vec{x}_{min}}^{T-\Delta T}|$ is the minimum absolute distance among particles at $T - \Delta T$, $|\vec{v}_{\vec{x}_{max}}^{T-\Delta T}|$ is the maximum absolute particle velocity in the problem domain at $T - \Delta T$, and $\Upsilon \geq 10$ is a parameter used for ensuring stability for the particle interaction method.¹⁰ Observe that T is unrelated to RPIM time t .

This way, CLDM is based on 6 well-defined steps: (a) definition of a preliminary rectangular discretization for the analysis domain (as in a structured rectangular grid), (b) to attribute equal electric charges for all the meshless discretization nodes, (c) to define support domains for CLDM (aiming at computational performance), (d) to move and fix nodes originally placed in the immediate neighborhood of scatterers to the closest media interfaces, (e) to fix nodes surrounding analysis region for confining nodes inside the domain of interest, and (f) to use the discretized Newton's second law (6) for moving the nonfixed nodes and restore force balance, naturally producing a conformal discretization node set.

The main advantages of CLDM (specifically for RPIM) are the simplicity of its computer implementation, the uniformity of the obtained node distribution in the analysis region (and inside support domains), and smooth transitions of the conformal spatial discretization among geometrically different scatterers. The generated node set can provide low interpolation errors due to conformal distribution of nodes on boundaries' vicinity.

3 | THE ECGGM

Near corners and edges of scattering objects, field singularities are observed. Local discretization refinements for proper numerical field representation are frequently used with FDTD and FEM.^{2,4} For this reason, we have adapted CLDM for naturally and controllably increasing node density over the neighborhood of these boundaries.

For nonuniform FDTD grids, it is recommended by Taflove and Hagness² that the grid should not contain cells edges changing drastically in space: Discretization density should be gradually changed for avoiding large local errors. In our experiments with nonuniform RPIM meshless discretization, we see that if discretization density is changing too abruptly, reflections are seen in free space, which is obviously physically incorrect, or simulations diverge. Because RPIM interpolation is performed with support domains (differently of what is done in local FDTD field calculations, which are performed using information from immediate neighbor cells), discretization density must be scaled over space even more gently. These smooth transitions must also be seen inside the support domains. Gaussian scaling meets these requirements.

In the methodology proposed in this paper, named ECGGM, Gaussian functions are used to set the magnitudes of the charges. The spatial variation of charge values is calculated using the coordinates of the scatterer's centroid as reference, in such way that a minimum charge value q_{\min} is set up at the border of an auxiliary (virtual) circle, as pictured by Figure 2. These values are set prior to the execution of CLDM iterations using either

$$q_i = 1 - (1 - q_{\min})e^{-\frac{\rho^2}{2\sigma^2}} \quad (8)$$

or

$$q_i = q_{\min} - (q_{\min} - 1)e^{-\frac{\rho^2}{2\sigma^2}}, \quad (9)$$

where ρ is the distance from the centroid of the scatterer to any scatterer node. For all the analyzed cases, we defined $\sigma = 8\Delta x$, which is the radius of the CLDM support domain. The parameter Δx is the spatial step of the preliminary rectangular grid of Figure 1, which is also used for free space discretization. Notice that modifications of charge values are performed only for nodes belonging to the scatterer. This condition ensures higher density nodes around the scatterer's corners and edges in the medium surrounding the object.

Equation 8 was applied for the scatterer of Figure 2A, and (9) was applied for the scatterer of Figure 2B. Different Gaussian functions were used for different scatterers because of the existence of corners in Figure 2B, around which high densities of nodes are controllably stimulated. This propensity is justified by the fact that the reduction of charge values at the corners, apexes, and neighboring nodes in the scatterer reduces the repulsion forces from these nodes on the nodes in the medium surrounding the scattering object.

Once the charge values are properly set throughout the nodes of analysis domain, CLDM is used much as defined in Sousa and de Oliveira¹⁰ (or Section 2), for iteratively repositioning the nodes. Thus, the movable points start to converge to the region around the scatterer and to create not only smooth transitions among conformal warps on space discretization (as in CLDM) but also soft transitions among different discretization levels. The process goes on until the condition of minimum potential energy is reached for each node.

It is important to highlight that, differently of what is done in Sousa and de Oliveira,¹⁰ in this work, when any node reaches the scatterer's surface, it is converted to an unmovable point at the boundary. Nodes do not need to be (and are not) instantaneously moved and fixed at the media interface. This is possible exactly because the application of (8) or (9) breaks the electrostatic force balance among the nodes, which are initially distributed in a periodic collocation (Figure 1). The charge gradation spontaneously produces a controlled level of convergence of nodes to the outer neighborhood of

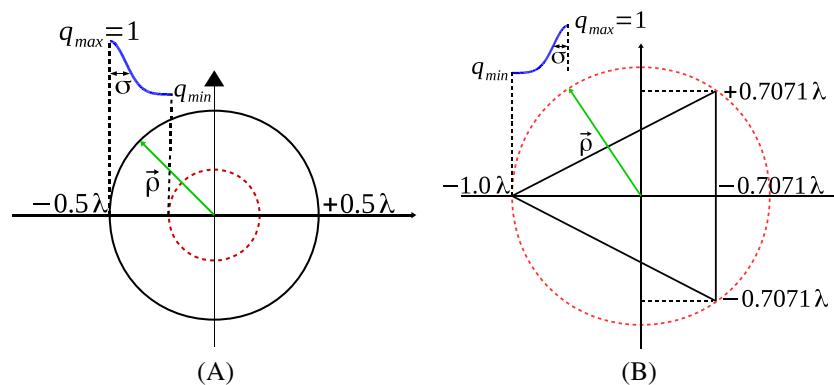


FIGURE 2 Perfectly conducting scatterers with charge reference at their centroids. The dashed red circle is over the virtual reference line where the Gaussian function reaches its minimum

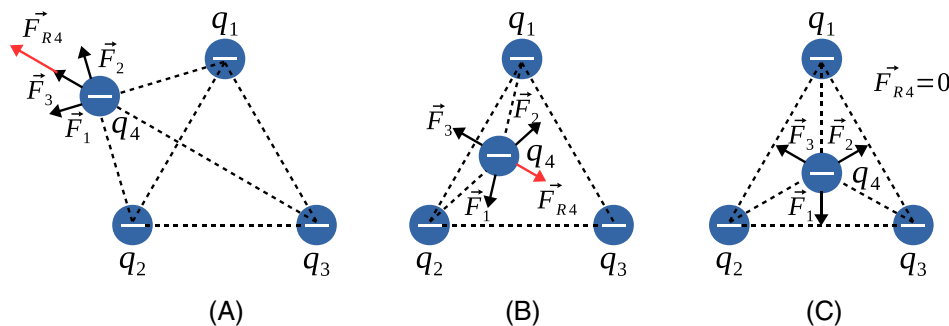


FIGURE 3 Resultant electric force in a system of four particles with equal charges. q_4 is the only a free node: A, when q_4 is initially positioned outside of triangle, F_{R4} pushes it away; B, charge q_4 is dragged by F_{R4} to the equilibrium point; and C, charge q_4 at the equilibrium point ($F_{R4}=0$)

TABLE 1 RPIM-ECGGM parameters for cases 1 and 2

RPIM-ECGGM parameters	Circular cylinder	Triangular cylinder
f , GHz	0.3	0.3
$\lambda = C/f$, m	1.0	1.0
Δx , m	$\lambda/20$	$\lambda/20$
Points used for RCS calculation	112	194
Number of time steps	6000	6000
Thickness of UPML, m	0.5	0.5

Abbreviations: ECGGM, Electric Charge Gaussian Gradation Method; RCS, radar cross section; RPIM, radial point interpolation method; UPLM, uniaxial perfectly matched layer.

the scatterers. The process can be tuned by modifying q_{\min} . This feature is important because it avoids the case illustrated by Figure 3A, which can take place near media interfaces using the unmodified CLDM if special care is not taken.¹⁰

Finally, an important feature must be discussed. Figure 1A shows the standard FDTD grid for the TMz mode. We see that the spatial coupling nature of electric and magnetic fields, as required by the curl operator, is properly characterized because every point at which the electric field is calculated is surrounded by points where magnetic field is computed (and vice versa).

Figure 1B shows the reference nodal arrangement that we have used to start the ECGGM algorithm. We observe that when ECGGM is applied, the charge gradation presented in the paper tends to maintain the distribution of nodes adequate to compute the curl operator for electric and magnetic fields near the boundaries of scatterers. Although the discretization level is increased near the media interfaces, the support domain radii are not reduced accordingly near the boundaries. Consequently, it is easier finding electric field nodes surrounding magnetic field nodes (and vice versa) in support domains near media interfaces. In CLDM, discretization levels are approximately constant all over the problem domain, and because it is difficult to preserve the reference nodal arrangement, instabilities may emerge.

4 | RESULTS AND DISCUSSION

To validate the proposed technique and quantifying its benefits, numerical experimentations are conducted by applying ECGGM for modelling the scatterers defined in Figure 2. RPIM interpolation is described in terms of Gaussian radial basis functions and polynomial basis of degree 1, such as described in Machado et al.⁹ Considering a constant magnitude for the shape factor c of the Gaussian basis usually does not lead to stable RPIM simulations for ECGGM node sets (the interpolation precision and the condition number of RPIM matrices are not favorable). For this reason, every support domain that had at least one node displaced by using ECGGM or CLDM had c optimized via the LSFCM technique.⁹ Precision of LSFCM calculations needs to be assured by means of 128 bits floating-point arithmetic. If this condition is not guaranteed in preliminary calculations, RPIM can diverge when using node distributions produced with ECGGM.

For all simulations performed using ECGGM-RPIM, we have $\Delta x = \lambda/20 = 0.05$ m. Every CLDM-RPIM-based simulation was also executed with $\Delta x = \lambda/20 = 0.05$ m. The RPIM computational domains are truncated by using an adapted

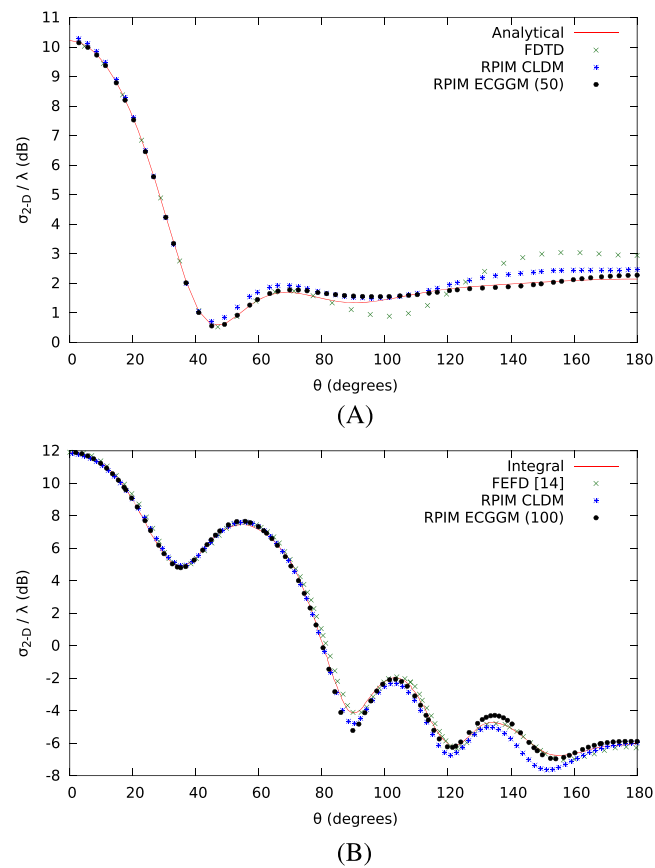


FIGURE 4 Radar cross section for A, circular (case 1) and b, triangular (case 2) cylinders. For all cases, $\Delta x = \lambda/20$. CLDM, Coulomb's law discretization method; ECGGM, Electric Charge Gradation Method; FDTD, finite-difference time-domain; FEFD, finite element frequency domain; RPIM, radial point interpolation method

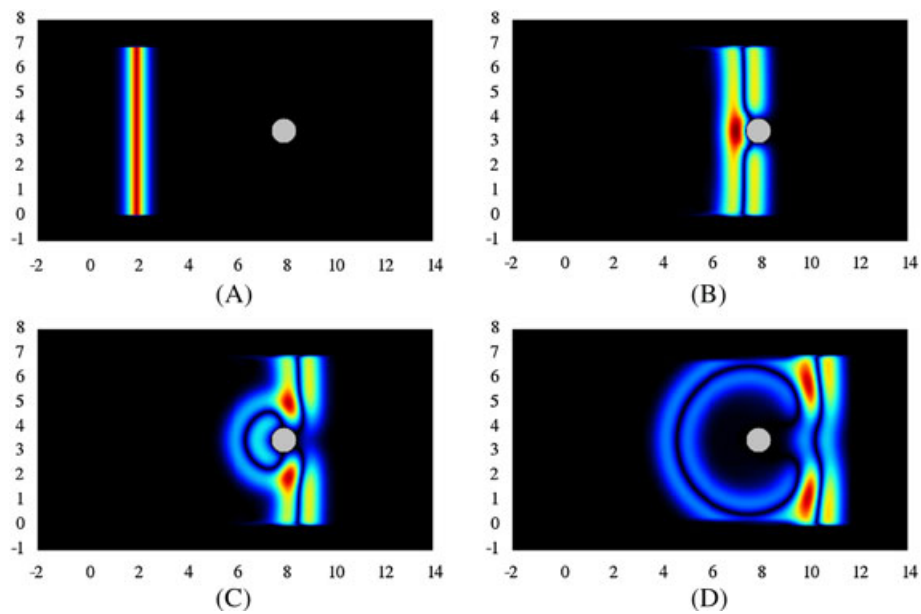


FIGURE 5 Spatial distributions of $|E_z|$ (total field) for the circular cylinder scatterer (case 1) for A, $t = 10.0$ ns; B, $t = 30.0$ ns; C, $t = 34.0$ ns; D, $t = 40.0$ ns. Spatial coordinates are given in meters

version of Gedney's uniaxial perfectly matched layer¹¹ for RPIM. An ultrawideband monocycle pulse¹² is used to excite a plane wave, which is scattered by the metallic objects. Parameters of all ECGGM-RPIM-based simulations are given in Table 1.

During the time loop of all RPIM simulations, transient electric field is registered at points distributed symmetrically around the scatterer. These signals are converted to frequency domain using discrete Fourier transforms considering $\lambda = 1$ m. Then, radar cross section (RCS)¹³ for the 2 scatterers was numerically calculated using the field line integrals given in Bavelis,¹⁴ for transforming near field to far field. Then, the Bavelis RCS-2D formulation, also given in Bavelis,¹⁴ was used. RCS curves obtained for all the cases subsequently described are given in Figure 4.

4.1 | Validation case 1—RCS for circular cylinder scatterer

The circular cylinder scatterer of Figure 2A was modelled with radius $r = 0.5\lambda$. RCS for that geometry has an exact analytical solution, which is given in Balanis.¹³ For this reason, this case was extensively explored in this work by tuning the parameter q_{\min} , defined in (8), in the interval $0.2 \leq q_{\min} \leq 0.9$ with a step of $\Delta q_{\min} = 0.1$. It is evident from (8) or (9) that $q_{\max} = 1$ (which is the charge used for nodes in the medium surrounding the scatterer).

For the sake of illustration, Figure 5 shows the spatial distributions of $|E_z|$, which is scattered by the circular conducting cylinder, for several values of t . Figure 4A shows RCS obtained for the circular scatterer using RPIM-ECGGM, FDTD (the finite-difference time-domain method)² and the analytical solution given in Balanis.¹³ To perform a fair comparison, the spatial step was set to $\lambda/20$ in the FDTD simulation. Ample numerical precision improvement is seen over FDTD and CLDM-RPIM for the entire angular range shown in Figure 4A when ECGGM-RPIM is used. Notice that the solution

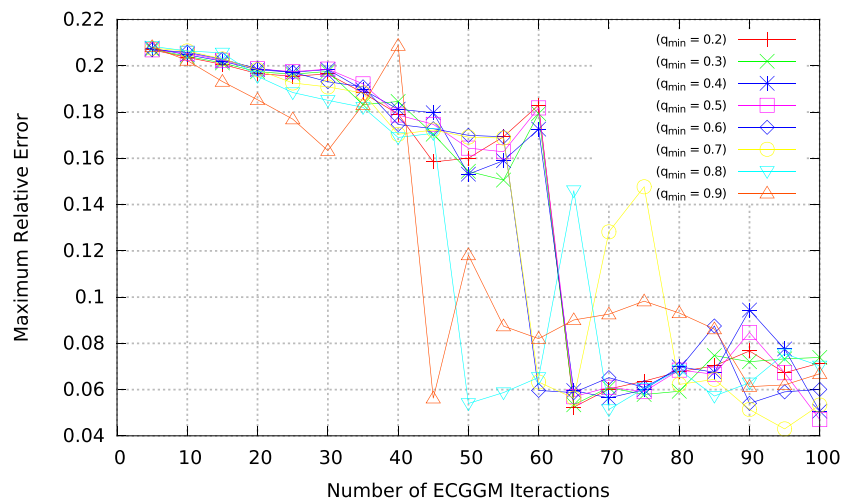


FIGURE 6 Maximum relative error for Electric Charge Gaussian Gradation Method (ECGGM) obtained for $0.2 \leq q_{\min} \leq 0.9$

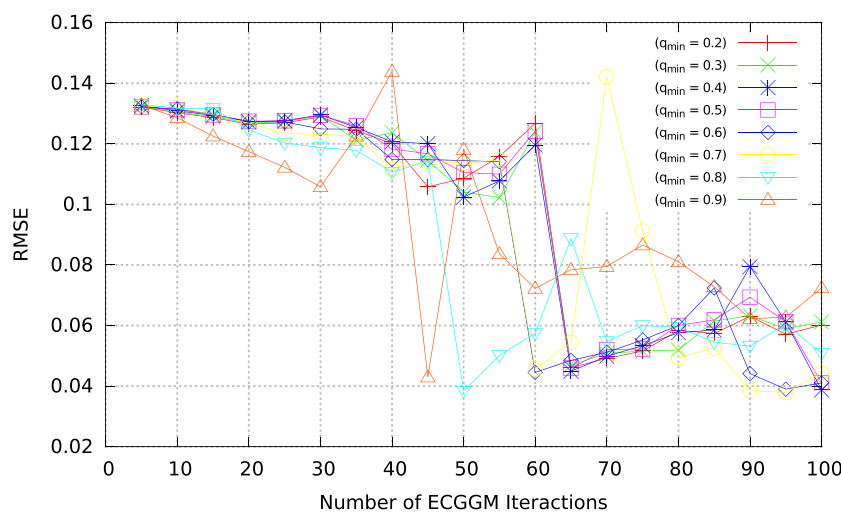


FIGURE 7 Root mean square error for Electric Charge Gaussian Gradation Method (ECGGM) obtained for $0.2 \leq q_{\min} \leq 0.9$

obtained with the proposed discretization methodology is almost identical to the analytical solution. A small deviation is seen for θ between 70° and 100° .

Figures 6 and 7 show the maximum relative error (MRE) and the root mean square error (RMSE) obtained for the circular cylinder RCS as functions of ECGGM iterations for several values of q_{min} . Each data point in Figures 6 and 7 is obtained by running a complete RPIM simulation. An important observation on both Figures is that for every value of q_{min} ,

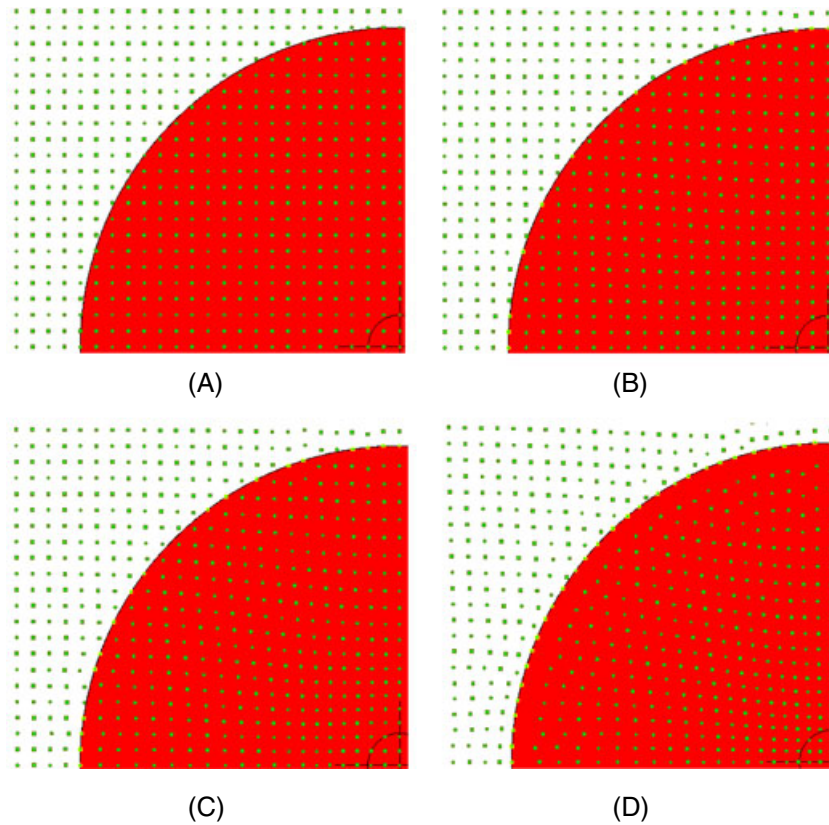


FIGURE 8 Application of Electric Charge Gaussian Gradation Method (ECGGM) for representing a circular scatterer (90° section) using $q_{min} = 0.8$. Repositioning of nodes after A, zero iterations (initial rectangular reference grid); B, 25 iterations; C, 50 iterations; and D, 100 iterations

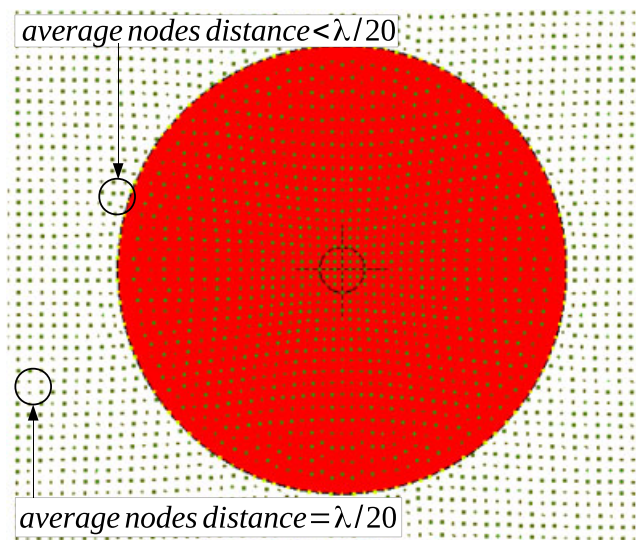


FIGURE 9 Electric Charge Gaussian Gradation Method discretization for the circular scatterer after 100 iterations using $q_{min} = 0.8$

MRE and RMSE tend to decrease as ECGGM iteration counting is increased. It is also noticed that for most values tested for q_{\min} , convergence is achieved after approximately 90 iterations, ie, error oscillates around a small average value from 90 iterations on. In addition, when $q_{\min} = 0.80$ is used, $MRE \approx 5\%$ and $RMSE \approx 0.04$ were obtained using 50 iterations. For this reason, RCS shown in Figure 4A and the spatial arrangements of points shown in Figure 8 were obtained for $q_{\min} = 0.80$. In contrast, the unmodified CLDM method requires about 150 iterations for obtaining converge for minimum error.¹⁰

An interesting remark is that the amount of nodes that are fixed at the media interfaces increases with the number of ECGGM iterations. For the case at hand, error converge for ECGGM was obtained when the amount of nodes that were set to be unmovable on the circular interface reached 76, which is equivalent to approximately 24.2 points per wavelength on the circular perimeter. This is related to the fact that the initial spatial increment produces 20 points per wavelength and final average separation of points neighboring the scatterer is about 24 points per wavelength (see Figure 9).

Table 2 shows numerical errors obtained using CLDM and ECGGM for Δx set to $\lambda/10$, $\lambda/20$, and $\lambda/30$. We see that ECGGM technique with $\Delta x = \lambda/20$ presents $MRE = 5.40$ and CLDM with $\Delta x = \lambda/30$ produces $MRE = 8.57$. Thus, we can say that ECGGM with 20 points per wavelength outperforms the numerical precision of CLDM with 30 points per wavelength. This is also true for the global error analysis, as RMSE indicates.

Processing times required for concluding RPIM simulations using both meshless discretization techniques are shown in Figure 10. Intel Xeon X5690 processor was used for executing the calculations in Slackware Linux 64 bits. For every

TABLE 2 Simulation parameters and numerical results for circular metallic scatterer RCS

Parameters	Circular cylinder (case 1)		
Δx , m (initial grid)	$\lambda/10$	$\lambda/20$	$\lambda/30$
f_c (GHz)	0.3		
$\lambda = C_0/f_c$, m	1		
Points used for RCS calculation	56	112	200
Number of points in analysis region	61004	185364	376924
Maximum Relative Error for ECGGM, %	18.85	5.40	3.41
Maximum Relative Error for CLDM, %	61.49	11.11	8.57
RMSE for ECGGM	0.1621	0.0383	0.04626
RMSE for CLDM	0.43500	0.1204	0.0650

Abbreviations: CLDM, Coulomb's law discretization method; ECGGM, Electric Charge Gaussian Gradation Method; RCS, radar cross section; RMSE, root mean square error.

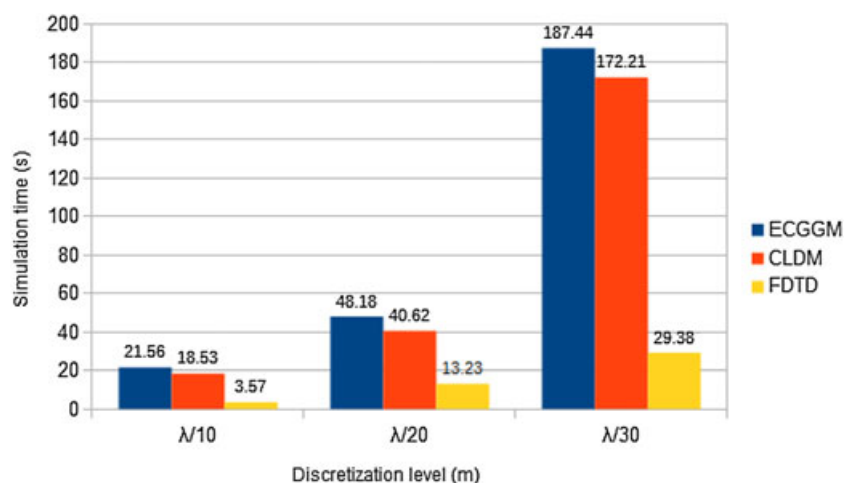


FIGURE 10 Radial point interpolation method processing time for spatial discretization performed with Electric Charge Gaussian Gradation Method (ECGGM) and Coulomb's law discretization method (CLDM)

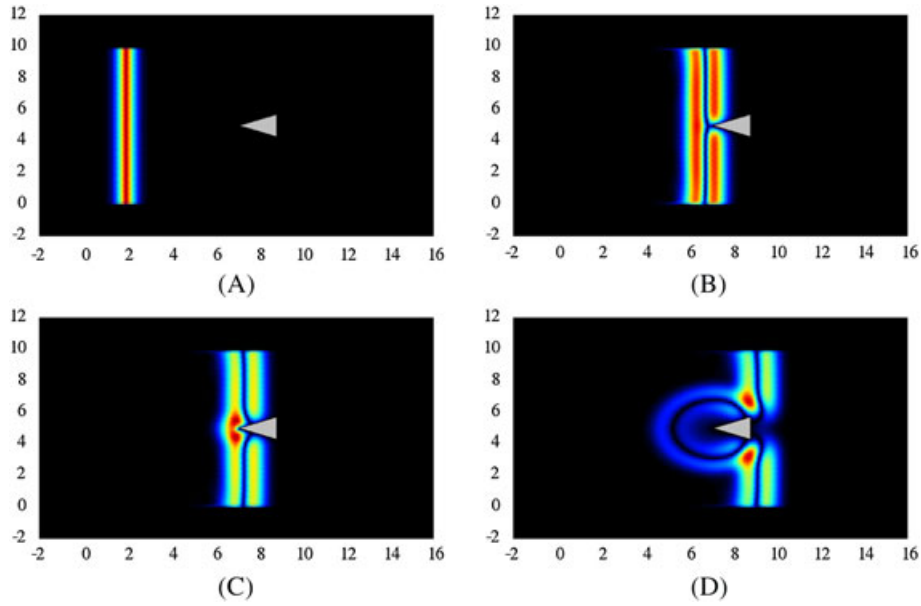


FIGURE 11 Spatial distributions of $|E_z|$ (total field) for the triangular cylinder scatterer (case 3) for A, $t = 10.0$ ns; B, $t = 28.0$ ns; C, $t = 30.0$ ns; D, $t = 36.0$ ns. Spatial coordinates are given in meters

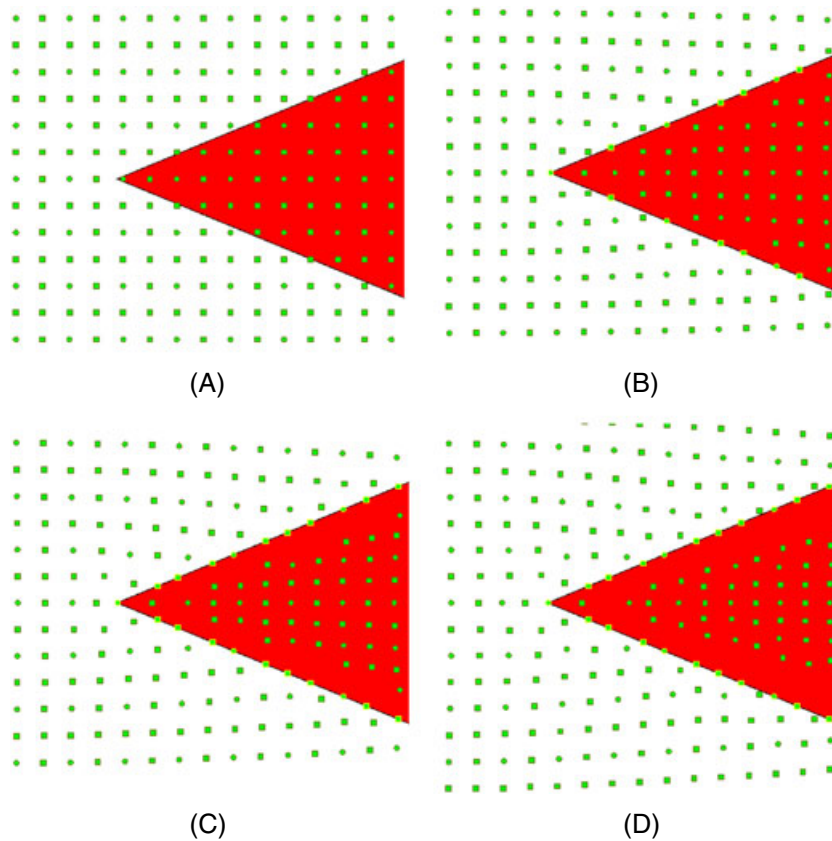


FIGURE 12 Electric Charge Gaussian Gradation Method discretization close to a corner of the triangular scatterer using $q_{min} = 0.9$ after A, zero iterations (initial rectangular reference grid); B, 25 iterations; C, 50 iterations; D, 100 iterations

case, it applied 99% of the Courant-Friedrichs-Lewy limit for defining the time step, which is mathematically given by

$$\Delta t = \frac{0.99}{v_{max} \sqrt{\frac{2}{\Delta_{min}^2}}} = 0.99 \frac{\Delta_{min}}{v_{max} \sqrt{2}}, \quad (10)$$

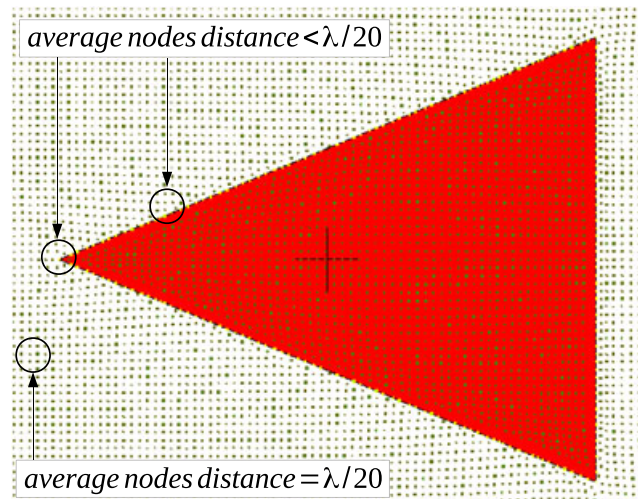


FIGURE 13 Electric Charge Gaussian Gradation Method discretization for the triangular scatterer after 100 iterations ($q_{min} = 0.9$)

where $\Delta_{min} = \min(\Delta_E, \Delta_H)$, Δ_E is the minimum distance among the points where electric field is calculated, and Δ_H is the minimum distance among the magnetic field nodes. Because ECGGM technique provides higher density of nodes around the scatterer, the time step given by (10) becomes smaller compared to CLDM time increment (for a given Δx). However, in Figure 10, one can observe that ECGGM with $\Delta x = \lambda/20$ requires 48.18 seconds of processing time. In the other hand, providing less accurate results, CLDM with $\Delta x = \lambda/30$ requires 172.21 seconds for concluding the RPIM simulation. This means that with the proposed meshless discretization method, one can substantially increase the numerical precision of RPIM with reduction of at least 78% on processing time.

4.2 | Validation case 2—RCS for triangular cylinder scatterer

In this case, the triangular scatterer shown in Figure 2B is modelled with ECGGM-CLDM method. The goal is to show that the proposed technique can provide substantial numerical precision improvements over CLDM for sharp geometries. The cross section of the analyzed scatterer is an isosceles triangle with base measuring $\sqrt{2}\lambda$ and its height measures $(1 + \sqrt{2})\lambda$. Figure 11 shows the spatial distribution of $|E_z|$ for various values of t .

To ensure symmetric distribution of nodes around the scatterer (Figures 12 and 13), the auxiliary circle used as minimum charge reference, which is illustrated in Figure 2B, is centered at the circumcenter of the isosceles triangle. For this case, calculations performed using the ECGGM-CLDM-RPIM method are compared with integral equations results calculated in Peterson and Castillo¹⁵ and finite element frequency domain (FEFD) results computed in Bavelis.¹⁴ Good agreement among the methods is seen in Figure 4B for all observation angles. It is important to notice that the results obtained with the methodology proposed in this paper bring substantial improvements over the results obtained with the original CLDM, as demonstrated by Figure 4B. Notice that $\Delta x = \lambda/20$ was used for the CLDM-RPIM simulation and for the ECGGM-RPIM calculations. Noteworthy differences from the reference RCS curve of the triangular scatterer are seen when CLDM-RPIM method is used. This improvement is attributed to the refined discretization obtained around the corners of the scatterer, which is visible in Figure 13 using $q_{min} = 0.9$.

The presented results show that ECGGM impacts positively in modelling sharp geometric shapes, such as corners, as long as substantial improvements were observed for the triangular scatterer over the results obtained in Sousa and de Oliveira¹⁰ with CLDM. Most important improvements were observed for $100^\circ \leq \theta \leq 180^\circ$.

5 | FINAL REMARKS

In this paper, we introduce a new technique called ECGGM, which is an important improvement on CLDM. With the proposed technique, it is possible to controllably increase the discretization level around borders and corners of scattering objects. This concentration of points around the interfaces among different media produces substantial improvements on numerical precision of RPIM because spatial variations of fields are more refinedly evaluated near these critical regions.

In addition, various other benefits are noticed when ECGGM is used. Among the several important advantages over the original CLDM technique, we have (1) remarkable improvement on field calculation precision when scatterers are present; (2) huge reduction of overall number of points in analysis domain in comparison with the original CLDM method for similar precision level; (3) reduced number of required CLDM iterations (from approximately 150 to about 50); (4) reduced processing time of each CLDM iteration, as long as the overall number of points is reduced; (5) drastic reduction of required processing time for RPIM simulations (at least 78%, considering the similar calculation precisions for the original CLDM and ECGGM); and (6) discretization of boundaries is naturally defined by fixing points as they cross the objects' borders (it is not necessary to have instantaneously moving points to scatterers' edges, as in the original CLDM for defining the boundaries) avoiding possible divergences in the discretization process for $0.2 \leq q_{\min} \leq 0.9$.

Scattering of plane wave for 2 metallic cylinders were simulated using FDTD and discretized using CLDM and ECGGM. The results obtained for the metallic circular cylinder (case 1) shows that the FDTD method produces a maximum relative error of 25.0% and a RMSE of 0.1996. For the original CLDM method, we have 11.11% and 0.1204, respectively, as shown in Figures 6 and 7. With respect to the exact solution, the results obtained using the ECGGM discretization method yield MRE and RMSE of around 5% and 0.0383, respectively, for a q_{\min} in [0.2,0.9] (see Figures 6 and 7), which clearly shows that ECGGM improves calculation precision for this problem. It is important to emphasize that ECGGM with 20 points per wavelength outperforms the numerical precision of CLDM with 30 points per wavelength.

In validation case 2 (triangular scatterer), the results obtained using the ECGGM-RPIM method were compared with results produced with the methods integral equations and FEFD. For the triangular scatterer, we see a huge agreement between FEFD and ECGGM-RPIM methods. Notice that this problem was simulated with ECGGM-RPIM and CLDM-RPIM using $\Delta x = \lambda/20$.

Numerical results show that the proposed discretization methodology (ECGGM), based on Gaussian charge gradation near boundaries, is adequate for properly representing edges and sharp corners for RPIM, providing relevant precision improvements to the original CLDM methodology. Undoubtedly, since discretization density changes smoothly in space, other charge gradation functions can be used, opening doors for producing further improvements in the future.

ORCID

Rodrigo M. S. de Oliveira  <http://orcid.org/0000-0001-7178-6387>

REFERENCES

1. Yee K. Numerical solution of initial boundary value problems involving Maxwell's equations in isotropic media. *IEEE Trans Antennas Propag.* 1966;14(3):302-307.
2. Taflove A, Hagness SC. *Computational Electrodynamics, The Finite-Difference Time-Domain Method*. 3rd ed. Boston, London: Artech House Inc.; 2005.
3. Dibben DC, Metaxas N. Frequency domain vs. time domain finite element methods for calculation of fields in multimode cavities. *IEEE Trans Magn.* 1997;33(2):1468-1471.
4. Polycarpou AC. *Introduction to the Finite Element Method in Electromagnetics*. 1st ed. Williston: Morgan & Claypool Publishers; 2006.
5. Wang JG, Liu GRs. A point interpolation meshless method based on radial basis functions. *Int J Numer Methods Eng.* 2002;54(11):1623-1648.
6. Yu Y, Chen Z. A 3-D radial point interpolation method for meshless time-domain modeling. *IEEE Trans Microwave Theory Tech.* 2009;57(8):2015-2020.
7. Afsari A, Movahhedi M. An adaptive radial point interpolation meshless method for simulation of electromagnetic and optical fields. *IEEE Trans Magn.* 2014;50(7):1-8.
8. Kaufmann T. The meshless radial point interpolation method for electromagnetics. *PhD Thesis*: ETH Zurich; 2011.
9. Machado PL, de Oliveira RMS, Souza WCB, Araújo RCF, Tostes MEL, Gonçalves C. An automatic methodology for obtaining optimum shape factors for the radial point interpolation method. *J Microw Optoelectron Electromagn Appl.* 2011;10:389-401.
10. Sousa WCB, de Oliveira RMS. Coulomb's law discretization method: a new methodology of spatial discretization for the radial point interpolation method. *IEEE Antennas Propag Mag.* 2015;57(2):277-293.
11. Gedney SD. An anisotropic perfectly matched layer-absorbing medium for the truncation of FDTD lattices. *IEEE Trans Antennas Propag.* 1996;44(12):1630-1639.
12. Farias RG, Dmitriev V, de Oliveira RMS. Application of particle swarm optimization to ultra-wideband multistatic radar used for protection of indoor environment. In: *Microwave and Optoelectronics Conference, 2007. IMOC 2007. SBMO/IEEE MTT-S International; 2007; Salvador.* 822-826.
13. Balanis CA. *Advanced Engineering Electromagnetics*. Hoboken: Wiley; 2012.

14. Bavelis K. Finite-element time-domain modelling of cylindrical structures with a modal non-reflecting boundary condition. *PhD Thesis: School of Engineering, University of Warwick*; 2010.
15. Peterson AF, Castillo SP. A frequency-domain differential equation formulation for electromagnetic scattering from inhomogeneous cylinders. *IEEE Trans Antennas Propag*. 1989;37(5):601-607.

How to cite this article: de Oliveira RMS, Brandão MBS, Sousa WCB. Electric charge gaussian gradation method (ECGGM): a technique for improving material interface representations for the radial point interpolation method. *Int J Numer Model*. 2017;e2303. <https://doi.org/10.1002/jnm.2303>

Capítulo 5

Artigo 3 - *A Meshless Discretization*

Methodology Based on Lennard-Jones Forces

IEEE ANTENNAS AND WIRELESS PROPAGATION LETTERS, VOL. 16, 2017

QUALIS (CAPES): A1

A Meshless Discretization Methodology Based on Lennard-Jones Forces

Rodrigo M. S. de Oliveira, Washington C. B. Sousa, and Wilson R. M. Rabelo

Abstract—A meshless discretization methodology based on the Lennard-Jones force is presented. The new methodology, named Lennard-Jones discretization method (LJDM), can be seen as an enhancement of Coulomb's Law discretization method (CLDM). Because CLDM is based on the repulsive Coulomb's forces, it can produce conformal discretization node sets with soft transitions in the space surrounding geometrically different objects. However, in CLDM, reference nodal arrangement (RNA) can be drastically modified, making it difficult to deterministically define a stop criterion and convergence using an invariable set of values for free parameters. This problem is solved in this letter by employing an adapted version of the Lennard-Jones vector force, which is a composition of repulsive and attractive contributions. The main role of attractive forces is preserving RNA, while repulsive forces produce conformal discretization. Analysis of simulation error as function of LJDM and CLDM iterations shows that the inclusion of attractive forces makes LJDM superior to CLDM because convergence and stability are found to be assured for constant sets of free parameters over the discretization iterations.

Index Terms—Lennard-Jones (LJ) forces, meshless discretization, molecular dynamics, radial point interpolation method (RPIM).

I. INTRODUCTION

NUMERICAL methods are powerful tools for modeling electromagnetic phenomena governed by Maxwell's equations. Among these methods, we can highlight techniques based on the finite-difference time-domain method (FDTD) [1], finite element methods [2], and the recent meshless (or mesh-free) techniques, such as the radial point interpolation method (RPIM) [3]. Meshless methods have received increasing attention in recent years, not only due to the absence of predefined meshes, but mainly because they enable accurate numerical representation of nonrectangular geometries (with high degree of geometrical compliance) for efficiently solving partial differential equations in time domain.

In terms of spatial discretization for meshless methods, the most common approaches in the literature are based on Delaunay triangulation or the Voronoi diagram [3], in which the set of nodes is extracted from unstructured meshes. In 2015, Sousa and Oliveira published a purely meshless discretization method called Coulomb's law discretization method (CLDM) [4], which

uses the repulsion among charges to generate a balanced distribution of nodes in space. When subjected solely to repulsive forces, the node set Ω behaves as a cloud of electrons. Although this physical system favors conformal meshless discretization and soft discretization transitions among geometrically different objects, it does not automatically favor the maintenance of an acceptable level of preservation of the reference nodal spatial arrangement (RNA), which is the local geometric configuration defining relative positions of nodes where electric and magnetic fields are calculated. With manual tuning of parameters during the CLDM discretization process, keeping RNA can be achieved in a nondeterministic way (it can be subjectively attained with user experience). As a consequence, without the periodic adjustment of parameters, instabilities can occur after a certain number of CLDM iterations, making it difficult to accurately define a stop criterion. In this context, as far as electrostatic interactions cannot account for all of the nonbonded particle interactions in physical system, the main objective of this letter is to propose an improved meshless discretization method based on the Lennard-Jones (LJ) potential [5], which is written in its general form as

$$u(r) = k\epsilon \left[\left(\frac{\sigma}{r} \right)^n - \left(\frac{\sigma}{r} \right)^m \right]. \quad (1)$$

In (1), $k = \frac{n}{n-m} \left(\frac{n}{m} \right)^{m/(n-m)}$, σ is the collision diameter, ϵ is the intensity of the interaction, and r is the distance of separation between atoms. This model is widely used in molecular dynamics. For example, liquid argon was modeled using this potential with a high degree of success [5]. A particle system regulated by the LJ potential can be in solid, liquid, or gaseous states, i.e., the attractive force of the potential is used to bind the system in the solid and liquid states, and the repulsive force prohibits collapse. In this work, the repulsive portion of the LJ force prevents the particles (nodes in Ω) from getting too close together, whereas the attractive contribution *automatically* prevents particles to break the desired nodal arrangement. These two parts work together to guarantee a stable connection among the particles (nodes) in Ω and to produce conformal meshless discretization. Thus, the method developed in this letter, named LJ discretization method (LJDM), can be seen as an improvement over CLDM.

II. THEORETICAL BACKGROUND

A. LJ Potential

In classical molecular modeling [5], a molecular system is represented by a collection of atoms held together by rigid or semirigid bonds. Usually, very small compact molecules are

Manuscript received October 19, 2016; revised December 24, 2016; accepted December 28, 2016. Date of publication December 30, 2016; date of current version June 5, 2017.

The authors are with the Department of Electrical Engineering, Federal University of Pará, Pará 66055-050, Brazil (e-mail: rmso@ufpa.br; csaksousa@gmail.com; rabelo@ufpa.br).

Color versions of one or more of the figures in this letter are available online at <http://ieeexplore.ieee.org>.

Digital Object Identifier 10.1109/LAWP.2016.2647198

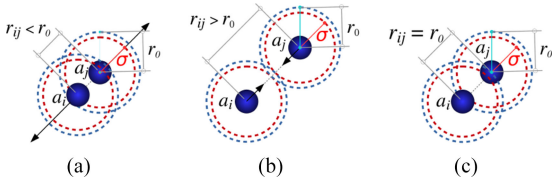


Fig. 1. LJ forces acting on a pair of interacting atoms: (a) $r_{ij} < r_0$ (repulsion); (b) $r_{ij} > r_0$ (attraction); and (c) for $r_{ij} = r_0$, $\vec{F}_{ij} = \vec{F}_{ji} = 0$.

modeled as rigid structures, and the interaction between atoms a_i and a_j is governed by a potential defining all forces acting between these atoms. In this context, a simple LJ potential is used to model van der Waals attraction and Pauli's repulsion forces. The original form of the LJ potential [5] is obtained using $n = 12$ and $m = 6$ in (1), where $r = r_{ij}$ is the distance between atoms a_i and a_j . The conservative force \vec{F}_{ij} that a_j exerts on a_i can be completely described as $\vec{F}(r_{ij}) = -\nabla u$. Thus, the force associated with the original LJ potential form is given by

$$\vec{F}_{ij} = \left[\left(\frac{A_{ij}}{r_{ij}^{12}} \right) - \left(\frac{B_{ij}}{r_{ij}^6} \right) \right] \vec{r}_{ij} \quad (2)$$

where $\vec{r}_{ij} = \vec{x}_i - \vec{x}_j$, $r_{ij} = |\vec{r}_{ij}|$, \vec{x}_k is the point vector defining the position of atom a_k in three-dimensional (3-D) space, $A_{ij} = 12\epsilon(r_0)^{12}$, $B_{ij} = 12\epsilon(r_0)^6$, $r_0 = 2^{\frac{1}{6}}\sigma = (A_{ij}/B_{ij})^{\frac{1}{6}}$, and finally $\epsilon = \epsilon_{ij} = B_{ij}/[12(r_0)^6]$. The distance separating a_i and a_j producing $\vec{F}_{ij} = 0$ is given by $r_{ij} = r_0 = (r_0)_{ij}$. Thus, attractive and repulsive forces in (2) can produce: 1) repulsion, Fig. 1(a), when $r_{ij} < r_0$; 2) attraction, Fig. 1(b), provided that $r_{ij} > r_0$; and 3) equilibrium state, Fig. 1(c), for $r_{ij} = r_0$.

For the case where there are a set of N atoms (a_1, a_2, \dots, a_N) , the total force \vec{F}_i on the atom a_i is given by the superposition principle [5]. Mathematically, we have

$$\vec{F}_i = \sum_{j=1}^N \vec{F}_{ij}, \quad \text{for } j \neq i. \quad (3)$$

Global equilibrium state is obtained when $\sum_{i=1}^N |\vec{F}_i| \rightarrow 0$.

B. LJ Forces in Complex Molecular Structures

The concepts discussed so far concerning the LJ force are general and can be applied to interactions of complex (poly-atomic) molecular structures. Therefore, it is necessary to understand that the molecular interactions can be classified in two groups: intramolecular interactions (forces \vec{F}^A holding together the atoms, making up molecules) and intermolecular interactions (forces \vec{F}^E holding molecules together). These forces are exemplified by using the illustrative model of Fig. 2, in which a molecule M_i is composed of four atoms a_1, a_2, a_3 , and a_4 associated with chemical elements I, J, K , and L . It is easy to see that \vec{F}_1^A (intramolecular force acting on a_1) is the result of the interactions of a_1 with all other atoms in M_i . Resultant intramolecular force is governed by (3) (superposition principle). This exact idea is also used for a system of two (or more) molecules M_c and M_d . It can be seen that intermolecular forces holding the molecules together result from the interaction

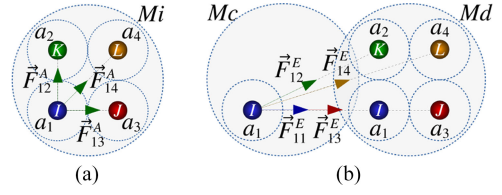


Fig. 2. Intramolecular interactions in M_i and intermolecular interaction between M_c and M_d : (a) Intramolecular force on atom a_1 (resulting in \vec{F}_1^A), (b) Intermolecular force on atom a_1 (resulting in \vec{F}_1^E).

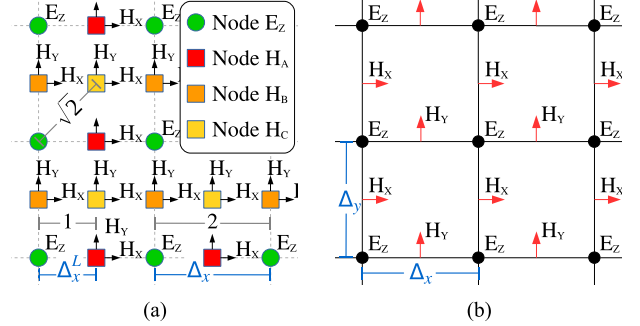


Fig. 3. Nodes and cells: (a) Ω_P and RNA for LJDM and (b) the Yee's grid.

among the elements $a_k \in M_c$ and $a_l \in M_d$. As it is illustrated by Fig. 2(b), total intermolecular force acting on $a_1 \in M_c$, due to elements in M_d , is given by $\vec{F}_1^E = \sum_{l=1}^4 \vec{F}_{1l}^E$.

It is of fundamental importance to notice that the parameters $(r_0)_{ij}$ and ϵ_{ij} are dependent on the chemical elements involved in the considered interaction. This means that parameters A_{ij} and B_{ij} in (2) are specifically calculated for each pair of atoms (which can be of different or equal chemical elements) for obtaining intramolecular or intermolecular forces [5].

III. LJ DISCRETIZATION METHOD

The meshless discretization method proposed in this letter (LJDM), similarly to CLDM, consists of four basic steps: 1) creation of preliminary domain (staggered distribution of electric and magnetic nodes); 2) definition of LJDM support domains $\Omega_{SL}(\vec{x}_i)$; 3) representation of media interfaces; and 4) iterative repositioning of nodes with progressive assessment of discretization quality. Specific details regarding each of the four steps in LJDM are given as follows.

1) *Preliminary Domain Creation*: The first stage of LJDM corresponds to the creation of a preliminary domain Ω_P , which consists on a staggered distribution of nodes in space, such as illustrated in Fig. 3(a). In Fig. 3(a), circular nodes represent points at which electric field is calculated. Nodes where magnetic field components are evaluated are presented by square nodes. These nodes are referred to in this letter as electric and magnetic nodes, respectively. Ω_P is based on the Yee mesh shown in Fig. 3(b). In order to assure initial force balance in Ω_P and to guarantee RPIM interpolation precision [4], magnetic nodes H_c are included at positions corresponding to the centers of Yee cells, as it can be seen in Fig. 3(a).

RNA is defined by the *relative positions* among nodes E_z, H_A, H_B , and H_C shown in Fig. 3(a), which tend to be

preserved within the iterations of LJDM due to attractive forces among the atoms. Naturally, due to repulsive forces, rotations of RNA come about in order to allow for conformal discretization, favoring electric nodes to be always surrounded by magnetic nodes (and vice versa).

In this letter, the global minimum distance [4] among nodes $\Delta_{\bar{x}_{\min}}^L$ is considered to be the minimum distance among electric and magnetic nodes in Ω_P . However, in order to perform LJDM iterations, all distances between every pair of nodes in Ω_P is normalized by $\Delta_{\bar{x}_{\min}}^L$. Therefore, $\Delta_{\bar{x}_{\min}}^L$ is considered to be one during the LJDM discretization process. Unmovable nodes around analysis region are set following [4].

2) *Definition of Support Domains*: The use of support domains $\Omega_{SL}(\bar{x}_i)$ in LJDM, for reducing computational costs during the discretization process, is feasible because \vec{F}_{ij} given by (2) is in essence inversely proportional to r_{ij}^8 for $r_{ij} > r_0$. Thus, for a given pair of atoms, the repulsive force obtained for $r_{ij} = 1$ is approximately 1526 times the force produced for $r_{ij} = 2.5$. Hence, we have set the radius of $\Omega_{SL}(\bar{x}_i)$ to $r_{SL} = 4\Delta_{\bar{x}_{\min}}^L$. This radius corresponds to half of the radius used in CLDM support domains, leading to an average reduction of 2/3 in the total amount of nodes in each support domain in comparison to CLDM.

3) *Repositioning of Nodes*: The discrete version of Newton's second law of motion, previously obtained in [4], is excited in this letter by LJ forces \vec{F}_i^T . LJ forces, calculated using (2) and (3), are used for displacing atoms (the RPIM nodes). Therefore, the position \bar{x}_i of a moving particle $p_i \in \Omega$ is calculated for time $T + \Delta T$ by

$$\bar{x}_i^{T+\Delta T} = \bar{x}_i^T + \left(\vec{F}_i^T \frac{\Delta T}{m_i} + \vec{v}_i^{T-\Delta T} \right) \Delta T \quad (4)$$

where $\Delta T = |\vec{\Delta}_{\bar{x}_{\min}}^{T-\Delta T} / \vec{v}_{\max}^{T-\Delta T}| / \Upsilon$. By successively applying (4) to each movable node $p_i \in \Omega$, minimum potential energy state tends to be reached. For LJDM, it was determined empirically that for $m_i = 1$, $\Upsilon = 30$ for ensuring stability for the iterative particle displacement procedure.

Aiming at RNA preservation, the parameters A_{ij} and B_{ij} in (2), for every pair of particles a_i and a_j , must take into account the specific values of $(r_0)_{ij}$ (obtained from RNA) and ϵ_{ij} due to specific chemical elements considered for nodes E_z , H_A , H_B , and H_C . For the considered RNA, Fig. 3(a) shows that $(r_0)_{ij} = 2$ for equal atoms separated horizontally or vertically. We also see that for different neighbor atoms separated horizontally or vertically, $(r_0)_{ij} = 1$. Finally, $(r_0)_{ij} = \sqrt{2}$ when neighbor atoms are separated along diagonals as indicated in Fig. 3(a). In order to accelerate convergence, mobility of nodes is increased by setting $(r_0)_{ij} = 2.2$ for E_z -nodes and by approximating $\sqrt{2}$ to 1.42. Values assumed by intensity of the interaction ϵ_{ij} have been optimized for the various pairs of interacting atoms in Fig. 3(a). For $E_z - E_z$ interactions, $\epsilon_{ij} = 2.4$. Additionally, we have: $\epsilon_{ij} = 0.3$ for $E_z - H_A$ and $E_z - H_B$; $\epsilon_{ij} = 1.0$ for $E_z - H_C$; $\epsilon_{ij} = 0.5$ for $H_A - H_C$ and $H_B - H_C$; $\epsilon_{ij} = 1.2$ for $H_A - H_A$, $H_B - H_B$, and $H_C - H_C$. Finally, $\epsilon_{ij} = 0.6$ for interactions between H_A and B_B .

4) *Progressive Definition of Media Interfaces*: In order to represent media interfaces, we introduce the concept progressive node displacement, in which the E_z -nodes in the

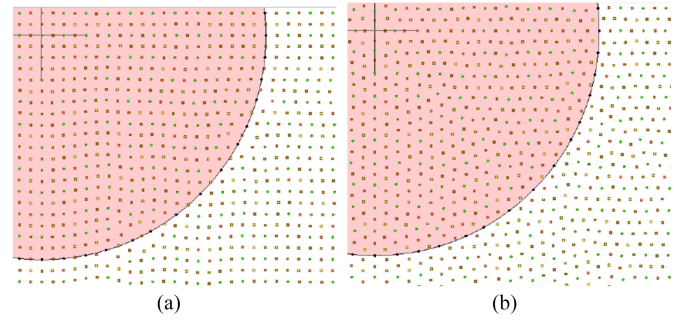


Fig. 4. Node distributions for representing the circular scatterer (90° section) after 200 iterations using $\delta_{dp} = 0.6$: (a) LJDM and (b) CLDM.

immediate neighborhood of a given media interface are gradually moved toward it. The progressive displacement is executed for a given node using the equation $\bar{x}_i^{T+\Delta T} = \bar{x}_i^T + \vec{\Delta}_{dp}$ for every LJDM iteration preceding the step at which the node intercepts the boundary. The progressive displacement vector is given by $\vec{\Delta}_{dp} = \frac{1}{100} \delta_{dp} \Delta_{\bar{x}_{\min}} \hat{a}_r$, where δ_{dp} is the progressive displacement factor and \hat{a}_r is the unit vector pointing from the displaced node to the nearest point of the interface. Via numerical experiments, we determined that $\delta_{dp} \leq 1.0$; otherwise, instabilities are seen in LJDM method. Once the progressively displaced node intercepts the boundary to which it is displaced, the node is fixed at the intercepting point at interface. Notice that all other nodes in Ω are moved using (4).

IV. RESULTS AND DISCUSSION

In order to validate the proposed technique, LJDM was applied for modeling the circular metallic scatterer, previously analyzed in [4]. For all simulations performed using LJDM-RPIM, CLDM-RPIM, and FDTD, we have $\Delta x = \lambda/20 = 0.05$ m (see Fig. 3) and $\Delta t = 2 \times 10^{-11}$ s. The monocycle pulse defined in [4] is used to excite a plane wave, which is scattered by the metallic object modeled with radius $r = 0.5 \lambda$. Ten-layer uniaxial perfectly matched layer [1] is used for truncating the analysis domain.

During the time loop of all RPIM simulations, transient electric field was registered at 112 points distributed symmetrically around the scatterer [4]. These signals are converted to frequency domain using discrete Fourier transforms considering $f = 300$ MHz. Then, radar cross section (RCS) [2], [6] for the scatterer was numerically calculated using the Bavelis RCS 2-D formulation and the field line integrals given in [2] for transforming near field to far field.

This scattering problem has an analytical solution, which is given in [6]. For this reason, this case was extensively explored numerically in this work by setting δ_{dp} in the interval $[0.2, 1.0]$ with steps of 0.2. Fig. 4(a) and (b) show part of the spatial discretization obtained by using LJDM and CLDM, respectively, after 200 iterations executed with $\delta_{dp} = 0.6$.

Fig. 5 shows RCS curves obtained by using LJDM-RPIM, CLDM-RPIM, RPIM with the rectangular node distribution of Fig. 3(a), FDTD, and the analytical solution given in [6]. Notice that the solution obtained with LJDM is the closest to the analytical solution. Small deviations are seen for θ between 60° and 100° and for $150^\circ \leq \theta \leq 180^\circ$.

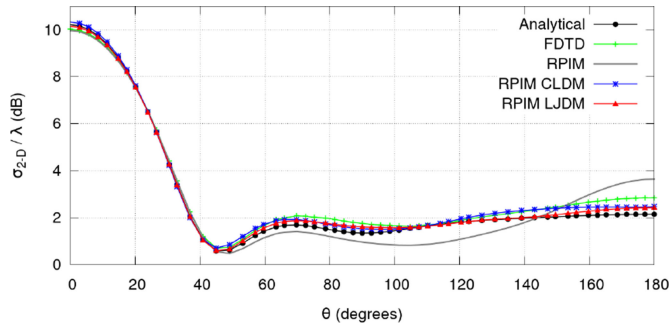


Fig. 5. RCS curves obtained for the circular scatterer using several methods.

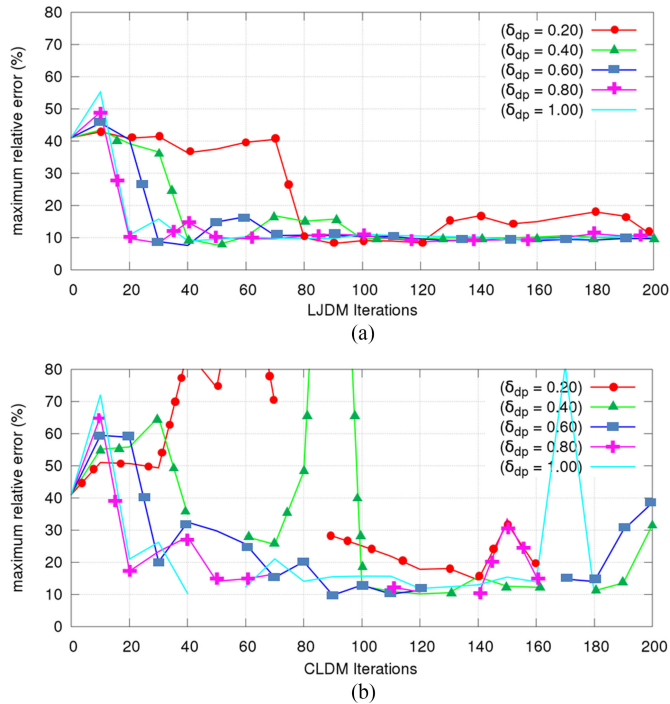
Fig. 6. MRE obtained for $0.2 \leq \delta_{dp} \leq 1.0$: (a) LJDM and (b) CLDM.

Fig. 6 clearly evinces the contribution of this letter. Fig. 6(a) and (b) shows the maximum relative error (MRE) obtained for the RCS of the circular cylinder as function of LJDM-RPIM and CLDM-RPIM iterations, respectively, for several values of δ_{dp} . Notice that every point in MRE curves is obtained with a full RPIM simulation. Using LJDM or CLDM, in both figures we see that MRE tends to decrease as iteration counting progresses. However, in Fig. 6(b) it is observed that CLDM produces discontinuous MRE curves, even when progressive displacement is employed with various values attributed statically to δ_{dp} . These discontinuities indicate that RPIM simulation diverged because RNA was completely decharacterized around at least a single node in Ω . As Fig. 6(b) indicates, it can be difficult to define a stopping iteration for CLDM.

On the other hand, Fig. 6(a) shows that LJDM produces continuous MRE functions for every value attributed to δ_{dp} . For the problem at hand, convergence is achieved in 70 iterations for $0.6 \leq \delta_{dp} \leq 1.0$. In addition, when $\delta_{dp} = 0.60$ is used, MRE is approximately 7% after 40 LJDM iterations. For this reason,

TABLE I
FEATURE COMPARISON BETWEEN LJDM AND CLDM

Method	Convergence	Nodes in Ω_S	Memory usage	Processing time
CLDM	Not assured	N_s	M	P
LJDM	Assured	$N_s/3$	$(2/5)M$	$0.95P$

RCS shown in Fig. 5 and the spatial arrangements of points shown in Fig. 4 were obtained for $\delta_{dp} = 0.60$.

In Fig. 6(b), $MRE \approx 9\%$ was obtained with $\delta_{dp} = 0.60$ after executing 90 CLDM iterations. However, RPIM diverged when more than 120 CLDM steps were executed because RNA was not preserved all over the domain. As it can be seen in Fig. 6(a), this problem is nonexistent when LJDM is used. If $0.40 \leq \delta_{dp} \leq 1.00$, convergence region is reached if at least 120 LJDM iterations are executed.

Finally, we show in Table I a feature comparison for the discretization processes based on CLDM and LJDM. These properties were statistically obtained based on executions of CLDM and LJDM for several 2-D discretization problems.

V. FINAL REMARKS

We introduced a new technique called LJ discretization method, which can be seen as an improvement of the CLDM. With the proposed technique, it is possible to generate domains with high-degree geometric compliance and smooth spatial discretization transitions among different geometries, and especially to maintain acceptable level of RNA preservation. Attraction forces are responsible for preserving RNA, which is held together because it is represented by a molecule stabilized by LJ forces while repulsive forces produce conformal discretization. Numerical experiments show that 200 LJDM iterations should be sufficient for achieving convergence to the optimized node distribution when $0.40 \leq \delta_{dp} \leq 1.00$. Also, we see that LJDM slightly improves precision over CLDM. For the analyzed problem, CLDM produces $MRE \approx 9.45\%$ and LJDM yields $MRE \approx 7.50\%$. Finally, it is observed that LJDM support domains contains approximately 1/3 of the amount of nodes in CLDM support domains, notably reducing computational memory usage and slightly shortening processing time of the discretization process.

REFERENCES

- [1] A. Taflov and S. Hagness, *Computational Electrodynamics: The Finite-Difference Time-Domain Method* (ser. Artech House Antennas and Propagation Library), 3rd ed. Norwood, MA, USA: Artech House, 2005.
- [2] K. Bavelis, "Finite-element time-domain modelling of cylindrical structures with a modal non-reflecting boundary condition," Ph.D. dissertation, School of Eng., Univ. Warwick, Coventry, U.K., 2010.
- [3] C. Fumeaux *et al.*, "Conformal and multi-scale time-domain methods: From unstructured meshes to meshless discretisations," in *Computational Electromagnetics-Retrospective and Outlook*, I. Ahmed and Z. Chen, Eds. New York, NY, USA: Springer-Verlag, 2015, ch. 6, pp. 139–165.
- [4] W. C. B. Sousa and R. M. S. Oliveira, "Coulomb's law discretization method: A new methodology of spatial discretization for the radial point interpolation method," *IEEE Antennas Propag. Mag.*, vol. 57, no. 2, pp. 277–293, Apr. 2015.
- [5] D. Rapaport, *The Art of Molecular Dynamics Simulation*. Cambridge, U.K.: Cambridge Univ. Press, 2004.
- [6] C. Balanis, *Advanced Engineering Electromagnetics*. Hoboken, NJ, USA: Wiley, 2012.

Capítulo 6

Aplicação do método LJDM na geração de domínios tridimensionais

Neste capítulo, são apresentados os resultados das simulações tridimensionais (3D) realizadas com os softwares e métodos desenvolvidos neste trabalho. O objetivo é validar o método RPIM com discretização espacial obtida através do LJDM para problemas tridimensionais (3D). O processo de validação tem a finalidade de garantir, através de estudos numéricos, que o método concorde com soluções analíticas, assegurando a consistência dos resultados.

6.1 RPIM aplicado nas equações de Maxwell 3D

Neste trabalho, utiliza-se uma abordagem em coordenadas retangulares, onde as equações de Maxwell no espaço tridimensional 3D, são representadas através das componentes de campo E_x , E_y , E_z , H_x , H_y e H_z , onde

$$\begin{aligned}\frac{\partial E_x}{\partial t} &= \frac{1}{\epsilon} \left(\frac{\partial H_z}{\partial y} - \frac{\partial H_y}{\partial z} \right), & \frac{\partial E_y}{\partial t} &= \frac{1}{\epsilon} \left(\frac{\partial H_x}{\partial z} - \frac{\partial H_z}{\partial x} \right), \\ \frac{\partial E_z}{\partial t} &= \frac{1}{\epsilon} \left(\frac{\partial H_y}{\partial x} - \frac{\partial H_x}{\partial y} \right),\end{aligned}$$

$$\begin{aligned} \frac{\partial H_x}{\partial t} &= \frac{1}{\mu} \left(\frac{\partial E_y}{\partial z} - \frac{\partial E_z}{\partial y} \right), & \frac{\partial H_y}{\partial t} &= \frac{1}{\mu} \left(\frac{\partial E_z}{\partial x} - \frac{\partial E_x}{\partial z} \right) \\ e & & \frac{\partial H_z}{\partial t} &= \frac{1}{\mu} \left(\frac{\partial E_x}{\partial y} - \frac{\partial E_y}{\partial x} \right). \end{aligned}$$

Ressalta-se que as leis de Gauss são automaticamente satisfeitas pelas leis de Faraday e Ampère em coordenadas retangulares [4].

As equações de (1)-(4) do artigo 1 podem ser usadas para construção das funções de formas $\phi(\bar{x}) = [\phi_1(\bar{x})\phi_2(\bar{x})\phi_3(\bar{x})\dots\phi_n(\bar{x})]$ (para cada domínio de suporte), como descrito em [13]. Desta forma sugere a equação (8) do artigo 1, descrita por

$$f^a(\bar{x}) = \sum_{j=1}^n f_j(\bar{x})\phi_j(\bar{x}) \quad (6.1)$$

Introduzindo a ideia da função de forma para derivadas parciais $\frac{\partial\phi_j}{\partial x}$, $\frac{\partial\phi_j}{\partial y}$ e $\frac{\partial\phi_j}{\partial z}$, nas equações de Maxwell 3D, tem-se

$$E_x^{N_t+1}(i) = E_x^{N_t}(i) + \frac{\Delta t}{\epsilon} \left(\sum_j^n H_z^{N_t}(j) \frac{\partial\phi_j}{\partial y} - \sum_j^n H_y^{N_t}(j) \frac{\partial\phi_j}{\partial z} \right), \quad (6.2)$$

$$E_y^{N_t+1}(i) = E_y^{N_t}(i) + \frac{\Delta t}{\epsilon} \left(\sum_j^n H_x^{N_t}(j) \frac{\partial\phi_j}{\partial z} - \sum_j^n H_z^{N_t}(j) \frac{\partial\phi_j}{\partial x} \right), \quad (6.3)$$

$$E_z^{N_t+1}(i) = E_z^{N_t}(i) + \frac{\Delta t}{\epsilon} \left(\sum_j^n H_y^{N_t}(j) \frac{\partial\phi_j}{\partial x} - \sum_j^n H_x^{N_t}(j) \frac{\partial\phi_j}{\partial y} \right), \quad (6.4)$$

$$H_x^{N_t+1}(i) = H_x^{N_t}(i) + \frac{\Delta t}{\mu} \left(\sum_j^n E_y^{N_t}(j) \frac{\partial\phi_j}{\partial z} - \sum_j^n E_z^{N_t}(j) \frac{\partial\phi_j}{\partial y} \right), \quad (6.5)$$

$$H_y^{N_t+1}(i) = H_y^{N_t}(i) + \frac{\Delta t}{\mu} \left(\sum_j^n E_z^{N_t}(j) \frac{\partial\phi_j}{\partial x} - \sum_j^n E_x^{N_t}(j) \frac{\partial\phi_j}{\partial z} \right), \quad (6.6)$$

e

$$H_z^{N_t+1}(i) = H_z^{N_t}(i) + \frac{\Delta t}{\mu} \left(\sum_j^n E_x^{N_t}(j) \frac{\partial\phi_j}{\partial y} - \sum_j^n E_y^{N_t}(j) \frac{\partial\phi_j}{\partial x} \right). \quad (6.7)$$

onde, $t = N_t \times \Delta t$ é o tempo (em segundos), Δt é o passo temporal para o RPIM, i é o índice do nó posicionado em \bar{x} e n é a quantidade de nós no domínio de suporte $\Omega_{SR}(\bar{x})$. Ressalta-se que neste trabalho, n varia entre 16 e 36, dependendo do domínio de suporte considerado.

6.2 Caso 1 - ressonador condutor perfeito na forma de um quarto de anel 3D

O ressonador condutor perfeito no formato de um quarto de anel tridimensional (3D), descrito em [29], foi escolhido para verificar a eficiência computacional do método LJDM na geração de discretização espacial *meshless* utilizada em problemas de propagação eletromagnética em ambiente 3D. Este caso é um estudo de propagação eletromagnética gerado dentro de uma cavidade tridimensional metálica (condutor perfeito) totalmente fechada no formato de um quarto (1/4) de anel com raio menor $r_a = 0.06\text{m}$, raio maior $r_b = 0.12\text{m}$ e altura $h=0.01\text{m}$ (eixo z). A Fig.6.1 ilustra a seção transversal (no plano-xy) e a projeção 3D (tridimensional) da região do problema. A onda eletromagnética se propaga dentro do ressonador e é excitada através da componente z do campo elétrico. A posição da fonte de excitação e do sensor podem ser vistas na Fig.6.1(a) e na Tabela 6.1. Ressalta-se que a distância entre os nós $\Delta_{\bar{x}}$ (definida para o domínio de análise Ω_a) deve ser menor ou igual a $\Delta_{\bar{x}\min} = \lambda_{\min}/10$ e a distância entre os nós que descrevem a fonte Δ^{fonte} deve ser igual a $\Delta_{\bar{x}}$.

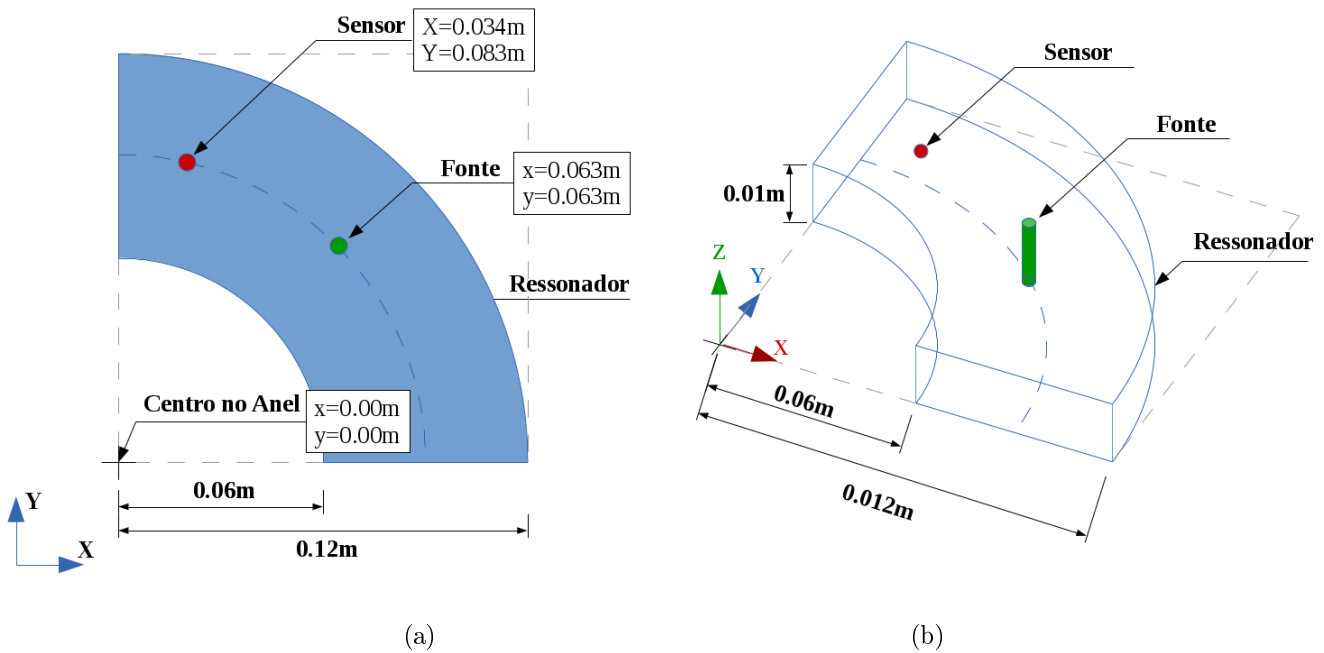
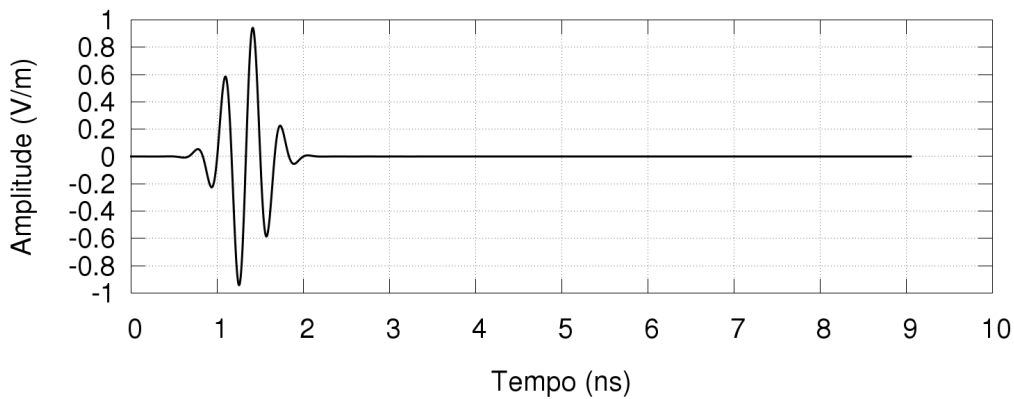


Figura 6.1: Representação do ressonador condutor perfeito na forma de um quarto de anel 3D. a) seção transversal no plano-xy e b) Projeção tridimensional (3D).

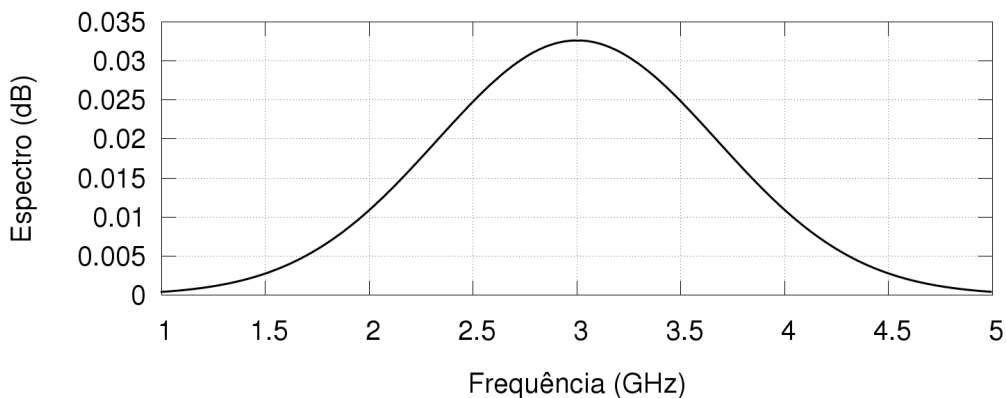
O sinal de excitação é descrito por um pulso gaussiano modulado dado por

$$J_z(t) = A_p \times e^{\left[-\frac{(t-t_0)^2}{\tau}\right]} \sin(2\pi f_c(t - t_0)), \quad (6.8)$$

onde $J_z(t)$ é a componente z da densidade de corrente (para $\frac{\partial E_z}{\partial t} = \frac{1}{\epsilon} \left(\frac{\partial H_y}{\partial x} - \frac{\partial H_x}{\partial y} - J_z \right)$), $A_p = 1$ é a amplitude do pico do sinal, $f_r = 3\text{GHz}$ é a frequência referência que possui maior amplitude em toda a banda no domínio da frequência, $\tau = \frac{1}{f_c}$ é um indicador da largura temporal do pulso e está relacionado à largura de banda (bw), $t_0 = 4\tau$ é o instante que corresponde ao centro do sinal gaussiano, e é a constante de Neper ($e \approx 2,71828$) e t é o tempo em segundos. Para este caso, utilizou-se a largura de banda igual a $bw \approx 4\text{GHz}$, frequência máxima de $f_{\text{max}} = 5\text{GHz}$. A Fig.6.2 mostra este sinal no domínio do tempo e da frequência.



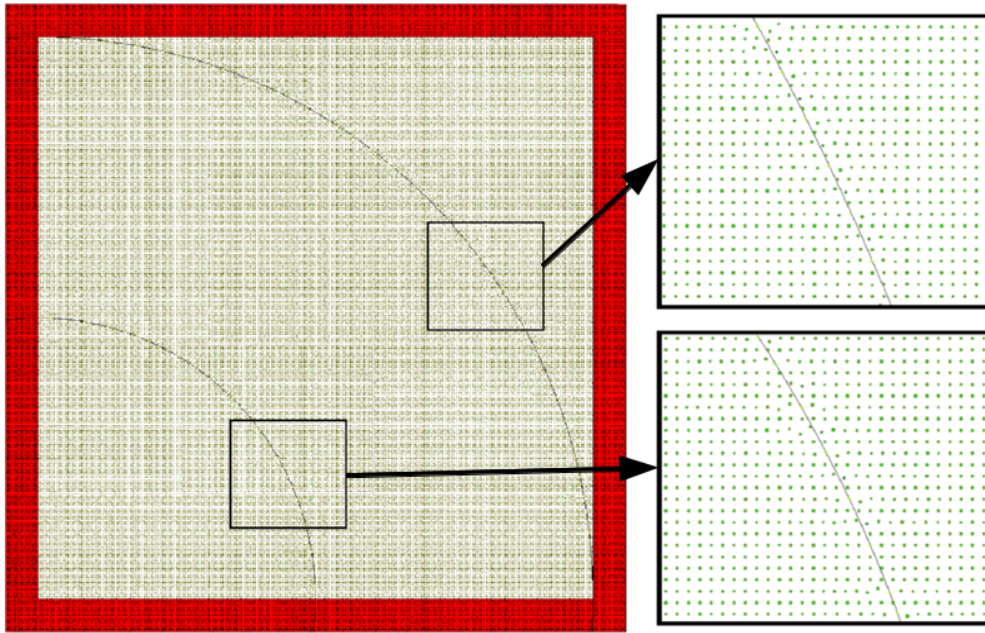
(a)



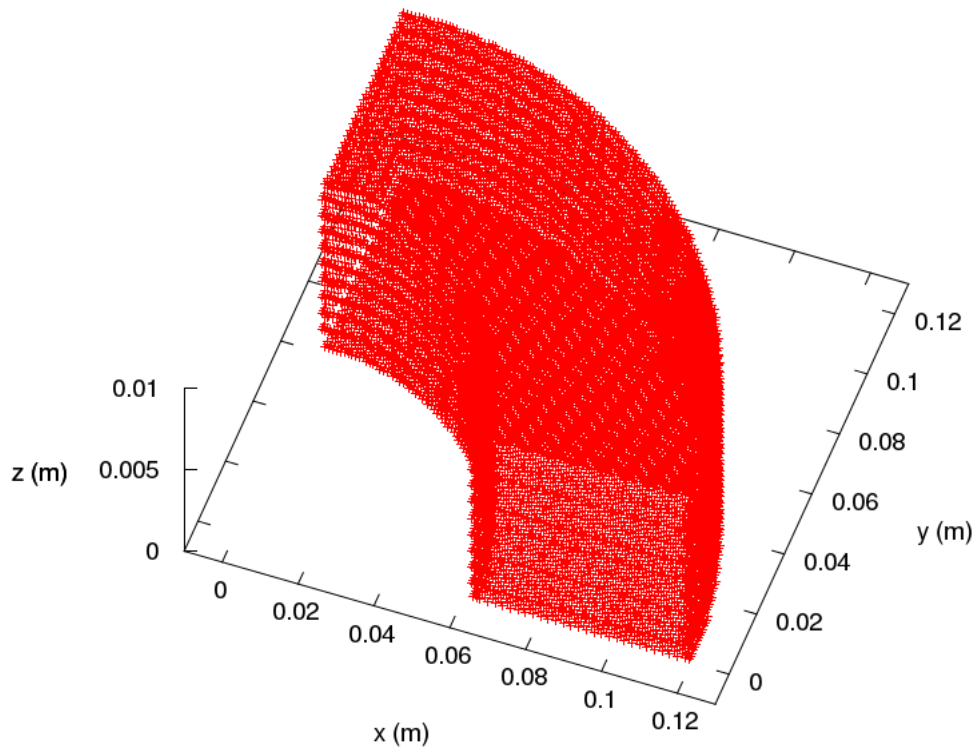
(b)

Figura 6.2: Sinal de excitação com largura de banda igual a $bw \approx 4\text{GHz}$ e a frequência máxima de $f_{\text{max}} = 5\text{GHz}$. a) Sinal gaussiano modulado no domínio do tempo, b) Espectro de frequência do sinal gaussiano modulado.

O método LJDM bidimensional (2D) foi adaptado para gerar o domínio tridimensional que representa o ressonador usado neste caso. Com base na simetria do problema, foi possível gerar um domínio bidimensional (Ω_{2D}) que represente adequadamente a região do problema no plano-xy (Fig.6.1(a)) e posteriormente foram realizadas projeções do Ω_{2D} no eixo z , criando assim um conjunto de camadas copias de Ω_{2D} , as quais, em conjunto, geram um domínio tridimensional (Ω_{3D}) capazes de representar o espaço tridimensional do problema, Fig.6.1(b). A distribuição dos nós no domínio foi gerada com base na distância entre os nós $\Delta_{\bar{x}}$, para $\lambda_r = C_0/f_r$, onde C_0 é a velocidade da luz e f_r a frequência referência (f_r deve ser menor que f_{\max} do pulso a ser aplicado). Para este caso, a distância entre os nós é dada por $\Delta_{\bar{x}} = \lambda_r/100 = 0.001$ metros (valor menor que $\Delta_{\bar{x}\min} = \frac{(C_0/f_{\max})}{10} = 0.006$ metros). É importante notar que para geração do domínio a partir do método LJDM utilizou-se $\Upsilon = 30$ equação (23) do artigos 1. A Figura 6.3 mostra a discretização espacial obtida após 65 iterações (para $\delta_{dp} = 0.25$) do método LJDM.



(a)



(b)

Figura 6.3: Discretização espacial na região próxima ao ressonador obtida após 65 iterações do método LJDM para $\delta_{dp} = 0.25$. a) Seção transversal no plano-xy, b) Visão 3D (tridimensional).

Como pode ser visto na Fig.6.3, a região do ressonador foi discretizada de modo conformal, representando de forma adequada a interface entre regiões e garantindo a qualidade da discretização espacial. É importante notar que, o método LJDM mantém a estrutura do arranjo nodal de referência (RNA), esta capacidade é a grande vantagem que o método LJDM possui em comparação com o CLDM.

Neste estudo de caso, foram realizadas simulações com os métodos: FDTD (diferenças finitas no domínio do tempo), RPIM com distribuição retangular (sem aplicação do LJDM) e RPIM (com LJDM), com a finalidade de comparar os resultados obtidos por cada método. Os parâmetros das simulações podem ser vistos na Tabela 6.1.

Tabela 6.1: Parâmetros de simulação

PARÂMETROS	RPIM	FDTD
Tamanho da Região de Análise		
$C_e \times L_e \times H_e$ (m)	0.12 x 0.12 x 0.01	0.12 x 0.12 x 0.01
Ressonador 1/4 de anel 3D - $r_a \times r_b$	0.06 x 0.12	0.06 x 0.12
Υ (Discretização via LJDM)	30	-
$bw[f_{\min}, f_{\max}]$ (GHz)	[1.0e-6, 5]	[1.0e-6, 5]
f_r (GHz) (frequência de referência)	3	3
dt (s)	9.62e-13	9.62e-13
A_p (V/m)	1	1
τ (s)	3.33e-10	3.33e-10
t_0 (s)	13.33e-10	13.33e-10
$\lambda = C_0/f_r$ (m)	0.1	0.1
$\lambda_{\min} = C_0/f_{\max}$ (m)	0.06	0.06
$\Delta_{\bar{x}}$ (m) (distância entre nós)	$\lambda/100$	$\lambda/100$
Δ_{\min} (m) (distância mínima entre nós)	$\lambda_{\min}/10$	$\lambda_{\min}/10$
Posição da fonte $x \times y$ (m)	0.063 x 0.063	0.063 x 0.063
Posição do sensor $x \times y$ (m)	0.034 x 0.083	0.034 x 0.083
Número de iterações no tempo	9400	9400

A propagação do sinal dentro do ressonador, obtida via simulação usando RPIM (com

LJDM), pode ser vista na Fig.6.4.

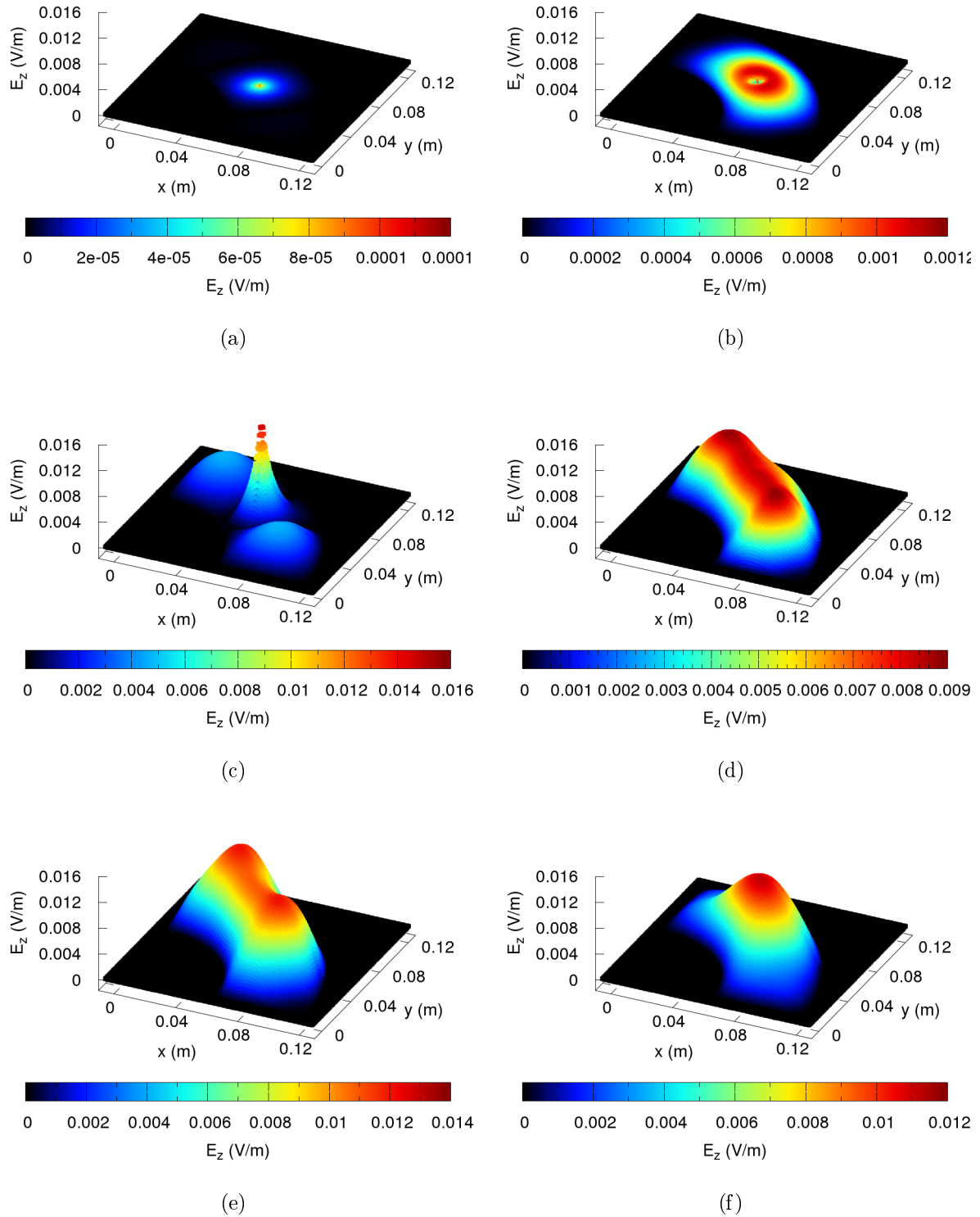


Figura 6.4: Distribuição da componente E_z total, secção transversal no plano-xy em $z = 0.005$. a) $t = 0.58\text{ns}$, b) $t = 0.96\text{ns}$, c) $t = 1.34\text{ns}$, d) $t = 1.93\text{ns}$, f) $t = 3.27\text{ns}$, g) $t = 4.91\text{ns}$.

Como explicado anteriormente, após 65 iterações do método LJDM foi gerado um domínio Ω para $\delta_{dp} = 0.25$ (fator de deslocamento) e uma simulação via RPIM foi realizada usando Ω . Para fins de comparação, mais duas simulações foram realizadas, uma usando o método FDTD e a outra o RPIM com distribuição retangular. Estas simulações geraram resultados no domínio do tempo que posteriormente foram convertidos para o domínio da frequência e comparados com a solução de referência descrita em [29]. A Fig.6.5 apresenta os resultados no domínio da frequência obtidos via: solução de referência, FDTD, RPIM com distribuição retangular e RPIM com LJDM (melhor resultado obtido com 65 iterações para $\delta_{dp} = 0.25$).

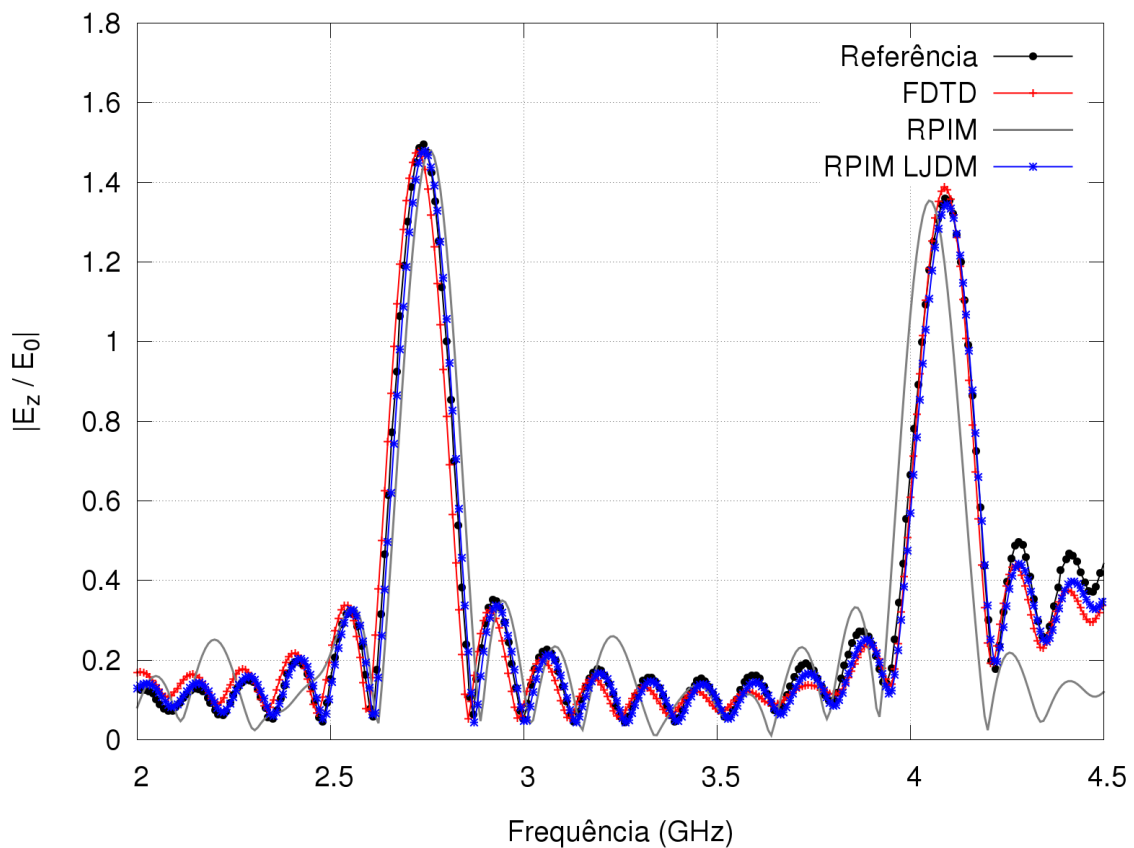


Figura 6.5: Comparação dos resultados no domínio da frequência para os métodos RPIM (com LJDM), RPIM (distribuição retangular), FDTD e solução de referência.

Comparando os melhores resultados obtidos pelo método LJDM e FDTD, nota-se que ambos os métodos possuem resultados muito bons, os quais se aproximam da solução de referência em quase toda a banda de frequência analisada. É importante notar que, o resultado obtido pelo método RPIM com distribuição retangular (sem utilizar nenhum

método de discretização espacial) foi o pior dos três resultados, se distanciando da solução de referência em vários pontos do gráfico. Além disso, apesar do maior tempo computacional, o resultado obtido via RPIM (com LJDM) foi melhor que o obtido pelo método FDTD, se aproximando mais do resultado de referência na maior parte do gráfico.

Desta forma, pode-se considerar que o método LJDM conseguiu gerar um domínio tridimensional conformal com elevada qualidade da discretização espacial, o qual consegue representar de forma adequada os objetos complexos inseridos na região de análise. Por este motivo, o RPIM (com LJDM) obteve resultado melhor que o FDTD e o RPIM com distribuição retangular. Baseando-se nos resultados obtidos, conclui-se que o método RPIM (com LJDM) foi desenvolvido e aplicado (de forma satisfatória) à problemas tridimensionais.

Capítulo 7

Considerações Finais e Propostas para Trabalhos Futuros

Ao longo dos anos de atividades que originaram este trabalho, foram desenvolvidas três novas metodologias de discretização espacial *meshless* com base nos potenciais de Coulomb e Lennard-Jones para criação de domínios que possam ser aplicados a problemas eletromagnéticos simulados com o método RPIM (Radial Point Interpolation Method).

O primeiro método está descrito no Artigo 1 e foi chamado de *Coulomb's Law Discretization Method* (CLDM) (CLDM), pois baseia-se na dinâmica analítica da lei de Coulomb, de tal forma que cargas virtuais (nós do domínio) são usadas para realizar discretização espacial. Basicamente, dois grupos de partículas são configurados: cargas móveis e fixas. As cargas fixas são usadas para criar um conjunto de nós sobre as regiões de fronteira (interfaces entre diferentes matérias) que representam os espalhadores inseridos no espaço de análise. Já as cargas móveis são empregadas para criar transições suaves na discretização espacial próxima dos vários objetos imersos no espaço. O processo de deslocamento das cargas (que produz equilíbrio de força entre partículas) é obtido naturalmente usando a dinâmica analítica da lei de Coulomb. A fim de assegurar a estabilidade numérica para o RPIM, a qualidade da interpolação (conforme definido no Artigo 1) é verificada e melhorada usando LSFCM quando necessário (otimização local do fator de forma c) durante o processo de discretização.

O CLDM foi aplicado com sucesso em problemas envolvendo espalhamento eletro-

magnético e filtros PBG com geometrias complexas. Alta precisão é observada para CLDM-LSFCM-RPIM quando as soluções analíticas são usadas como referência porque a representação geométrica sem malha (por CLDM) é conformal, diferentemente das malhas FDTD, que sofre com uma representação não muito adequada para estruturas não-retangulares, gerando *staircase* [30]. Além disso, a precisão das interpolações é melhorada ao empregar otimização local de c . O artigo 1 mostra que os conjuntos de nós gerados por discretização CLDM tendem a ter maior qualidade de discretização do que os gerados por discretização *meshless* com base em *Delaunay*.

Apesar de conseguir gerar discretização espacial *meshless* com elevado nível de conformidade, o método CLDM não garante a qualidade da discretização para todos os domínios gerados, pois em muitos casos não consegue manter de forma adequada o RNA (arranjo nodal de referência) em todo espaço de análise, mais especificamente nas regiões próximas dos espalhadores, causando problemas na precisão numérica do RPIM, pois as variações espaciais dos campos não conseguem ser avaliadas de forma mais precisa perto dessas regiões críticas. Nestas condições, surgem os métodos descritos nos artigos 2 e 3, como resultados de pesquisas adicionais com o intuito de aperfeiçoar o método CLDM.

O artigo 2 apresenta uma melhoria importante no CLDM chamada de *Electric Charge Gaussian Gradation Method* (ECGGM). Com esta técnica, é possível aumentar de forma controlável o nível de discretização em torno das interfaces (bordas e cantos) dos espalhadores contidos na região de análise. Este efeito é produzido utilizando função gaussiana para alterar gradualmente a magnitude das cargas (nós do domínio) próximas das fronteiras desses espalhadores. Essa concentração de nós em torno das interfaces entre diferentes materiais produz melhorias substanciais na precisão numérica do RPIM, pois as variações espaciais dos campos são avaliadas de forma mais precisa perto dessas regiões críticas. Outras vantagens importantes do método ECGGM sobre o CLDM, estão descritas no artigo 2, tais como: 1) melhoria notável na precisão do cálculo do campo eletromagnético quando os espalhadores estão presentes; 2) redução do número total de nós no domínio de análise em comparação com o método CLDM para um nível de precisão semelhante; entre outras.

Dois estudos de caso foram realizados com base no espalhamento eletromagnético para

cilindros metálicos, usando onda plana. Para estes casos foram realizadas simulações com FDTD e RPIM (com CLDM e ECGGM). Os resultados obtidos para o cilindro circular metálico (caso 1) mostram que, com relação à solução exata, o método de discretização ECGGM produz Máximo Erro Relativo (MRE) e Raiz do Erro Médio Quadrático (RMSE) de cerca de 5% e 0,0383, respectivamente, para um q_{\min} em $[0.2, 0.9]$. Desta forma, o ECGGM gerou resultados melhores que os obtidos pelo FDTD e CLDM (como mostram as Figuras 6 e 7 do artigo 2), demonstrando claramente que ECGGM melhorou a precisão de cálculo para este problema. No caso de validação 2 (espalhador triangular), os resultados obtidos utilizando o método ECGGM-RPIM foram comparados com resultados produzidos usando as equações integrais de métodos e FEFD. Para o espalhador triangular, vemos uma grande concordância entre os métodos FEFD e ECGGM-RPIM. Observe que este problema foi simulado com o ECGGM-RPIM e CLDM-RPIM usando $\Delta_x = \lambda/20$. Os resultados numéricos mostram que a metodologia de discretização proposta ECGGM, com base na gradação de cargas por equação gaussiana perto das fronteiras entre materiais, é adequada para representar corretamente bordas e cantos, já que a densidade da discretização muda suavemente no espaço, o que agrega relevantes melhorias na precisão do método CLDM.

No artigo 3, foi introduzida uma nova metodologia chamada *Lennard-Jones Discretization Method* LJDM, que pode ser vista como uma melhoria do CLDM. Esta metodologia baseia-se no potencial de Lennard-Jones (e nas forças de atração e repulsão associadas a este potencial), para gerar uma distribuição totalmente *meshless*.

A força de Lennard-Jones é composta por duas parcelas (repulsiva e atrativa) que atuam em conjunto e conseguem representar sistemas de partículas nos estados sólido, líquido ou gasoso. As forças repulsivas atuam para gerar a conformidade da discretização, enquanto as forças de atração são responsáveis pela preservação do RNA (arranjo nodal de referência), que é conservado porque foi modelado como uma molécula estabilizada por forças de LJ. Sendo assim, é possível gerar domínios com elevados graus de conformidade geométrica, e principalmente, manter um nível aceitável de preservação do RNA.

Os experimentos numéricos realizados mostram que 200 iterações do LJDM devem ser suficientes para alcançar a convergência para distribuição dos nós no domínio, quando o

fator de deslocamento progressivo está na faixa de $0.40 < \delta_{dp} < 1.00$ (tendo em vista que o processo de deslocamento progressivo é aplicado para o LJDM e CLDM, na representação das interfaces entre matérias). Nota-se que o LJDM melhora ligeiramente a precisão sobre CLDM. Para o problema analisado, o CLDM produz $MRE \approx 9,45\%$ e LJDM produz $MRE \approx 7,50\%$. É importante ressaltar que os domínios de suporte usados pelo LJDM contêm aproximadamente $1/3$ da quantidade de nós em relação aos domínios de suporte usados pelo CLDM, reduzindo principalmente o uso de memória computacional e diminuindo o tempo de processamento do processo de discretização espacial em aproximadamente 95% .

Neste trabalho, além dos três artigos, foi realizado um estudo de caso tridimensional, com o intuito de validar a aplicação do método LJDM para casos 3D. Foram desenvolvidas versões dos métodos LJDM e RPIM, adaptadas para simular problemas eletromagnéticos regidos pelas equações de Maxwell no espaço tridimensional. O problema proposto para este estudo foi o ressonador de condutor perfeito com formato de $1/4$ de anel 3D, descrito em [29].

Analisando os resultados gerados com base na solução de referência, nota-se que alta precisão numérica foi obtida usando o método RPIM-LJDM aplicado a este problema 3D. O resultado obtido com o método RPIM-LJDM é muito mais próximo do resultado de referência do que os obtidos via FDTD e RPIM com distribuição retangular. Sendo assim, pode-se considerar que o método LJDM obteve um desempenho satisfatório para o problema tridimensional em questão.

Como pôde ser visto, a utilização dos conceitos físicos de interação entre partículas se mostrou muito eficaz no desenvolvimento de metodologias de discretização espacial *meshless* aplicadas a problemas eletromagnéticos simulados com o método RPIM (Radial Point Interpolation Method).

Deste modo, foi possível a publicação dos três artigos científicos que servem como base para esta tese de doutorado, escrita a partir da agregação dos mesmos. Com base no exposto, pode-se concluir que os objetivos pretendidos foram alcançados, contribuindo para o desenvolvimento de novos métodos de discretização espacial totalmente *meshless*.

Além dos artigos, foram desenvolvidos *softwares* para auxiliar na aplicação dos métodos propostos, dentre os quais estão: 1) uma interface gráfica bidimensional (2D) que

auxiliou na criação dos cenários que representam as regiões de análise dos problemas estudados, possibilita também, a visualização dos domínios gerados por cada um dos métodos; 2) um software que gera domínios tridimensionais a partir de domínios bidimensionais, para problemas cuja estrutura não varia em uma das direções; 3) dois simuladores com base nas equações de Maxwell com RPIM (formulação 2D e 3D respectivamente), o quais possibilitaram a simulação em RPIM dos problemas de propagação eletromagnética, propostos neste trabalho.

É importante ressaltar que o processo de geração da distribuição dos nós está totalmente automatizado para todos os três métodos, fazendo com que a interação humana seja necessária apenas para iniciar o processo.

Futuramente, outras implementações podem ser desenvolvidas a fim de melhorar a aplicação destes métodos. Entre elas estão:

- Paralelização - possibilitando a modelagem de problemas mais complexos, com região de análise e número de elementos maiores. Esta implementação é fundamental para a aplicação dos métodos CLDM, ECGGM ou LJDM em problemas 3D;
- Acoplamento ao simulador - na implementação atual o processo de geração da distribuição dos nós está separado do processo de simulação. Porém é possível acoplar o simulador à interface gráfica (associada à aplicação dos três métodos), criando um único *software*, possibilitando assim a automatização total do processo.
- Truncagem por CPML - A CPML [31] é uma técnica ABC que se mostra adequada para método *meshless*.
- Com base no ECGGM é importante ressaltar que outras funções (tais como linear e tansig) podem ser utilizadas na gradação das cargas, abrindo portas para produzir mais melhorias no futuro.
- Considerar permissividade e condutividade elétrica como arbitrários.
- Trabalhar com meios dispersivos.

As implementações mencionadas são apenas exemplos de melhorias que podem ser desenvolvidas, a fim de dar continuidade a este trabalho e contribuir para a evolução dos

métodos em questão.

Ressalta-se que os métodos propostos (CLDM, ECGGM e LJDM), dada as suas relativas simplicidades de implementação em comparação com métodos para geração de malhas não-estruturadas, mostraram-se alternativas viáveis aos geradores (de malha) comerciais e aos complexos algoritmos de geração de malhas não-estruturadas. Além disso, os algoritmos permitem avaliar previamente se o conjunto de nós funcionará adequadamente com o método RPIM. Mesmo com geradores comerciais, a qualidade da discretização (para o método *meshless*) não é assegurada automaticamente, pois instabilidades numéricas podem ser observadas quando malhas de elementos finitos (com alta qualidade para o FEM) são empregadas em métodos *meshless*.

Destaca-se que as principais vantagens dos métodos propostos são: possibilitar a geração de discretização espacial conformais, conseguir aumentar o nível de discretização apenas em regiões específicas do espaço de análise diminuindo problemas de precisão do método RPIM e preservar o arranjo nodal de referência (RNA). Estas vantagens garantem maior qualidade da discretização e aumentam a precisão dos resultados numéricos da equação de Maxwell com RPIM. Estas características associadas às técnicas desenvolvidas são a principal contribuição deste trabalho.

Referências Bibliográficas

- [1] F. P. Preparata and M. I. Shamos, *Computational Geometry: An Introduction*, 1st ed. Springer-Verlag, 1985.
- [2] C. Balanis, *Advanced Engineering Electromagnetics*. Wiley, 1989.
- [3] A. Thom and C. J. Apelt, *Field Computations in Engineering and Physics.*, 1st ed. London: D. Van Nostrand, 1961.
- [4] A. Taflove and S. Hagness, *Computational Electrodynamics: The Finite-Difference Time-Domain Method*, 3rd ed., ser. Artech House Antennas and Propagation Library. Artech House, 2005.
- [5] T. Hughes, *The Finite Element Method: Linear Static and Dynamic Finite Element Analysis.*, 1st ed. Dover Publications, 2000.
- [6] P. P. Silvester and R. L. Ferrari, *Finite elements for electrical engineers.*, 3rd ed. ed. New York: Cambridge, 1996.
- [7] K.-J. Bathe, *Finite Element Procedures.*, 1st ed. New Jersey: Prentice Hall, 1996.
- [8] J. Thompson, B. Soni, and N. Weatherill, *Handbook of Grid Generation*. Taylor & Francis, 2010.
- [9] A. Quarteroni and A. Valli, *Numerical Approximation of Partial Differential Equations*, xvi ed. Springer-Verlag, 1994.
- [10] R. Gingold and J. Monaghan, “Smoothed particle hydrodynamics - Theory and application to non-spherical stars,” *Monthly Notices of the Royal Astronomical Society*, vol. 181, pp. 375–389, Nov. 1977.

- [11] S. N. Atluri and T. Zhu, “A new Meshless Local Petrov-Galerkin (MLPG) approach in computational mechanics,” *Computational Mechanics*, vol. 22, no. 2, pp. 117–127, 1998.
- [12] G.-R. Liu and Y. Gu, “A point interpolation method,” in *4th Asian-Pacific Conference on Computational Mechanics*, Singapore, December 1999, pp. 1009–1014.
- [13] J. G. Wang and G. R. Liu, “Radial point interpolation method for elastoplastic problem,” in *1st International Conference on Structural Stability and Dynamics*, Taipei, Taiwan, December 2000, pp. 703–708.
- [14] Y. Yu and Z. Chen, “A 3-d radial point interpolation method for meshless time-domain modeling,” *Microwave Theory and Techniques, IEEE Transactions on*, vol. 57, no. 8, pp. 2015–2020, 2009.
- [15] P. L. Machado, R. M. S. Oliveira, W. C. B. Souza, Ramon C. F. Araújo, Maria E. L. Tostes, and C. Gonçalves, “An automatic methodology for obtaining optimum shape factors for the radial point interpolation method,” *Journal of Microwaves, Optoelectronics and Electromagnetic Applications*, vol. 10, no. 2, pp. 389–401, 2011.
- [16] S. Lipschutz and M. Lipson, *Matemática Discreta: Coleção Schaum*. BOOKMAN COMPANHIA ED, 2004.
- [17] J. Shewchuk, *Delaunay Refinement Mesh Generation.*, 2nd ed. John Wiley, 2000.
- [18] A. Okabe, B. Boots, K. Sugihara, and S. N. Chiu, *Spatial Tessellations - Concepts and Applications of Voronoi Diagrams.*, 2nd ed. John Wiley, 2000.
- [19] W. B. d. Sousa and R. M. e. S. d. Oliveira, *Metologia de discretização espacial para o método radial de interpolação por pontos (RPIM) aplicada para solução numérica das equações de Maxwell*. 2013., n.d. [Online]. Disponível em: <http://search.ebscohost.com/login.aspx?direct=true&db=cat02764a&AN=ufpa.196903&lang=pt-br&site=eds-live&authtype=ip,cookie,uid>
- [20] J. H. Ferziger and M. Peric, *Computational Methods for Fluid Dynamics.*, 1st ed. Springer, 1998.

- [21] S. Li and W. K. Liu, *Meshfree Particle Methods.*, 1st ed. Springer, 2007.
- [22] S.A.Viana, “Meshless methods applied to computational electromagnetics.” PhD thesis, University of Bath, 2006.
- [23] K. Shanazari and M. Hosami, “A two-dimensional adaptive nodes technique in irregular regions applied to meshless-type methods,” *Engineering Analysis with Boundary Elements*, vol. 36, no. 2, pp. 161 – 168, 2012.
- [24] Q. Du, M. Gunzburger, and L. Ju, “Meshfree, probabilistic determination of point sets and support regions for meshless computing,” *Computer Methods in Applied Mechanics and Engineering*, vol. 191, no. 13, pp. 1349–1366, 2002.
- [25] D. Burgarelli, “Modelagem computacional e simulação numérica adaptativa de equações diferenciais parciais evolutivas aplicadas a um problema termoacústico.” PhD thesis, Departamento de Matemática da PUC-RIO, 1998.
- [26] D. Appleby and J. VandeKopple, *Programming Languages: Paradigm and Practice*, ser. McGraw-Hill International Editions. McGraw-Hill, 1997.
- [27] L. Books, S. Wikipedia, and B. Group, *Object-oriented Programming Languages: COBOL, Java, C++, Perl, Fortran, Python, PHP, Eiffel, Smalltalk, Ruby, Blitz BASIC, Turbo Pascal, List of Object-oriented Programming Languages, Self, Common Lisp, Objective-C, Lua, Pike, BETA, Objective Caml, Z++, XLISP, Oxygene.* General Books, 2011.
- [28] B. Stroustrup, *The C++ Programming Language.* Addison-Wesley Professional, 2000.
- [29] F. Liu, D. Su, and Y. Zhang, “A 3-d unconditionally stable laguerre-rpim meshless method for time-domain electromagnetic computations,” vol. 31, pp. 279–293, 01 2013.
- [30] R. Holland, “The case against staircasing,” in *6th Annual Review of Progress in Applied Computational Electromagnetics*, Monterey, CA, Mar. 1990, pp. 89–95.

- [31] Y. Yu and Z. Chen, “The CPML Absorbing Boundary Conditions for the Unconditionally Stable Meshless Modeling,” *Antennas and Wireless Propagation Letters, IEEE*, vol. 11, pp. 468 –472, 2012.